Paleomagnetism of Silurian to Carboniferous magmatic rocks in the Orkney Islands

Thomas Viken

Thesis submitted for the degree of Master of Science in
Structural Geology and Tectonics
60 credits

Department of Geosciences
The Faculty of Mathematics and Natural Sciences

UNIVERSITY OF OSLO

02.03 / 2021

Paleomagnetism of Silurian to Carboniferous magmatic rocks in the Orkney Islands

2021

Paleomagnetism of Silurian to Carboniferous magmatic rocks in the Orkney Islands

Thomas Viken

http://www.duo.uio.no/

Trykk: Reprosentralen, Universitetet i Oslo

Abstract

Earlier paleomagnetic studies of the Orkney Islands, Scotland, have encountered difficulties with identifying the oldest components seen in the Devonian rocks. Poor quality of remanence in the samples alongside few data points in some cases have thrown the reported paleo poles into question. The estimated ages of the rocks in the earlier studies have also been uncertain, with wide error margins.

Newly published, well constrained ages of the Hoy Volcanic member and of a part of the Lamprophyre dike swarm on Orkney yielded emplacement ages of 378 Ma and 304 Ma, respectively. In this study, the hope was that the new ages could help explain the results and difficulties previously encountered. Newer laboratory equipment and proper documentation during the fieldwork was also thought to give an advantage to overcome the earlier troubles.

Neither the previously published, nor the new paleo poles for the Devonian volcanics in this study match what is expected for Devonian rocks on Scotland, falling over 30° eastwards from the 380 Ma reference pole. The sampled Carboniferous dikes fit better with the expected paleo pole for the Carboniferous, but there have been some shift eastwards of the paleo pole for the dikes as well, though not to the same extent as the volcanics. The characteristic remanence found in some of the volcanics and sediments resembles the remanences seen in the dikes, so there is likely some overprinting in the volcanic of the same age as the dikes.

That both the Devonian volcanics and the Carboniferous rocks have paleo poles that have been moved counterclockwise from the expected reference, but to different degrees, is suggested to reflect a large-scale rotation of the Orkney Islands throughout the period of volcanism and dike emplacement.

Acknowledgements

I would like to express my deepest gratitude to the following people at the University of Oslo:

Anders Mattias Lundmark for being my supervisor, proofreader, and for general encouragements throughout the process.

Mathew Domeier for being my supervisor and teaching me all there is to know about paleomagnetic fieldwork and lab work, and for ample inputs during the writing process.

Lars Eivind Augland for being my supervisor, for always being available during meetings and open to supply knowledge of the Orkney Islands.

Petter Silkoset at the Centre for Earth Evolution and Dynamics (CEED) for frequent assistance and tutelage during the laboratory work, and for being available for questions when needed.

John Flett Brown and Cynthia for their hospitality during the fieldwork.

“Hutch” from Rackwick, who served tuna sandwiches and drinks after a long, wet day in the field and provided ample conversation about the state of the islands.

Special thanks to Anders Mattias Lundmark and Mathew Domeier for their hard work during the two weeks in the field, it was a fantastic experience to have you accompany me during the fieldwork.

Thanks to friends and family for their support during this long process and being there when I needed a little extra boost to write.

Table of Contents

1. Introduction and aim of study

There have been several previous studies of Paleomagnetism on the Orkney Islands in the 70's and 80's (Storetvedt and Pettersen, 1971; Storetvedt and Meland, 1985; Storetvedt and Otterå, 1987; Robinson, 1985). The target has been volcanic rocks, the Hoy volcanics, and lamprophyric dikes. The goal of these studies has been to establish the location of the paleo pole in the Middle Devonian, which some of the rocks of Orkney has been dated to.

In the liquid magma of 400 million years ago, the magnetic minerals aligned themselves with the magnetic field of the earth, like a compass. When the magma cooled to form the volcanic rocks of Orkney we can see today, these magnetic particles were locked in place, and formed what we call remanent magnetism. By measuring this property of the rocks today, we can see the apparent pole position, and combined with the position of the Orkney Islands today we can say something about the movement and previous whereabouts of the Orkney Islands.

There have been problems in the previous paleomagnetic work. From the earlier studies, we know that there has been significant overprinting of the magnetism following emplacement of the rocks (Storetvedt and Pettersen, 1972), making it difficult to find the oldest remanent magnetism and paleo pole position. The ages of some of the investigated rocks have also been uncertain.

Recent studies have given us new information. New age dating of the lamprophyric dikes on Orkney shows that at least some of the dikes are millions of years older than previously suggested by some investigations (Rian, 2018), but millions of years younger than assumed in some of the paleomagnetic work (Storetvedt and Meland, 1985). The new dating of these dikes might help us explain some of the previous overprinting of the Devonian volcanics, and give us a more in depth look of the paleomagnetic history of Orkney. The precise position of the Devonian paleo pole of the British Isles remains elusive to this day (Domeier and Torsvik, 2014).

With state-of-the-art laboratory equipment at the Ivar Giæver Geomagnetic Laboratory and thorough fieldwork, I hope to gather new information on the paleo pole for the Devonian and to explain some of the difficulties with the data found in the volcanic rock of the Orkney Islands.

Aims:

- Collect samples from a varied set of Devonian volcanic rocks on Mainland Orkney and on the island of Hoy. And from the Carboniferous camptonite dikes in the western part of Mainland.
- Conduct a well constrained paleomagnetic study using new equipment and properly document where samples were gathered to examine variations between sites.
- Further constrain the Devonian paleo pole position at 378 Ma.
- Investigate a possible link between the overprint of the Devonian Volcanics and lamprophyre dike emplacement.
- Compare to previous studies to see if new equipment can uncover new information.

2. Background

2.1 General background

The Orkney Islands is a group of islands situated to the northeast of Scotland and is Scottish territory. The Orkney Islands consists of a number of islands, the biggest being Mainland and the island of Hoy to the south. The terrain on Orkney is dominated by steep cliffs on the western side; low terrain and little vegetation save for some cultivated land and extensive moors.
The oldest rocks in Scotland are found on the Outer Hebrides and in the northern parts of Scotland, with younger sediments forming the southern and central parts of Scotland (Gillen, 2003). The Orkney Islands today are almost completely built up of sandstones and flagstones from the middle and upper Old Red Sandstone (ORS; Fig. 1), the regional term for mainly Devonian terrestrial sediments (Mykura, 1976). In addition to the flagstones there are some scattered volcanic rocks from the Devonian (Mykura, 1976) as well as an extensive suite of over 200 lamprophyre dikes (Wilson and Knox, 1936) from the Permo-Carboniferous (Rock, 1983)

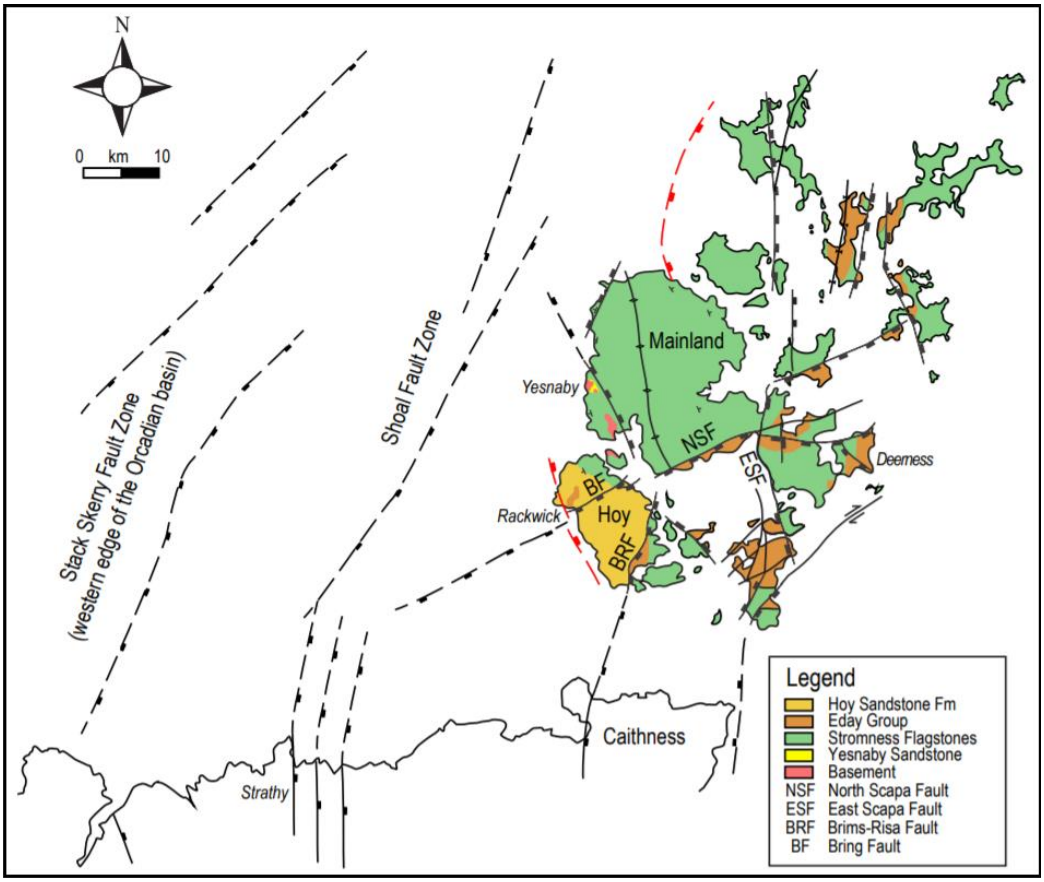

Figure 1: Geologic overview of the Orkney Islands, and selected Devonian faults in the surrounding areas. From Rian (2018), modified in Lundmark et al., (Submitted), used with permission

2.2 Geologic background

The geologic history of the Orkney Islands is closely linked to the history of Scotland. Being one of the birthplaces of modern geology, the area has been extensively studied for hundreds of years, and was described geologically already in the 1600s (Speed, 1666).
Scotland has a geologic history stretching back over 3.0 Ga, and has been a part of five possible supercontinents during this time (Macdonald & Fettes, 2007).

Scotland's earliest magmatic history is found in the form of igneous rocks found in the Lewisian Gneiss Complex dating back to about 2.7-3.1 Ga (Macdonald & Fettes, 2007). At this point Scotland was part of the Kenorland supercontinent (Macdonald & Fettes, 2007), and the Lewisian Gneiss Complex is a deep part of the Laurentian plate from prior to the Caledonian Orogeny (Gillan, 2003). The igneous rocks dating back to this age are granodiorites and tonalites, which underwent metamorphosis sometime around 2.5-2.7 Ga during a tectonothermal event (Macdonald & Fettes, 2007).

The Lewisian gneisses were uplifted and exposed around 1200 Ma, during the Grenvillian Orogeny that eventually led to the formation of the supercontinent Rodinia around 1100-900 Ma (Li *et al*., 2008). During this period of continent collisions, rivers in what is now Canada and Greenland deposited thick layers of sediments on top of the Lewisian gneisses on the northwestern part of Scotland. These sediments form what is now called "The Torridonian". These are the oldest sedimentary rock sequences found in Great Britain (Gillen, 2003).

Between 1000-870 Ma Scotland formed part of a slowly subsiding basin, with deposition of marine sand and clay that now make up the Moine schists (Gillen, 2003). The Moine schists dominates the Northern Highlands and is proposed to form a part of the basement beneath the Orkney Islands (Mykura, 1976; Strachan, 2003). The Northern Highlands is bounded by the Great Glen fault to the southeast and by the older Hebridean terrane to the northwest (Fig. 2).

Across the Great Glen fault lie the Grampian Highlands, which are dominated by the Neoproterozoic Dalradian rocks. These rocks are similar to the Moine schists, and forms a broad belt from the Shetland Islands southwestwards through the central parts of Scotland (Prave *et al.,* 2009). The Dalradian sediments were deposited between 750-600 Ma during the breakup of Rodinia and the opening of the Iapetus Ocean (Gillen, 2003).

In the early Palaeozoic, the three paleocontinents of Laurentia, Baltica and Avalonia started to drift together, closing the Iapetus ocean and going through the series of tectonic events that lasted from

the Cambrian to the early Devonian (McKerrow *et al*., 2000), and make up the Caledonian Orogeny (Chew and Strachan, 2014).

The British Isles were situated on the northern edge of Avalonia, and was at the forefront in the collision between the three paleocontinents of Avalonia, Laurentia and Baltica (Macdonald & Fettes, 2007). After the collision, the movement between the three continents became orogen-parallel, and lasted to about 410 Ma (Macdonald & Fettes, 2007). The Great Glen Fault running through the north of Scotland is probably responsible for taking up a huge part of the sinistral movement during this period (Dewey and Strachan, 2003). The actual length of displacement is disputed, but could be up to 700km in length (Dewey and Strachan, 2003).

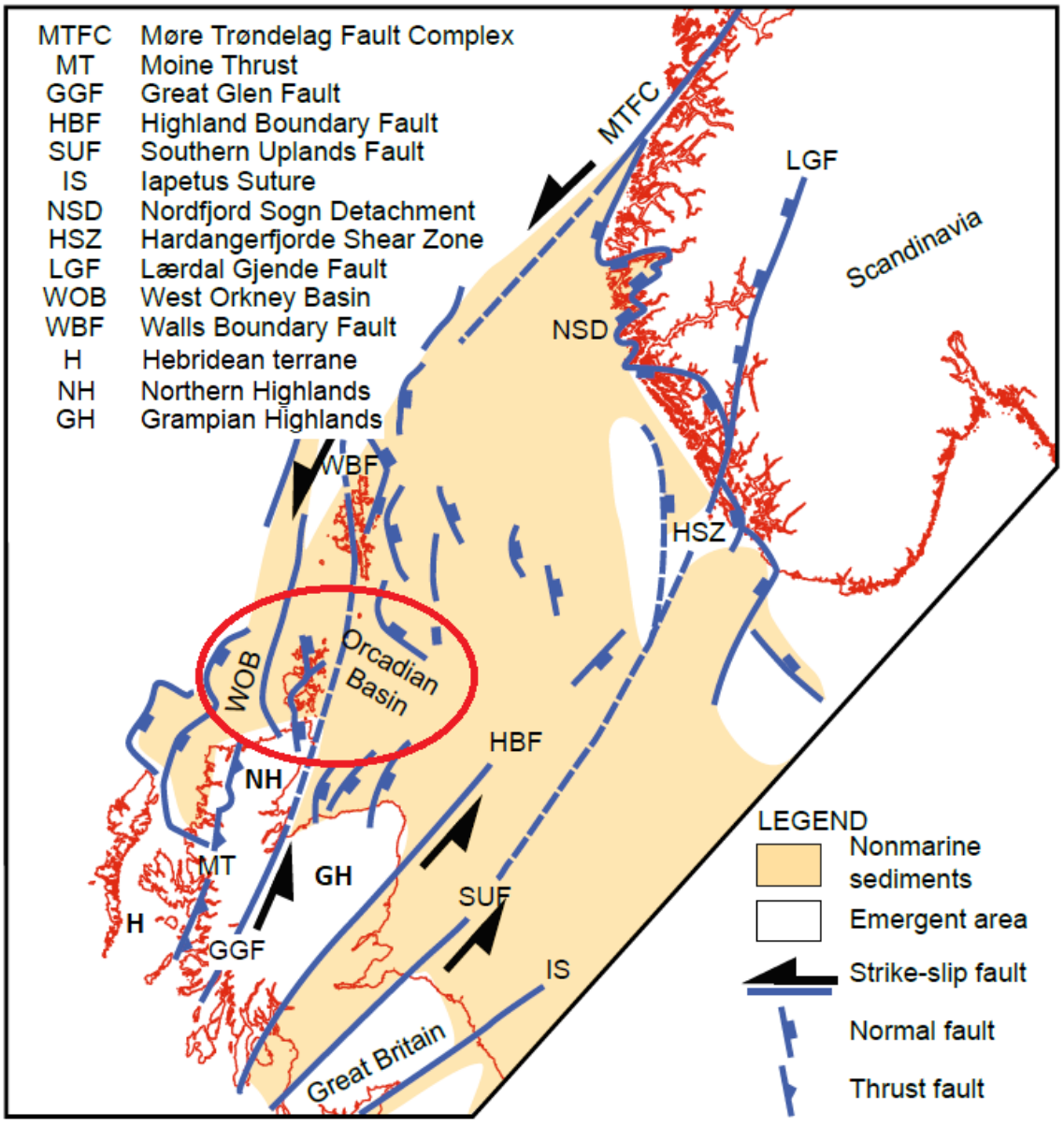

Figure 2: The Orcadian Basin (circled), with an overview of the transcurrent and extensional faults that caused it to form. Originally from Coward et al., 2003; Fossen 2010, modified in Lundmark et al., submitted; and modified further here.

2.2.1 Hoy and Deerness Volcanics, Orkney Islands

Following the Caledonian Orogeny, a subsequent post-orogenic collapse after 410 Ma gave rise to the Orcadian basin and provided accommodation space for the Old Red Sandstone (ORS) sediments within it (Dewey and Strachan, 2003). Extensional sinistral movement along the faults led to large pull-apart structures creating the Orcadian basin with associated rifting (Fossen, 2010; Bird, 2014). The basin consisted of northeast trending half-grabens, from the Moray Firth to Shetland (Parnell *et al*., 1985), and bounded to the west by the Stack-Skerry Fault Zone (Bird, 2014) and to the east by the continuation of the Highland Boundary Fault (Marshall and Hewett, 2003). Sedimentation continued during this period of northwest-southeast extension within the basin (Coward *et al*., 1989). Fault block rotations within the half-grabens underneath the Orcadian basin led to episodic footwall uplifts and local unconformities, growth faults, uneven sedimentation rates and most importantly for this thesis, episodes of local volcanism (Mykura, 1976; Astin, 1985; Coward *et al.,* 1989; Marshall and Hewett, 2003; Bird, 2014).

The Orcadian basin was at this point during the Devonian situated around 20-30°S (Domeier and Torsvik, 2014) with an arid to semi-arid climate (e.g. Astin, 1990).
The Orcadian basin experienced shifting periods of domination by the Orcadian Lakes or by alluvial and fluvial systems (Astin, 1990). The Old Red Sandstone sediments elsewhere are shown to be deposited from the Silurian to the Carboniferous (Kendall, 2017), but is on Orkney limited to the Devonian. The ORS on Orkney is divided into the "Lower", "Middle" and "Upper" Old Red Sandstone (Enfield and Coward, 1987) and currently make up most of the exposed rocks on Orkney (Mykura, 1976). The middle ORS on Orkney is divided further into the Stromness Flagstones and Rousay Flagstones in the bottom half with the Eday Flagstones above (Mykura, 1976). The Eday Sandstones can be further divided into the lower, middle, and upper Eday Sandstone formations (Fig. 3; Mykura, 1976).

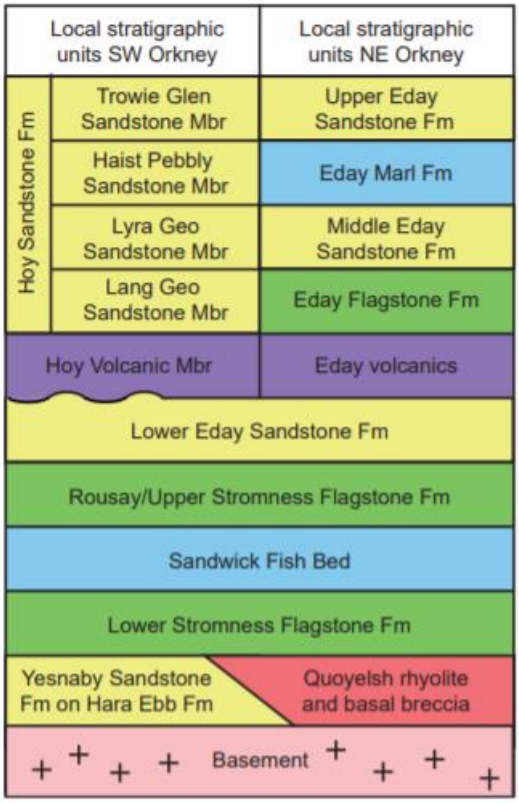

Figure 3: Stratigraphic column from Orkney. Used with permission from Lundmark et al. 2020. The basement consist of Moine schist and Caledonian granites (Lundmark et al. 2019), sediments and Devonian volcanics were deposited in the Orcadian basin, and the entire stratigraphy is cut by younger lamprophyre dikes (Rian, 2018; not shown in the column).

There are two known episodes of Devonian volcanic activity found on Orkney, consisting of the Quoyelsh rhyolite found on Mainland extruded into/onto the Lower Stromness Flagstones (Bjerga, 2017) and the slightly younger Hoy and Eday Volcanics (Fig. 3; Mykura, 1976).
After the Caledonian collision and collapse which gave birth to the Hoy and Eday volcanics there was a time of quiescence, though the Orkneys and Shetland experienced a period of magmatism in the mid-Devonian (McDonalds and Fettes, 2007). At the beginning of the Carboniferous, there was again an increase in magmatic activities, with over 3000 mafic dikes being emplaced in Northern Scotland. On the Orkney Islands, there are over 200 dikes reported (Wilson and Knox, 1936). The dikes have been proposed to reflect three pulses of volcanic activity around 325, 290 and 250 Ma (Baxter and Mitchell, 1984).

The Hoy Volcanic Member is exposed along Too of the Head at Rackwick, on the west coast of Hoy, making it available for study (Fig 1). Stretching almost 700 meters, the Hoy volcanics at Rackwick consists of around 100 meters of volcanic tuffs and columnar jointed basalts (Odling, 1999a). The volcanic tuffs underneath the basalts are around 20 meters thick, with alternating layers of sediments. The volcanics are overlain conformably by the Lang Geo Sandstone, a Member of the Hoy Sandstone Formation (Fig. 3; McAlpine, 1978).
Underneath the Hoy Volcanics, there is an unconformity with the Lower Eday Sandstone formation (Geikie, 1879; Mykura, 1976). The shape of the Hoy Volcanics at Too of the Head seem to indicate an infilling of lavas in an already occurring valley or hollow (Mykura, 1976).

The different isolated exposures of the Hoy Volcanics do not reveal if they are the result of a single lava flow or if they represent separate events (Mykura, 1976).
It is not possible to reconstruct the geometry of the lava flow, but Lundmark *et al*. (submitted) has shown that the different exposures on the north side of Hoy all share a similar geochemical signature, and propose that they formed from one effusive event.

The outcrop of lava at Melsetter is situated on the south side of Hoy, far away (10km) from the other exposures. The lava here is heavily altered and amygdaloidal, but shares characteristic geochemical signatures seen in the other Hoy volcanics (Lundmark *et al*., submitted), suggesting this exposure too is from the same event.

2.2.2 Age of the Hoy volcanics

Earlier reports on the age of the Hoy Volcanics have suggested an age of 379 ± 10 Ma from ^{40}Ar-^{39}Ar dating of exposed rocks at Hellia and Rackwick (Halliday *et al*., 1977, 1982). The ages however are imprecise and widespread alterations and sericitisation of the dated rocks from Hellia throws some uncertainty on the exact ages of these rocks. Another source of uncertainty is the low number of samples, with only two seeming to form the basis of the age estimation (Halliday *et al.,* 1977). These rocks were dated using ^{40}Ar-^{39}Ar age spectras and step-wise heating allowing for dating where some subsequent argon loss has occurred (Halliday *et al.,* 1977).

Recent fieldwork and analysis by Lundmark *et al*. (submitted) sampled a lighter colored horizon at the base of the columnar basalt at Rackwick for zircon U-Pb geochronology. Ten zircons are concordant with an age estimate of 381 Ma to 378 Ma, with eight zircons clustering within a small window giving a weighted mean $^{206}Pb/^{238}U$-age of
378.32 ± 0.19 Ma (Lundmark *et al*., submitted).

This new age constraint of the basalts fits well with the earlier estimate by Halliday *et al.* (1977; 1982) and further constrains the stratigraphic interpretations (Lundmark *et al*., submitted). The underlying Lower Eday Sandstone has been previously dated to be of Givetian age, 387.7-382.7 Ma (Cohen *et al*., 2013, updated 2020/03), from marine micro-fauna found in the Eday Marls lying between the Middle and Upper Eday Sandstones (Marshall *et al*., 1996; Marshall *et al*., 2011).
The Hoy Sandstone formation lying conformably above the Hoy Volcanics has previously been interpreted to be a part of the Upper ORS and of late Devonian age (McAlpine, 1978), 382.7-358.9 Ma (Cohen *et al*., 2013, updated 2020/03). This sandstone formation however has more recently been correlated to the Eday Group found on the eastern parts of the Orkney Islands (Astin, 1990; Marshall *et al*., 1996). The Hoy Volcanics have therefore been correlated with the Eday volcanics found on northeast Orkney, therefore, both volcanic units are situated below the Givetian Eday Marl (Marshall and Hewett, 2003).

2.2.3 The Deerness Volcanics

The Deerness Volcanics are a part of the Eday Volcanics, interbedded with the Eday Flagstones. The volcanic rocks here are placed at the same stratigraphic level as the Hoy Volcanics (Marshall and Hewett, 2003), but geochemical analyses show that they are probably not from the same event

(Thirlwall, 1979). The chemical analysis and sedimentological correlation hint that the Deerness volcanics may be slightly younger than the Hoy Volcanics (Odling, 1999b).

2.2.4 Lamprophyre Dikes

Numerous lamprophyre dikes outcrops across Mainland. The dikes form two groups, a camptonite-bostonite dike swarm and a monchiquite dike swarm; these have recently been dated by Rian (2018), which is one of the main reasons for the new paleomagnetic survey (this study). Being of a younger age than the Hoy and Deerness Volcanics, they can give us a new angle to study for the paleomagnetic development from the Devonian and to the origin of these dikes, and may be related to the previously observed paleomagnetic overprinting of the Devonian volcanics (Storetvedt and Petersen, 1971).

The Orkney dikes were previously thought to belong to the youngest of three pulses of magmatic activity in the Permo-carboniferous (Brown, 1975; Halliday *et al*., 1977; Mykura, 1976). Smythe *et al*. (1995) compared the strikes of the dike swarm to that of the ca. 300 Ma (Monaghan and Parrish, 2006) tholeiitic quartz dolerite dikes found in Northern Britain and the North Sea. Lundmark *et al*. (2011) dated the Orkney dikes using LA-ICPMS U-Pb, and found evidence of an emplacement age considerably older than the previous ca. 250 Ma K-Ar ages, at ca. 313 Ma.
This was further constrained by Rian (2018), who dated the camptonite-bostonite dikes on Orkney to 304 Ma. These are the dikes sampled in this study. The other set of dikes sampled by Rian (2018), the monchiquites, were dated to 281 Ma (Rian, 2018).

2.2.5 Recent geologic history

In the early Jurassic (201.3-174.1 Ma; Cohen *et al*., 2013, updated 2020/03) north-western Europe experienced widespread extensional forces during the breakup between the paleocontinent Laurasia and the supercontinent Gondwana, with the formation of the North Atlantic Ocean (Macdonald and Fettes, 2007). In Scotland, this was mostly marked with the volcanic sequences associated with the rifting in the North Sea during the middle Jurassic (Macdonald and Fettes, 2007).
By the late Cretaceous (100.5-66 Ma; Cohen *et al*., 2013, updated 2020/03) the expansion of the North Atlantic had resulted in the breakup of Greenland from Eurasia, and the arrival of the Iceland Plume marked the onset of Paleogene magmatism (Macdonald and Fettes, 2007).

The Paleogene was a period of crustal growth for Scotland, with large volumes of basic magma being added to the Scottish crust as extrusive rocks and intrusions, showing up as seaward-dipping reflectors in seismic studies (Macdonald and Fettes, 2007).

Throughout all of this, the Orkney Islands have been relatively undeformed following the emplacement of the dikes.

2.3 Previous paleomagnetic studies on the Orkneys

2.3.1 The Hoy volcanic member

There has been three previous paleomagnetic studies of the Hoy Volcanics, in 1971, 1973 and in 1985. The goal was to find the paleo pole for the Middle-Upper Devonian. In the 1971 study by Storetvedt and Petersen the volcanic rocks of Hoy were sampled. Samples were collected from Rackwick and from the Old Man of Hoy on the western side of Hoy (Fig. 4). From 30 hand samples collected from both lavas and tuffaceous sediments beneath them, 60 specimens were made. From this set 7 specimens showed a slightly southwestern direction, just below the vertical at declination 205°, inclination 8.4°. The low number of specimens in the final calculations is caused by few specimens where the final direction can be properly determined. This component is said to be held in a spinel phase in the lavas, while the principal carrier in the ashy tuffs is haematite. This is supported by the thermal stability observed during the demagnetization process, where the lavas would lose 50% intensity by 200°C. The tuffs did not reach a similar demagnetization level until 600°C.

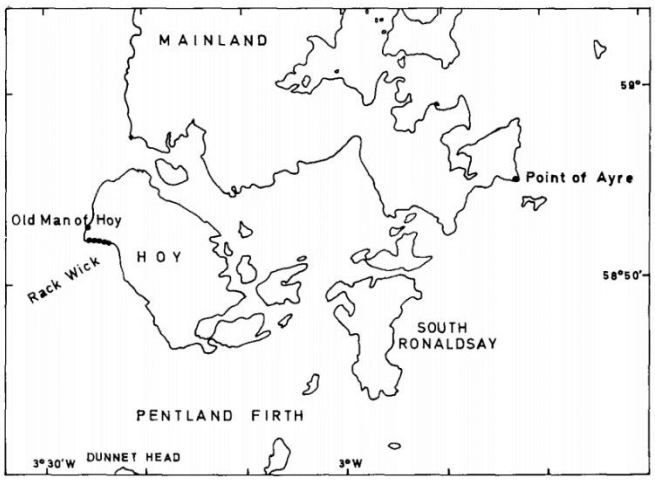

Figure 4: Sample map from the first study by Storetvedt and Petersen, 1971.

Storetvedt and Petersen concluded that chemical magnetization (CRM) plays an important role in the magnetization of the Orkney volcanics due to the high oxidation state of the minerals together with the dual polarity directions supplied by the haematite (Storetvedt and Petersen, 1971). They

identified the spinel phase as exclusively one polarity, indicating it to be more limited in time than the haematite and probably formed close in time to the emplacement of the volcanic rocks. The component carried in the haematite is concluded to be of a later date, possibly from the Middle Devonian-Middle Carboniferous (Storetvedt and Petersen, 1971).

Storetvedt and Meland went back to Orkney in 1985 to resample the same rocks. With the advances in technology and techniques they hoped to get a better understanding of the paleomagnetic data on Orkney (Storetvedt and Meland, 1985).

Samples were again collected from Rackwick and from the Old man of Hoy (Fig. 5). The results this time around were better, from 76 analyzed specimens, 41 gave remanence results able to be separated into distinct groupings (Storetvedt and Meland, 1985). The clearer results are attributed to a few different changes from the first study. AF demagnetization was used on the Rackwick samples over thermal, giving clearer results. The sediments beneath the Old Man of Hoy, which are new to this study, gave good results without the component overlap encountered in the volcanics. Lastly the new equipment available at this point enabled less measuring scatter during demagnetization, helping to determine higher field and temperature end points (Storetvedt and Meland, 1985).

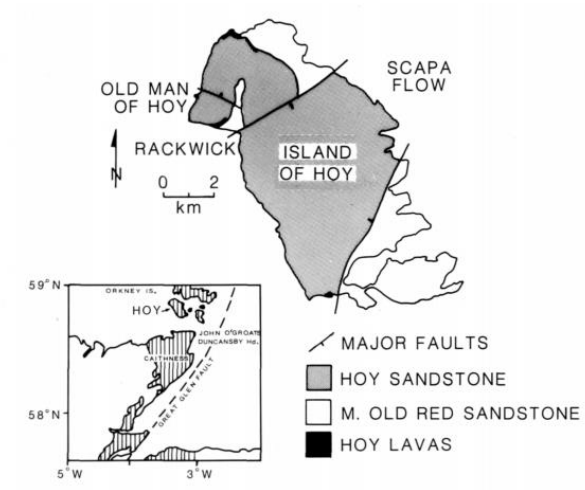

Figure 5: Sample map from the second study of the Hoy volcanics. From Storetvedt and Meland, 1985.

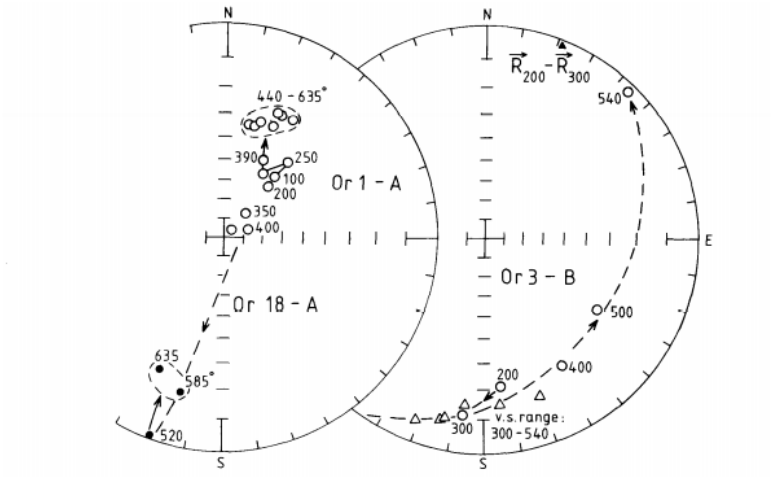

Figure 6: Examples of behavior seen in the Hoy Volcanics. From Storetvedt and Meland, 1985.

From the samples from the Old Man of Hoy, they encountered the same two-polarity remanence as they had previously seen (Fig. 6, left), with one direction towards the southwest and one towards the northeast (Storetvedt and Meland, 1985).

In the sediments below the Old Man they saw another magnetization directed almost directly south with an upwards inclination of around 30° (Storetvedt and Meland, 1985).

The lava specimens of Hoy are found to contain two magnetic phases, one with a Curie temperature around 560-580°C and one with a Curie temperature over 600°C. These are thought to be held in a cation-deficient spinel (titanomaghemite) and haematite respectively (Storetvedt and Meland, 1985). This correlates with the previous study from 1971, where the two components were thought to be held in a spinel phase and haematite (Storetvedt and Petersen, 1971).

The Rackwick lava samples gave 15 specimens with a stable end point in the southwest. Storetvedt and Meland also observed a movement towards the northeastern quadrant in a few of the thermally demagnetized specimens, suggesting a presence of the two-polarity magnetization seen previously.

Storetvedt and Meland defines three groupings of components, with the upwards facing southern component named A, the northeastern component named B1 and the southwestern component named B2 (Fig. 7).

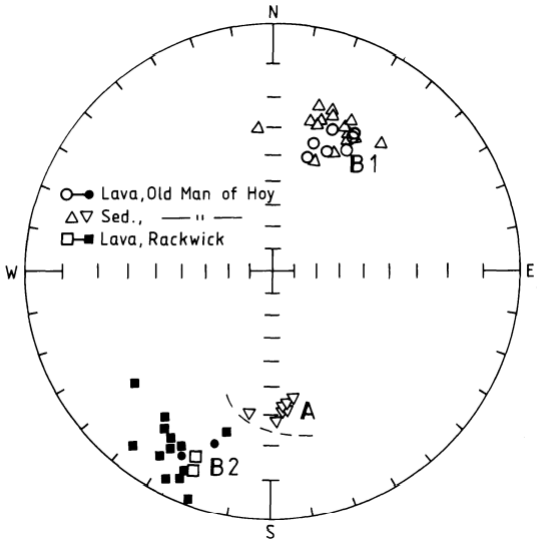

Figure 7: Component map of the three distinct groups. From Storetvedt and Meland, 1985.

From the high amount of low temperature oxidation observed in their samples, with little unaltered titanomagnetite left in the rocks, they speculate that the southwestern component, named B2, is of a younger date than the B1 component in the northeast. They propose that the discrepancy between this B1 component and the regional Devonian reference field is explained by a tectonic shift in the bedding prior to the acquisition of the B2 and A components through chemical magnetization (Storetvedt and Meland, 1985).

The upwards facing southern direction (named A in their study), is said to correspond with a Permian Age, due to its direction and polarity (Storetvedt and Meland, 1985). This is supported by similar directions seen in rocks from the Caithness region and the Helmsdale granite in previous studies by Storetvedt and co-authors (Storetvedt and Meland, 1985).

The third study was carried out by Morris *et al*., (1973). They sampled rocks from Lounders Fea, Melsetter and Rackwick among others, but not all sites were demagnetized. The reported NRMs fall at a medium steep, downwards facing south-southwestern direction.

2.3.2 The Eday volcanic member

Robinson (1985) sampled the Eday volcanics and a wide set of sediments from the southeastern parts of the Orkney islands. Among the rocks sampled where the same basalts from Deerness sampled in this study.

This set of samples consisted of 88 samples from the Eday group sediments and 85 from the Eday volcanics and its baked contact. Samples were collected from eastern Mainland as well as from the islands of Burray, South Ronaldsay, Black Holm (Copinsay) and from Shapinsay, a total of 21 localities (Fig. 8; Robinson, 1985). The majority of the specimens were demagnetized thermally, with a total of 10-15 temperature steps between 100°C and 600°-700°C (Robinson, 1985). The localities numbered 19, 20 and 38 are situated at Deerness, where our samples were collected.

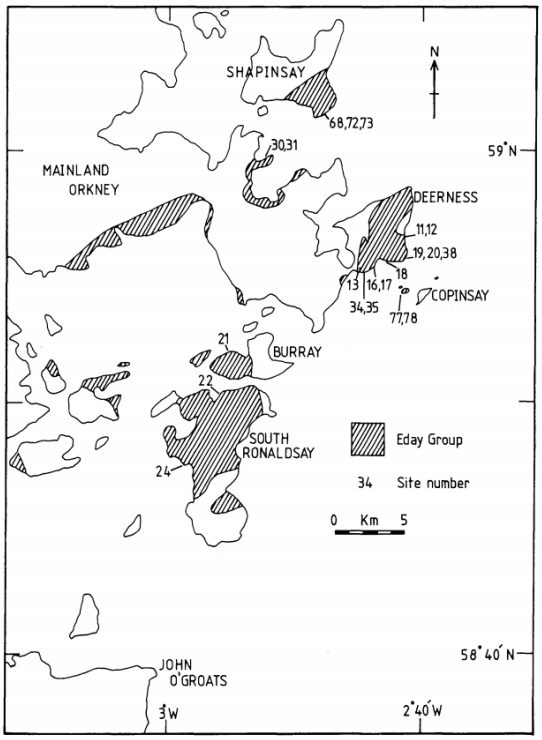

Figure 8: Sample map for the Eday volcanics and sediments. From Robinson, 1985.

The progressive thermal demagnetization found two different behaviors in the Eday lavas. One had a single component pointing steeply downwards and does not match up with any known European Phanerozoic direction (Robinson, 1985). The origin of this magnetization is unknown, but Robinson speculates that this could be a drilling induced magnetization (Robinson, 1985).

The other group displays a low stability component falling close to the present earth's magnetic field, with a higher stability component falling downwards to the south (Robinson, 1985). There is no stable magnetization above 585°C.

The contact test beneath the Deerness lavas showed a similar low stability component close to the present earth's magnetic field, and a higher stability component falling downwards towards the south (Fig. 9, top left; Robinson, 1985). The baked contact zone, as far away as 20cm from the volcanics shows a noteworthy agreement with the mean directions seen in the above-lying lavas (Robinson, 1985).

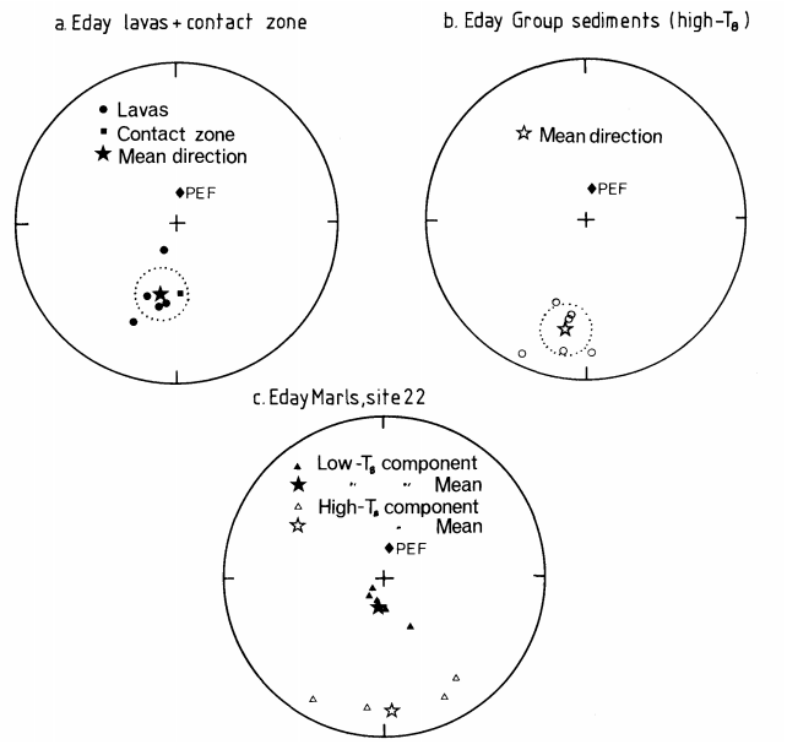

FIG. 3. Stable component distributions. Solid symbols represent directions in the lower hemisphere of the stereographic projection. (a) Lavas and contact zone site means dip corrected; (b) Eday Group sediments, high-T_B component site means (see Table 2), *in situ*; (c) Site 22, Eday Marls. Shows both low-T_B and high-T_B components, at sample level.

Figure 9: Component map for the Eday volcanics and sediments. From Robinson, 1985.

The southern direction seen in the lavas and the contact zone is believed to be a primary direction (Robinson, 1985). The magnetization is held in magnetite, and the correspondence between the lavas, the baked contact and in iron rich sediments below the lavas suggests that the direction does not have a common chemical origin (Robinson, 1985). Robinson points out that this southern direction was found by Storetvedt and Petersen in their 1971 study, but not recognized (Robinson, 1985).

2.3.3 Previous work on the dikes

In 1987, Storetvedt and Otterå carried out a paleomagnetic survey of the lamprophyre dikes that cuts through the Middle Old Red Sandstone and into the Upper Old Red Sandstone. The aim of this study was to see if the paleomagnetic data in the dikes supported a paleogeographic model where the dikes corresponds with a 600km sinistral movement along the Great Glen Fault in the upper Middle Devonian (Storetvedt and Otterå, 1987).

Figure 10: Sample map of the dikes. From Storetvedt and Otterå, 1987.

Samples were collected from 13 dikes along the west and middle Mainland, with a total of 61 hand samples (Fig. 10). From this set of samples, a total of 144 specimens were demagnetized either thermally or using AF demagnetization (Storetvedt and Otterå, 1987). Specimens exhibited increasing erratic behavior as demagnetization proceeded, and some end points were not able to be determined (Storetvedt and Otterå, 1987).

Storetvedt and Otterå found that most samples had a low stability component close to the present earth's magnetic field, and above that one of two characteristic components (Storetvedt and Otterå, 1987). One, which they call component A, lies at 172° declination, -24° inclination, while the other, B, lies at 169° declination, 4° inclination (Fig. 11; Storetvedt and Otterå, 1987). In the samples from the Birsay dike (Fig. 10, site nr. 1 and 2), the A component dominated, but it was seen that the direction shifted towards component B during the last 15% of magnetic moment during demagnetization. The B component is always of higher stability in the specimens where the two components were found together (Fig. 12; Storetvedt and Otterå, 1987).

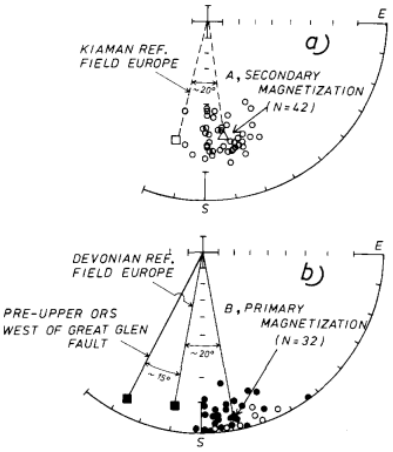

Fig. 6. Stereoplots showing the distribution of the two fossil magnetization populations, components A (a) and B (b), in conjunction with relevant palaeomagnetic reference axes. The overall palaeomagnetic directions for the dykes are shown by △. Note that both remanence groupings are rotated anticlock-

Figure 11: Component map. From Storetvedt and Otterå, 1987.

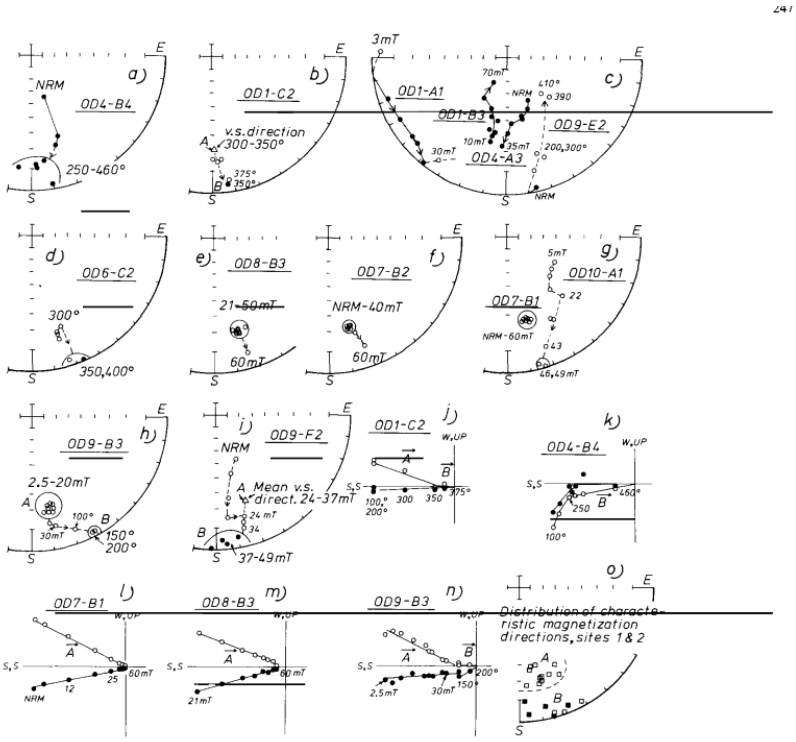

Fig. 2. Examples of demagnetization results from sites 1 and 2. Note the co-existing A- and B-magnetizations in various samples (cf., OD1-C2, 9-B3 and 9-F2). Plots are stereographic projections (Figs. a–i, o), on which ● (○) represent directions in the lower (upper) hemisphere, or in orthogonal vector diagrams (Figs. j–n) for which projections in the vertical and horizontal planes are marked by open and closed symbols respectively. Alternating peak field values are in mT.

Figure 12: Samples from the Birsay dike. From Storetvedt and Otterå, 1987.

The two components seen by Storetvedt and Otterå is interpreted by the authors to be from two distinct magnetization events, with the shallow B direction thought as primary and the steeper A direction being of secondary origin (Fig. 11; Storetvedt and Otterå, 1987).

The A component is said to be of Permo-carboniferous age, while the B component corresponds with Devonian-Lower Carboniferous magnetic fields (Storetvedt and Otterå, 1987). The components seen on Orkney however is rotated about 20° counterclockwise from the comparable northwestern European reference fields (Storetvedt and Otterå, 1987). This shift in components is claimed to be caused by a large-scale strike-slip displacement along the (Slightly curved) Great Glen Fault, which was one of the goals of the study to find out (Storetvedt and Otterå, 1987). The primary B component is theorized to be acquired during the initial period of 600km sinistral displacement along the fault, while the A component was a result of reactivation of the Great Glen Fault during the Middle Carboniferous to Upper Permian, leading to a 300km dextral movement along the fault (Storetvedt and Otterå, 1987). This dextral movement is what led to the 20° counterclockwise rotation observed in the dikes today (Storetvedt and Otterå, 1987).

Storetvedt and Meland, 1985, theorized that the true age of the dikes were closer to that of the volcanics (350-370 Ma), and that the lower age seen when analyzed with K/Ar dating was due to the same argon loss that was observed in the Hoy Volcanics by earlier studies (Halliday, 1977; Storetvedt

and Meland, 1985). This older age is repeated in Storetvedt and Otterås 1987 study as a supporting fact for the 20° rotation seen in the magnetic field (Storetvedt and Otterå, 1987).
Recent high precision dating of the camptonite dikes by Rian (2018) has shown that these are 304 Ma.

Tarling (1985) summarized the previous paleomagnetic work on the Orcadian Basin. Going through studies dating from 1958 to 1983, he found that the general consensus was the presence of two major components, called A and B, but the main disagreement lay in the age of the magnetizations. The A component has declinations between 170° to 214° and inclinations between -37° to -55°, meaning a southern-southwestern angle, at medium steepness downwards.
The B component lies between dec: 181° to 211°, inc: 2° to 14°, so a southwestern, slightly upwards facing component (Tarling, 1985).
Most of these studies are from samples taken in the greater area around Orkney, with many from the north of Scotland. For the studies specific to the Orkney Islands, the 1971 Storetvedt and Petersen falls within component group B, while an early study on the Orkney sandstones and a combined study of Shetland and Orkney both grouped outside the two specified groups.

3. Theory

3.1 Paleomagnetism

There are four important core concepts when it comes to paleomagnetism: magnetic moment, magnetization, magnetic fields, and magnetic susceptibility (Butler, 1992).
Magnetic monopoles, an isolated magnetic charge, does not exist naturally for any period of time, so the smallest unit of magnetic charges is found in the magnetic dipole (Butler, 1992). The magnetic dipole moment, or just magnetic moment can be either a pair of charges or a loop of electrical current (Butler, 1992).

The magnetic moment ***M*** for a dipole with two charges is the magnitude of the charges times the distance between the two (Fig. 13, left). For a loop this looks at the area of the loop times the current, times a vector **n** standing perpendicular to the loop, with the direction of n going upwards out of a loop going counterclockwise (Fig. 13, right; Butler, 1992).

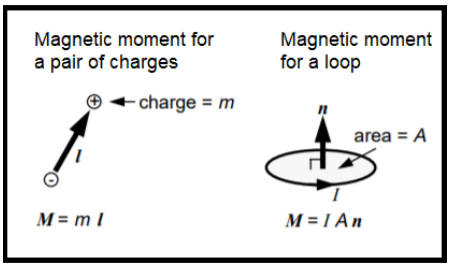

Figure 13: **Left***: Magnetic dipole consisting of a positive and a negative charge with distance l.* **Right**: *Magnetic dipole of a loop with current I, area A and unit normal vector n. Modified from Butler, 1992*

A magnetic field, ***H***, in a region is defined by the force the positive unit of a dipole will experience. A magnetic moment that is free to rotate will align itself to the magnetic field (Butler, 1992), just like a compass needle. The energy required to align a magnetic moment to the magnetic field looks at the magnetic moment, the strength of the magnetic field and the angle between the two (Butler, 1992). The minimum energy configuration is achieved when the magnetic moment is parallel with the magnetic field (Butler, 1992).

The magnetization or magnetic intensity is a measure of the net magnetic moment per unit volume. The vector sum of magnetic moments seen in a material is divided by the volume they take up (Butler, 1992). There are two types of magnetization, induced magnetization which occurs when a material is exposed to a magnetic field, and remanent magnetism. Remanent magnetism is the recording of past magnetic fields that has acted on a material (Butler, 1992). The remanent magnetism will record both the inclination and declination of the past magnetic field that acted on the material (Butler, 1992).

The last part is the magnetic susceptibility, how easily a material can be magnetized. This takes into account both how easily magnetization happens in the direction of the magnetic field, and how that field affects the other direction through a material (Butler, 1992).

The minerals in a rock (or really materials in general) will respond differently to an applied magnetic field, for example the Earths geomagnetic field created in the outer core of the Earth (Butler, 1992). A mineral in a rock can either acquire a small induced magnetization vector that is opposite of the applied field, these minerals are **diamagnetic** and once the applied field is removed the induced magnetization vanishes (Butler, 1992). The strength of the magnetization is linearly dependent on the applied field, and is not affected by outside factors like temperature (Butler, 1992).

The second response seen in minerals happens when the applied field induces a positive magnetization parallel to the applied field; this is a **paramagnetic** response (Butler, 1992). The magnetic moments in the rocks have no interaction between them, and once the applied field is removed the magnetization goes back to zero (Butler, 1992). Paramagnetic minerals are affected by thermal energy, any temperature above absolute zero will cause the crystal lattice in the mineral to vibrate, causing magnetic moments in the atoms to oscillate rapidly and in random directions, causing the overall magnetization to equal zero (Butler, 1992). An applied magnetic field will apply torque on the magnetic moments, causing some of the magnetic moments to align themselves with the new field (Butler, 1992).

The third response is seen in **ferromagnetic** minerals; these minerals have magnetic moments that, unlike in paramagnetic materials, will interact strongly with adjacent magnetic moments (Butler, 1992). This interaction can cause the magnetization of the mineral to be magnitudes greater than what would be seen in paramagnetic materials under the same applied magnetic field (Butler, 1992). The ferromagnetic properties are temperature dependent, ferromagnetic materials will have a saturation temperature; a temperature point where increasing the intensity of the magnetic field will not create greater magnetization (Butler, 1992). The strength of the saturation magnetization will further decrease with increased temperature, eventually reaching the point where the magnetization reaches zero. Above this point, the mineral is paramagnetic (Butler, 1992).
The most important factor of ferromagnetic materials in correlation to paleomagnetism is their ability to remember the direction of the applied magnetic field in the form of remanent magnetism. Once the applied field is removed the magnetization in the rock will not return to zero, instead holding on to a remanence of the applied field, which can be studied later (Butler, 1992).
One of the sources of stability for remanent magnetism is the way a ferromagnetic material will

magnetize easier along certain crystallographic directions, caused by electron orbitals being forced to rotate as the magnetic moments in the atoms rotates in accordance to the applied magnetic field (Butler, 1992). The arising magnetocrystalline anisotropy affects the exchange energy, the energy exchanged between adjacent atomic magnetic moments, along certain directions depending on the crystal lattice (Butler, 1992). The exchange coupling produced can be either parallel or antiparallel depending on the direction the adjacent magnetic moments take (Fig. 14). In ferromagnetic materials, layers within the material are parallel coupled, but adjacent layers can have opposite directions, causing the material to be antiferromagnetic as the adjacent layers cancel each other out (Butler, 1992).

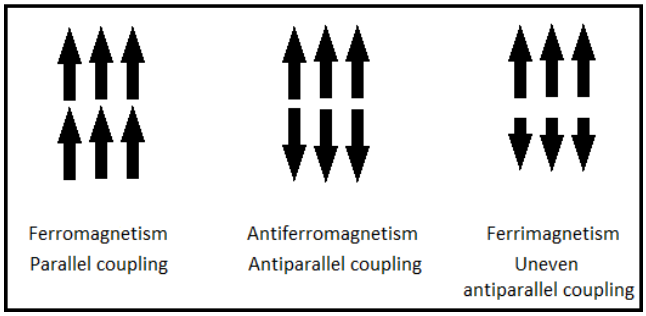

Figure 14: The three possible parallel couplings, creating ferromagnetic, antiferromagnetic and ferrimagnetic behavior. Redrawn from Butler, (1992)

The most important ferromagnetic minerals are the iron-titanium (FeTi) oxides, with titanomagnetites and titanohematites being of special interest due to their magnetic properties (Butler, 1992).

Rocks will have a mixture of ferromagnetic, paramagnetic, and diamagnetic minerals of varying grain sizes, all affecting the overall magnetization of the entire rock (Butler, 1992). The behavior of the magnetic charges in a rock is dependent on the size of the magnetic grains found in the rock and their orientation. Smaller grains can only hold a single field, called single domain; while larger grains will be able to have several fields concurrently potentially pointing in different directions, all of which affect the overall field generated by the sample (Fig. 15). Both the different orientations of magnetic fields found in a rock and any anisotropies seen in size and shape will alter the total magnetic field seen in a rock (Butler, 1992).

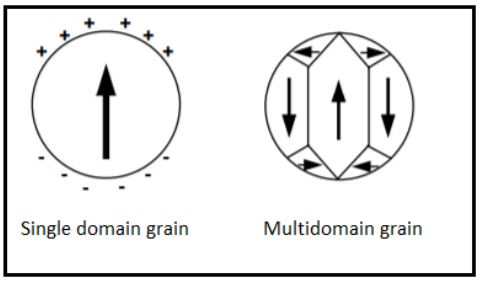

Figure 15: **Left**: *Single domain grain with a positive and negative charged surface. Arrow showing the overall saturation.* **Right**: *Multidomain grain, arrows showing the saturation direction within domains. Modified from Butler, 1992*

The limit of where a grain will favor single domains is dependent on the mineral, but with decreasing size, grains will hit a point where the energy required to develop a domain wall separating domains within a single grain will be greater than the decrease in magnetostatic energy gained in dividing the grain into different domains (Butler, 1992). Single domain grains have dramatic different behavior than multidomain particles, since a single grain will only hold a single field and direction and can be very efficient carriers of remanent magnetization (Butler, 1992).

The magnetic remanence of a rock will decay over time; which is called *Magnetic relaxation*. Relaxation times varies over orders of magnitude, from superparamagnetic single domain grains who will decay shortly after the magnetizing field is gone to the grains holding on to their imparted field over geologic timescales (Butler, 1992).
Relaxation time has a strong size and temperature dependency, for example going from less than one microsecond at 575°C, to longer than the age of the earth at 510°C in a 0.1μm x 0.02μm single domain magnetite grain (Butler, 1992). The temperature point where the relaxation time exceeds a predetermined point, for example 10^3 years is called the *blocking temperature* (Butler, 1992).

The Natural Remanent Magnetization (NRM) is the magnetization found in the rock naturally (Butler, 1992). The overall magnetization is a combination of the natural primary component acquired during the formation of the rock, and any secondary components that has been acquired thereafter (Butler, 1992). Secondary components can alter or completely hide the original primary component (Butler, 1992).

3.1.2 Primary components

Natural Remanent Magnetism can come from several possible sources; the most common is thermoremanent magnetism, usually found in igneous rocks. Thermoremanent magnetism is acquired in lavas and magmas cooled from above the Curie temperature in the presence of a magnetic field. Once below the Curie temperature of the mineral the magnetic remanence will start to accumulate, and below the blocking temperature of the material, the NRM should be stable over

geologic time (Butler, 1992).

Chemical remanent magnetism can be acquired from the growth of new ferromagnetic grains below the Curie temperature. Alterations of minerals can change them into ferromagnetic minerals, or ferromagnetic minerals can precipitate from a solution (Butler, 1992). Because of this, chemical remanent magnetism may be developed in a rock millions of years after the rock was formed, making this form of remanent magnetism a source of secondary, later magnetization (Butler, 1992). This form of remanence is often found in sedimentary rocks (Butler, 1992).

Another form of remanent magnetization found in sedimentary rocks can come from detrital remanent magnetism (Butler, 1992). Developed in sedimentary rocks during deposition and lithification from sediments containing ferromagnetic minerals, most often in the form of magnetite (Butler, 1992). The magnetized grains can align themselves physically both during deposition, and later during settlement before complete consolidation (Butler, 1992).

3.1.3 Secondary components

Any later alterations or additions to the natural remanent magnetization of a rock can be referred to as secondary components. The sources of these are varied, and the same environment that gave birth to the oldest components can return at later stages to re-magnetize the same rocks. Examples are later magmatic events that reheat the rocks and enabling new acquisition of thermoremanent magnetism or the slow growth of ferromagnetic minerals forming chemical remanent magnetism.

Secondary components of the NRM can also be acquired through **Viscous remanent magnetism (VRM)**. VRM comes from the exposure of weak magnetic fields over the long ages since the formation of the rock (Butler, 1992).

Laboratory experiments has shown that acquisition of secondary components is made easier with higher temperatures over time (Fig. 16). The higher the temperature the more VRM is acquired over shorter time (Butler, 1992). The equation for VRM is [S log t], where t is the time in seconds VRM is acquired and S is the viscosity coefficient (Butler, 1992). From this, we can see that at higher temperatures a greater part of the NRM will be secondary components more closely aligned to the present magnetic field. Grains with shorter relaxation times

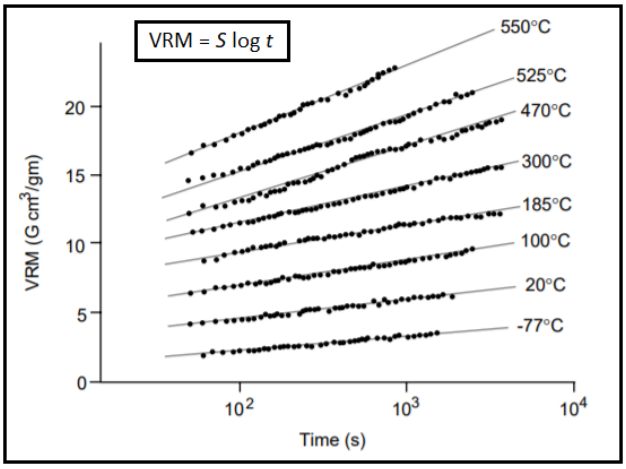

Figure 16: Acquisition of VRM as a function of time and temperature. Modified from Butler, 1992

will be more susceptible to VRM, which is size and shape dependent, smaller grains will be more likely carriers of VRM since it is easier to overwrite the older remanence found in these grains (Butler, 1992).

Prolonged exposure to high temperatures, but still below the Curie temperature may cause metamorphism in the rock, but the NRM can still be held in the rock, so even the oldest remanence has a chance to survive over the ages (Butler, 1992).

Secondary components can also be acquired from short exposures to strong magnetic fields with constant temperature, called **isothermal remanent magnetism (IRM;** Butler, 1992). In nature, this is the result of lightning strikes, which will expose any rock within a meter of the strike to magnetic fields of 10-100 mT, causing significant buildup of IRM (Butler, 1992). The short range of a lightning strike is compensated for by the frequency of thunderstorms and the wealth of time since formation of the rock, so IRM can be a significant source of problems in areas prone to strikes like the tropics or elevated ridges (Butler, 1992).

3.1.4 Characteristic NRM (ChRM)

The NRM of a rock can consist of multiple components, acquired at different times and pointing in different directions. The identification and removal of these components are done through partial demagnetization techniques in the laboratory (Butler, 1992). Some components will start to disappear sooner than others, making them able to be identified. The easier removed components are said to possess low stability, while more resistant components are of higher stability.
The higher stability components can usually be considered the primary components, since these are harder to remove or alter, but this is not always the case (Butler, 1992). A good example would be the later growth of hematite in a rock where the older remanence is held in magnetite grains, the Curie temperature of magnetite is 580°C, while the Curie temperature of hematite is at 680°C. A partial demagnetization technique utilizing heat would see that the component held in magnetite disappears before the newer component caught by the hematite.

Since the highest stability component may not always be the oldest, it is more common to characterize the highest stability component as the **Characteristic component of NRM (ChRM)** instead of primary. Isolation and identification of this component is done through the partial demagnetization process (Fig. 17), but it is usually not possible to determine if this is the primary, oldest component left in the rock (Butler, 1992).

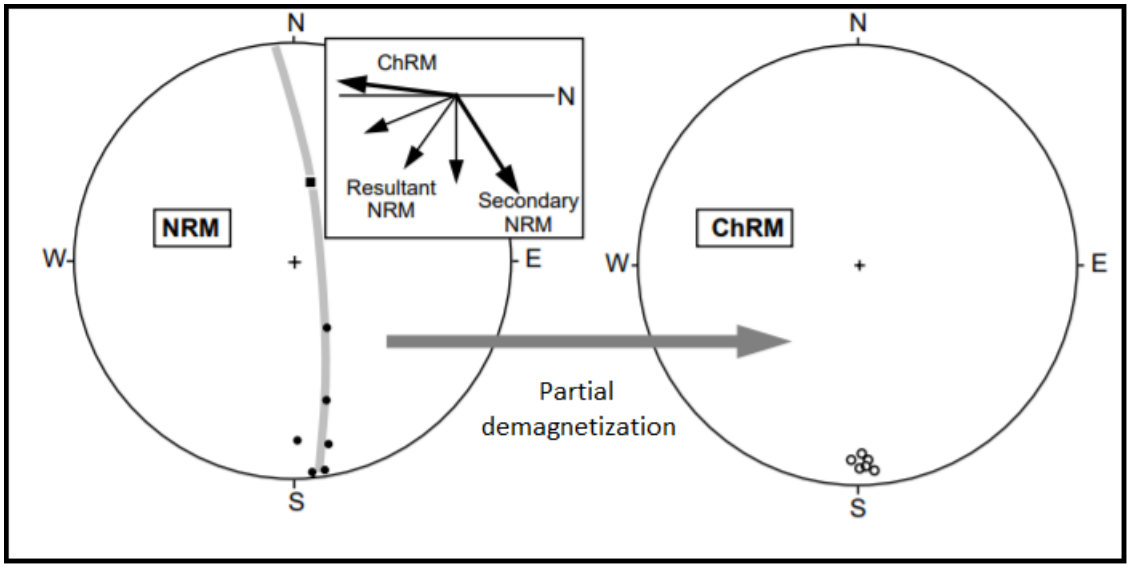

Figure 17: Partial demagnetization removes the lower stability components from the NRM, revealing the ChRM. Modified from Butler, 1992

3.2 Partial demagnetization procedures

The measured NRM in the laboratory will be a vector sum of the primary NRM from the formation of the rock and any secondary components acquired at a later point (Butler, 1992).

Identification and removal of these secondary components is done in a laboratory through partial demagnetization of the samples. Since the primary NRM component might be masked or obscured by one or more secondary components it is advised to take samples from various sites to see if there are any trends or common components emerging during demagnetization (Butler, 1992).

During partial demagnetization the measured NRM should start to shift and change direction as the demagnetization progresses, since the total vector sum will be less affected by secondary low stability components and hopefully closer to the ChRM (Butler, 1992).

3.2.1 Thermal demagnetization

During thermal demagnetization, the sample is heated to a predetermined temperature (below the Curie temperature of that sample) then allowed to cool to room temperature in a shielded environment with no magnetic fields (Butler, 1992). This will cause all grains in the sample with a blocking temperature less than or equal to the demagnetization temperature to lose any NRM held in these grains. The NRM is then measured, before the sample is reheated to a slightly higher temperature. Over repeated steps, the low stability component(s) will be gradually removed, and

the highest stability component should be made visible (Butler, 1992).

The temperature steps at the beginning can be quite large, and then progressively shorter once the temperature approaches the Curie temperature of the magnetic minerals.

The Curie temperature for magnetite is 580°C, and hematite is 680°C, which is one reason secondary components in some cases can have higher stability than the primary component you are looking for if the hematite is later in origin than the magnetite (Butler, 1992).

3.2.2 Alternating Field (AF) demagnetization

During AF demagnetization, the sample is subjected to an alternating magnetic field with a sinusoid waveform (Fig. 18). The intensity will drop of linearly from a preset intensity level while the sample is rotated to evenly spread the new magnetic field along all axes (Butler, 1992).

This new magnetic field will overwrite any grains in the specimen with a coercive force less than the intensity of the new field to the direction the alternating field is pointing.

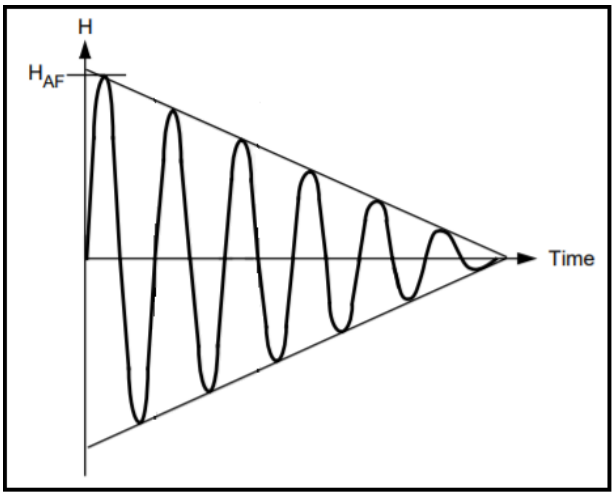

Figure 18: Alternating field demagnetization. The decreasing strength and alternating direction of the applied field will cause opposing magnetic moments to average out to zero. Modified from Butler, 1992.

The alternating field will, for example during the 10 mT demagnetization step, set any grain with coercive force less than or equal to 10.0 mT to the direction we can define as *up*. The field then rotates downwards and sets any grain with coercive force 9.99 mT to *down*. This repeats until the entire set of grains with forces at or below 10 mT to either up or down along all axes. The result of this is since all grains with coercive forces between

10.0 and 9.99 mT is pointing up, 9.99 mT to 9.98 mT pointing down etc., these sets of grains should roughly cancel each other out, giving a net sum of magnetic moments of zero (Butler, 1992).
During AF demagnetization the steps in intensity levels are small in the beginning and then progressively larger.
During AF demagnetization, larger multidomain grains will be the first to be affected, since they generally have a coercive force < 20 mT, while single domain grains can have far larger thresholds. This makes AF great at removing secondary NRMs and isolating ChRM (Butler, 1992).

3.2.3 Finding which technique to use

Rocks and minerals respond differently to demagnetization techniques, so it is good to start the laboratory work with a small subset of samples from each locality to see which technique works better for that set of samples.
Two specimens from two samples from each locality was selected and demagnetized using thermal or AF demagnetization, then the results of these measurements were used to determine which method worked better, in that they gave clearer results that were easier to interpret. That technique was then utilized for the rest of the samples from that locality.

3.3 Anisotropy of Magnetic Susceptibility (AMS)

As mentioned during the paleomagnetism part above, the magnetic moment is held in small grains in the rock, and these can respond differently to magnetization along different directions due to the configuration of the crystal lattice or variations in the distribution of ferromagnetic grains versus dia- and paramagnetic grains in the rock (Butler, 1992). The anisotropy of how susceptible a rock is to magnetization can be measured, and is called the Anisotropy of Magnetic Susceptibility, or AMS.

The anisotropy of the magnetic susceptibility is measured by applying a weak magnetic field (≤ 1mT) along three perpendicular axes and measuring the corresponding response from the sample rock (Butler, 1992; Pueyo Anchuela *et al*., 2006).

The resulting magnetic anisotropy is expressed using an ellipsoid with principal axes $\boldsymbol{K_1}$ for the direction of maximum susceptibility, $\boldsymbol{K_2}$ for the direction of intermediate susceptibility and $\boldsymbol{K_3}$ for the

direction of minimum susceptibility (Raposo, 1995; Butler, 1992). The shape of the magnetic susceptibility ellipsoid is dependent on the relative strength of the three axes (Butler, 1992). An ellipsoid where $\boldsymbol{K_1} = \boldsymbol{K_2} = \boldsymbol{K_3}$ is spherical, while a $\boldsymbol{K_1} = \boldsymbol{K_2} > \boldsymbol{K_3}$ ellipsoid is flattened/oblate and a $\boldsymbol{K_1} > \boldsymbol{K_2} = \boldsymbol{K_3}$ is cigar-shaped/prolate in shape (Butler, 1992).

The anisotropy of the rock can show the fabric and flow direction of a rock even when this is not readily apparent to the naked eye (Ort *et al*., 2015). The principal axis K_1 tend to orient itself along the flow direction due to the way both intrusive and extrusive lava processes are subjected to hydrodynamic forces during emplacement. (Ort *et al*., 2015). The cases where the K_1 axis is oriented along the flow direction is called a *normal* fabric, but in some cases the K_1 axis will orient itself perpendicular to the direction of flow (Ort *et al*., 2015; Delcamp *et al*., 2015). This is an *inverse* fabric and can be caused by a domination of single domain magnetite grains or by turbulence during flow, which disrupts the normal orientation (Ort *et al*., 2015).

4. Methods

4.1 Fieldwork

Fieldwork was carried out over a two-week period from the 26th of August 2019 to the 6th of September, 2019. Sample locations were chosen to get a mix of older volcanic rocks from Mainland and from the island of Hoy, together with five volcanic dikes from all along the western coast of Mainland.

Samples were taken in the field using a chainsaw modified to function as a drill. Pomeroy in California, USA, produces the drill equipment and the cores drilled are 25.4mm wide, making them suitable for the paleomagnetic equipment used at IGGL. The cores were supposed to be sufficiently long to yield 3-4 samples once cut, but hidden fractures in the rocks sometimes proved this difficult.

Measurements of magnetic azimuth and plunge was taken with a combined sun and magnetic compass, also produced by Pomeroy, before the cores were marked with their orientation and extracted. Solar compass measurements were taken whenever the weather allowed it. The solar compass measurement can help to correct for any magnetic interference on the compass from the surrounding rocks when taking measurements.

As a part of the application to take samples an agreement with the National Heritage Office of Scotland was reached for us to conceal our drill sites to the best of our ability. Various methods from just simple filling with available materials to carrying with us cement was considered, but in the end with the input of the National Heritage Office we settled on filling with hammered in loose rocks and gravel of the same rock as the drilled hole.

4.2 Laboratory work

4.2.1 Preparation of samples

The cores were cut with a saw consisting of two diamond-edged copper blades giving a standardized size of each sample. Samples were marked according to sampling locality, core number and the cut samples were marked A to E starting from the bottom depending on the length of the sample. Shape is an important factor when measuring AMS, so any broken samples were glued back together using PELCO® High Performance Ceramic Adhesive. This adhesive has been tested for its non-magnetic properties, making it suitable for paleomagnetic work.

4.2.2 Anisotropy of magnetic susceptibility

The anisotropy of magnetic susceptibility (AMS) was tested using an AGICO MFK1-FA Multifunction Kappabridge with an automatic rotator.

The software used for measurements was Safyr6 – Kappabridge Control Software (version 6.1.12) by AGICO, Inc.
The data is displayed using Anisoft42 – Anisotropy Data Browser by AGICO, Inc.

4.3 Remanence measurements, demagnetization, and component identification

The natural remanence of the rock was measured using an AGICO JR-6A – Dual Speed Spinner Magnetometer with the software REMA6W – JR-6A Instrument Control v. 6.1.3 by AGICO, Inc.

For the rocks that were partially demagnetized using thermal demagnetization, the samples were heated using a Magnetic Measurements Thermal Demagnetiser MMTDSC.

The Alternating Field demagnetization procedure was done with an AGICO LD5-A AF Demagnetizer using the tumbling specimen option.

4.3.1 Demagnetization procedure

The temperature steps used, and the strength of the AF steps varied slightly between some samples depending on the demagnetization up to that point, but most used the same steps as was used for the pilot samples (Table 1).

Each sample was measured for NRM, before undergoing one step of the demagnetization procedure. The remanence is then re-measured and the procedure repeats.

The intensity of the remaining remanence will gradually drop as more and more of the remanent magnetism is removed. Once the remaining intensity drops below 10% of the starting strength, the components seen can start to act erratically, no longer holding any old remanence and instead acquiring a new direction during demagnetization. The demagnetization of that sample is then stopped at that point. The consequence of this is that for some samples the last component seen never reaches a stable end point during demagnetization, so some results had to be disregarded during the analysis.

Step #	Thermal °C	AF mT		Step #	Thermal °C	AF mT
NRM	-	-				
1	100	2		**15**	585	50
2	175	4		**16**	595	60
3	250	6		**17**	600	70
4	300	8		**18**	605	80
5	350	10		**19**	610	90
6	400	12		**20**	615	100
7	450	15		**21**	620	110
8	500	18		**22**	630	120
9	520	21		**23**	640	130
10	535	24		**24**	650	140
11	545	27		**25**	660	150
12	555	30		**26**	670	-
13	565	35		**27**	680	-
14	575	40		**28**	690	-

Table 1: The demagnetization steps used

4.3.2 Possible difficulties using Alternating Field demagnetization

After the pilot sample was concluded, a problem with the Alternating Field demagnetization process was identified. Over time, some of the specimens developed some erratic behavior, with the magnetic direction often drifting to the right, and in some cases moving towards and circling around the vertical axis when seen in specimen-specific coordinates (Fig. 19). To counteract this the process was changed for the remaining specimens. During the pilot, the specimens were demagnetized using

the tumbling specimen option of the AGICO LD5-A AF Demagnetizer. The countermeasures were to utilize the tri-axial demagnetization option instead of tumbling, as well as alternating the orientation of the specimen in the holder at each step of the demagnetization process.

This was accompanied by a demagnetization of the coil twice a day by running the machine at 200 mT to remove any possible trapped fields affecting the specimens during demagnetization.

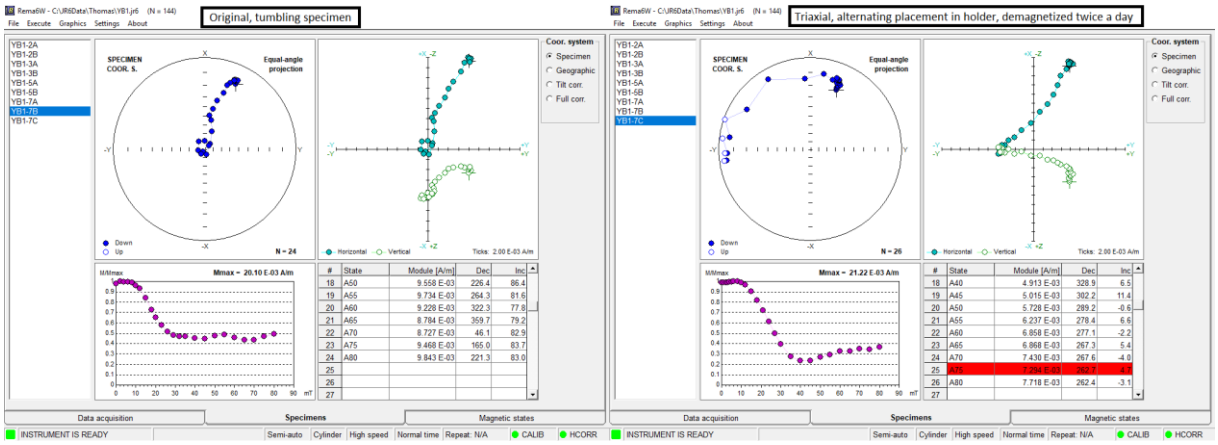

Figure 4: YB1-7B (Left) and YB1-7C (Right). The YB1-7B sample is from the pilot, while YB1-7C was demagnetized using the countermeasures. Some improvements can be seen, but there is still some unusual behavior.

4.3.3 Identifying components

Once the demagnetization procedure was concluded the data acquired was displayed using the Remasoft 3.0 Paleomagnetic data browser and analyzer software by AGICO Inc.

Using this software, the different components can be isolated and identified by looking at how the direction the NRM moves as the specimen gradually demagnetizes. In the example in figure 20, the horizontal direction (blue) starts moving eastwards, before turning upwards as the specimen demagnetizes, revealing that at least two components were present in this rock. These are the results that determined whether a rock responded better to thermal demagnetization or AF, some specimens taken from the same sample core would look radically different depending on the method used.

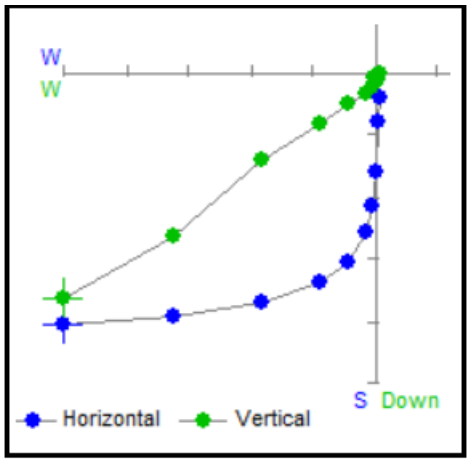

Figure 20: Zijderveld diagram used to project a 3D plot onto two axes. Used for identifying components.

5. Results

The results are presented with the Devonian volcanic rocks from Hoy and Deerness first, followed by the Permo-Carboniferous dikes (Fig. 21). For each locality the locality itself will be presented, then the measurements of the AMS and paleomagnetism will follow.

All declination and inclination angles are given in geographic coordinates.

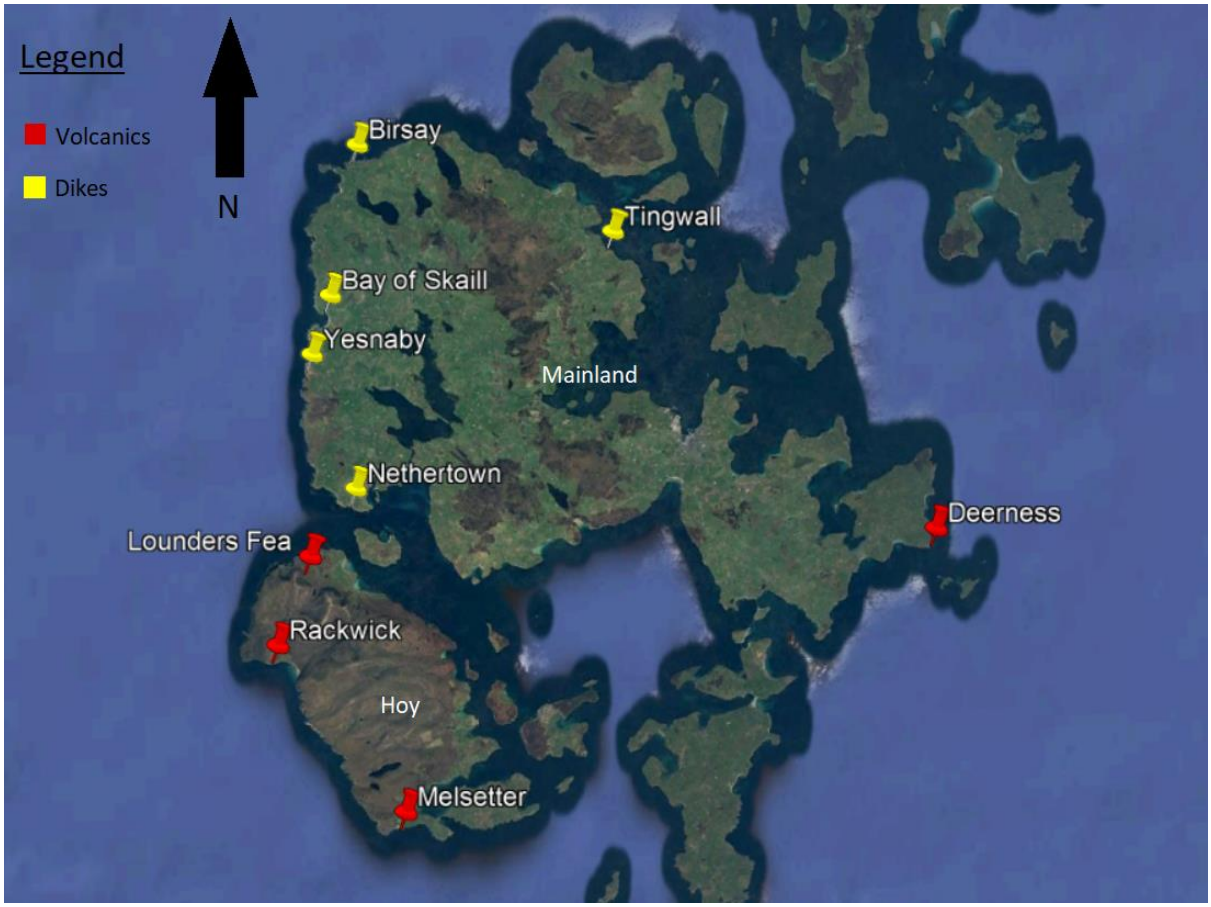

Figure 21: Map of sample locations on the islands of Hoy and Mainland. Red pins for the Devonian volcanics and yellow for the Carboniferous dikes.

5.1 Devonian volcanic and sedimentary rocks

5.1.1 Rackwick

Coordinates:	58.869N 3.399W	Locality 1
	58.869N 3.400W	Locality 2 - 5

Rackwick sits on the western side of Hoy and is a wide bay with magnificent red sandstones on the southern side, and columnar jointed volcanic basalts over red ashy tuffs on the northern side. The samples were collected from the basalts on the northern shore as well as from the volcanic ashes beneath (Fig. 22). The volcanic rocks transition over into sandstones westward along the coast. The columnar basalts start about 20 meters up a steep hillside, so sampling proved adventurous. The volcanic tuffs are unsorted and alternate with sandstones upwards towards the basalts above. The area is faulted at both the east and west ends with a syncline in the basalts in the middle, possibly made as a result of collapse between the east and west faults. The bedding planes in the ashy tuffs provided a means to estimate the paleohorizontal (Fig. 23), which shows a shallow dip to the northwest with a mean dip-dir/dip direction of 312/13.

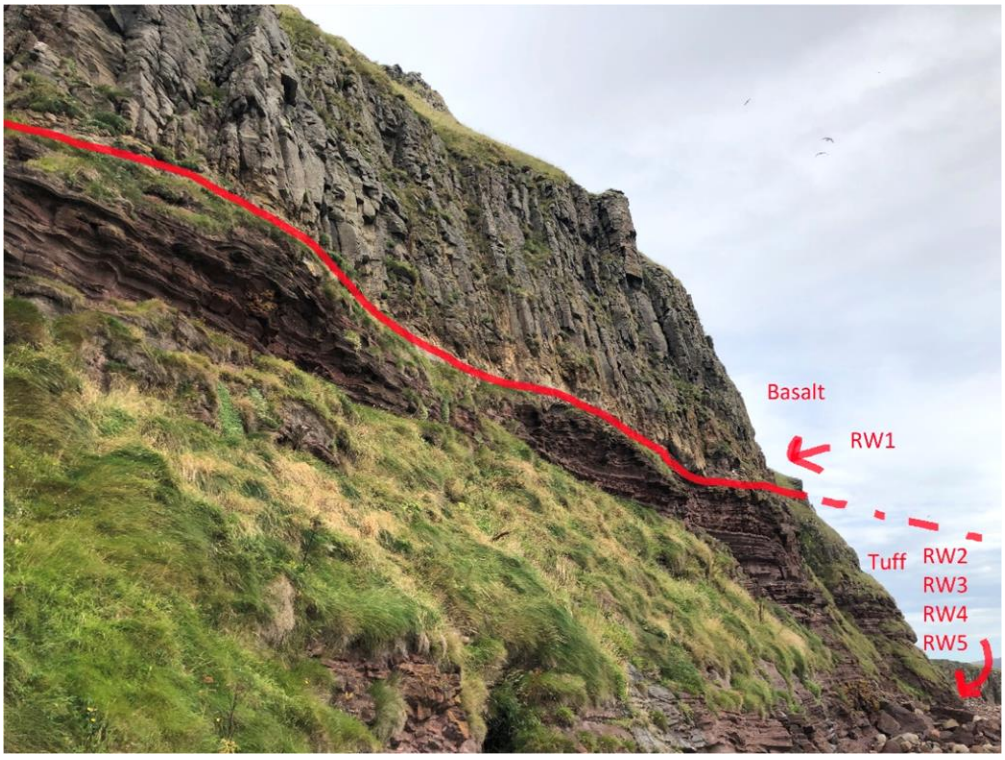

Figure 22: The columnar basalts sitting on top of volcanic sediments and sandstones, Too of the Head, Rackwick

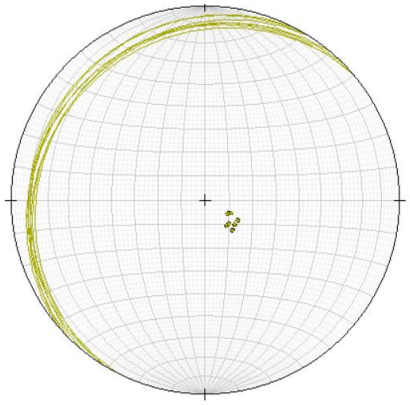

Figure 23: Stereo plot of the Rackwick bedding measurements

From Rackwick, one site (RW1) of eight samples of basalt was collected from the bottom of the 70m or so tall columnar basaltic cliff (Fig. 22, 24). Four additional sites were also gathered from the volcanic tuffs that lie beneath the basalt (RW2-5; 25 samples in total). AMS and demagnetization experiments were conducted on both the basalts and tuffs, as described below.

Figure 24: Sampling sites from Rackwick.

AMS results

AMS results from the basalt samples (Fig. 25, left) show a clear correspondence to the measured structural plane (Fig. 23), in that the K3 (Kmin) axis is approximately parallel to the measured bedding plane, i.e. reflecting a slight tilt towards the west – north-west. By contrast, the volcanic tuffs (Fig. 25, right) are much more scattered and do not provide any additional help in constraining the orientation of the paleohorizontal plane; however, the well-resolved structural measurements and the similar results from the AMS data from the basalts suggests that our paleo-horizonal estimates are well-determined and reliable.

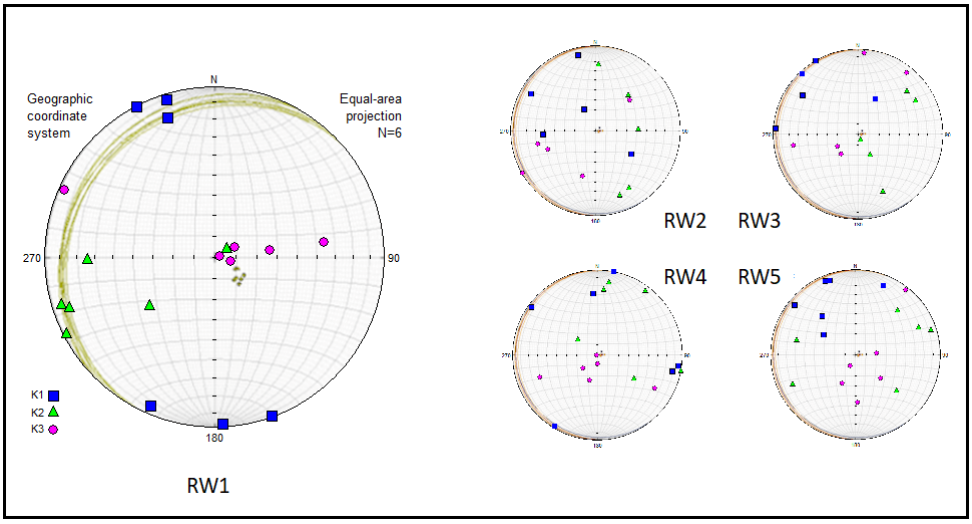

Figure 5: AMS results from the five Rackwick sets. Left: *Volcanic rocks, showing a slight tilt towards the northwest.* Right: *Volcanic tuffs, no discernable patterns.*

Demagnetization

Basalt (RW1)

All eight specimens were demagnetized thermally following the pilot project. The two specimens demagnetized using AF during the pilot show similar behavior as the thermal results, but due to the possible AF bias thermal was chosen for the entire locality. The specimens all behave in the same manner during demagnetization: an interval of remanence stability is followed by a steepening decay after ~300°C to < 10% intensity reached at 535°C – 545°C (Fig. 26). This decay is normally associated with two distinct directional components: first a weak, low stability component that falls to the northwest of the vertical is removed at low temperatures, revealing a high-temperature component that is directed shallowly to the south. These two components are well clustered and

separated, so I will call them component A (Blue in figure 27, left) for the lower stability component and component B (Red in figure 27, right) for the higher stability component.

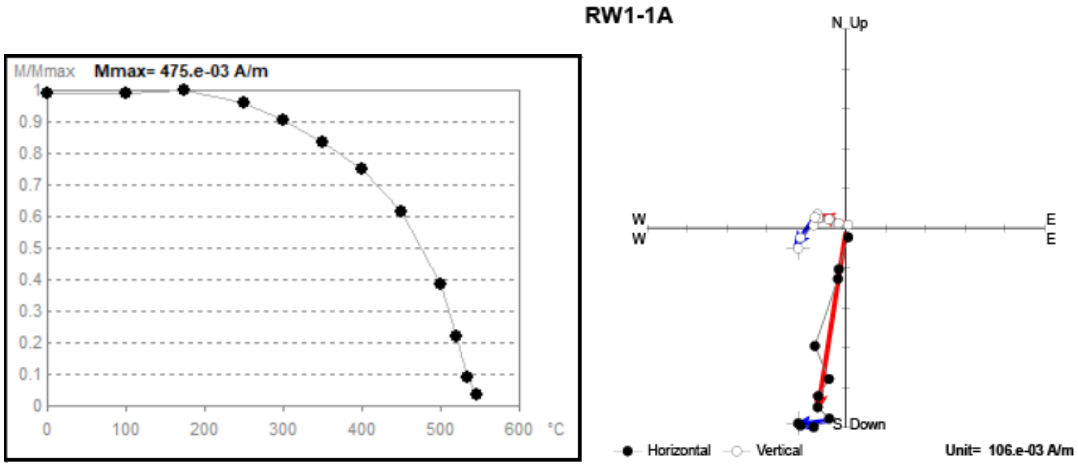

Figure 6: Typical demagnetization behavior and Zijderveld diagram of the RW1 samples

At the site-level, the low stability component (Fig. 27, left) has a mean direction of: D (declination) = 307.4°, I (inclination) = 68.3°, *k* = 14.19, A_{95} = 15.2°. The high stability component (Fig. 27, right) has a mean direction of: D = 187.7°, I = -4.5°, *k* = 287.33, A_{95} = 3.3°.

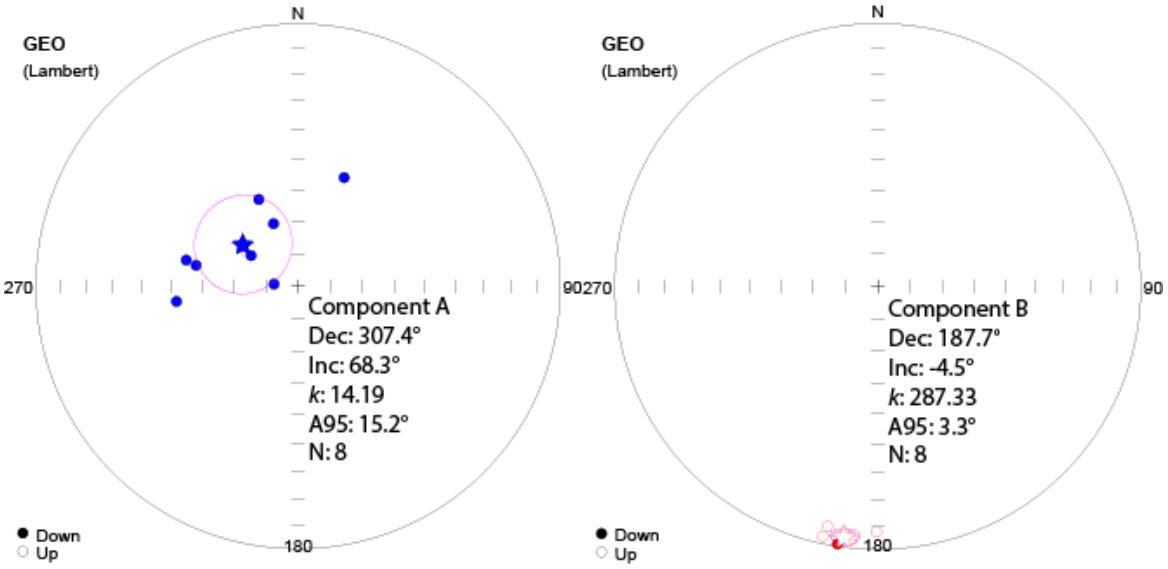

Figure 27: ***Left:*** *Low stability components.* ***Right:*** *High stability components found at the RW1 locality, with mean and* A_{95} *confidence*

The volcanic tuffs, RW2 - 5

In general, the volcanic tuffs demagnetized poorly and were associated with erratic directional changes and abrupt remanence changes. Sites RW3 and RW5 were associated with especially poor behavior and were not demagnetized beyond the pilot samples, and will not be discussed further. The other two sites (RW2 and RW4) also showed mostly erratic behavior, but a few samples exhibited behavior somewhat similar to that seen in RW1. In Fig. 28 we show three examples of such samples.

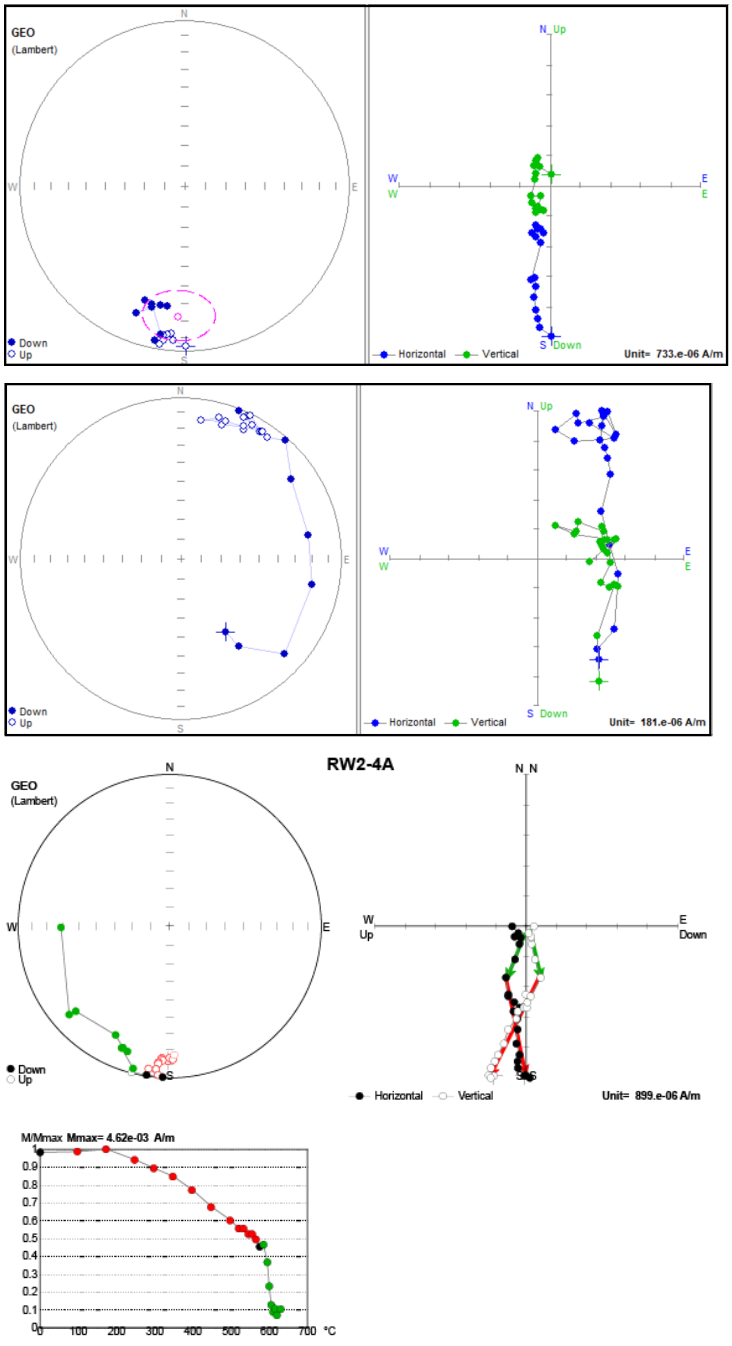

Figure 28: Some examples of interpretable samples from sites RW2 and RW4.

Sample RW2-1A (Fig. 28, middle row) is especially interesting because the direction the NRM moves to, very shallow and towards the north-east, is approximately antipodal to the other high stability directions observed in these samples (Fig. 28 upper and lower rows), as well as the B component seen in RW1. Note that the intensity of this sample is still at over 70% remaining strength at 620°C, so this component might be an antipodal direction held in hematite. Indeed, sample RW2-4A (Fig. 28, lower row) may exhibit the same behavior: the NRM begins pointing towards a shallow, upwards facing southern direction, then starts to travel towards the north-west after the temperature passes the curie temperature of magnetite. Notably, this same behavior was observed in previous studies from the Hoy volcanics (Storetvedt and Petersen, 1971).

In Fig. 29 we show the sample-level results from those samples which yielded interpretable behavior from sites RW-2 and RW-4 (again because most samples exhibited erratic demagnetization behavior). Higher temperature directions could be recognized in some samples (as shown in Fig. 28), but did not yield well-defined linear components (not usually reaching a stable end-point).

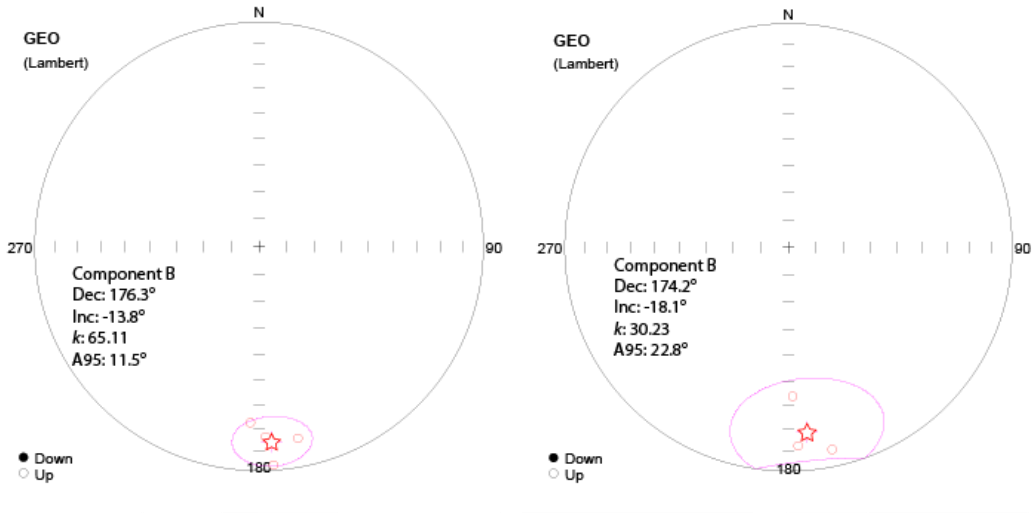

Figure 29: Three samples from the RW2 tuffs (Left) and RW4 (Right) had discernible high stability components.

5.1.2 Lounders Fea

Coordinates:	58.917N 3.366W	Locality 1
	58.919N 3.369W	Locality 2

Located on the northern side of Hoy, the Lounders Fea locality is a volcanic bench situated below hills of sandstone. The two sample localities are separated by about 200 meters with a possible fault running between them down from the hills above (Fig. 30). No discernible height difference can be observed between the two localities. Structural measurements were taken of both the volcanics and on select exposures of the sandstones in the hills above and reveal a shallow dip to the west (average dip-direction/dip of 261/12; Fig. 31). The volcanics are weathered and heavily covered in lichen showing its age. The exposures are only about 40 meters wide, and there are no more exposures further north towards the Bay of the Tongue.

Figure 30: Overview of the Lounders Fea area. LF1 to the left of the picture and LF2 to the right.

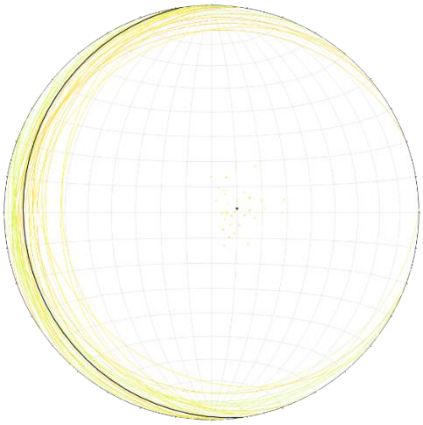

Figure 31: Stereo plot of the Rackwick bedding measurements

The Lounders Fea locality is divided in two sites with nine samples collected at LF1 and eight samples collected from LF2 (Figs. 30, 32).

Figure 32: Sampling sites from Lounders Fea

AMS

Both the localities at Lounders Fea show similar groupings with a slight tilt towards the southwest. The measurements at LF2 is a bit more dispersed than at LF1 but show a similar trend (Fig. 33).

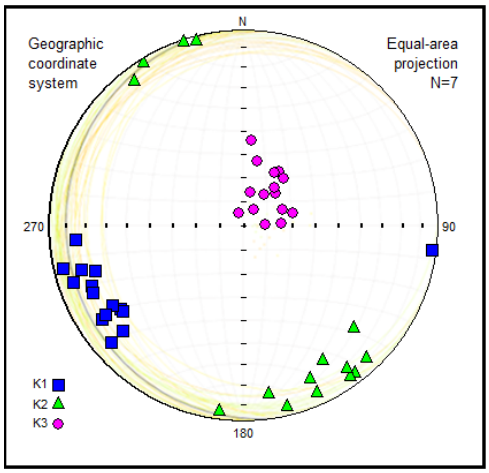

Figure 33: AMS results from all samples from LF1 and LF2.

Demagnetization

LF1

From the pilot examination, both AF and thermal seemed to give similar results, with thermal demagnetization results looking a little cleaner than the AF results. All the LF1 samples show either a gradual demagnetization down to 535°C – 555°C or a progressive drop with an increased descent reached at 450°C – 500°C (Fig. 34). Directionally, the LF1 samples exhibit at least two, but often three components. In many samples, an initial, weak component that is directed moderately to steeply downward is removed at low temperatures (component A), revealing a higher temperature component that is generally directed shallowly to the south (component B; Fig. 34, top). However, at even higher temperatures, the direction often tracks toward the east, with a slightly steeper inclination (Fig. 34, bottom). Unfortunately, in many cases (one exception shown in Fig. 34, bottom), this highest temperature component cannot be isolated, and instead is only recognized from great-circle trajectories (Fig. 35). Unfortunately, these great circles are near parallel (Fig. 35), giving no real intersection to look for, though the Remasoft software suggests a great circle intersection at 179.5°/5.5°, close to the B component seen in the other sites.

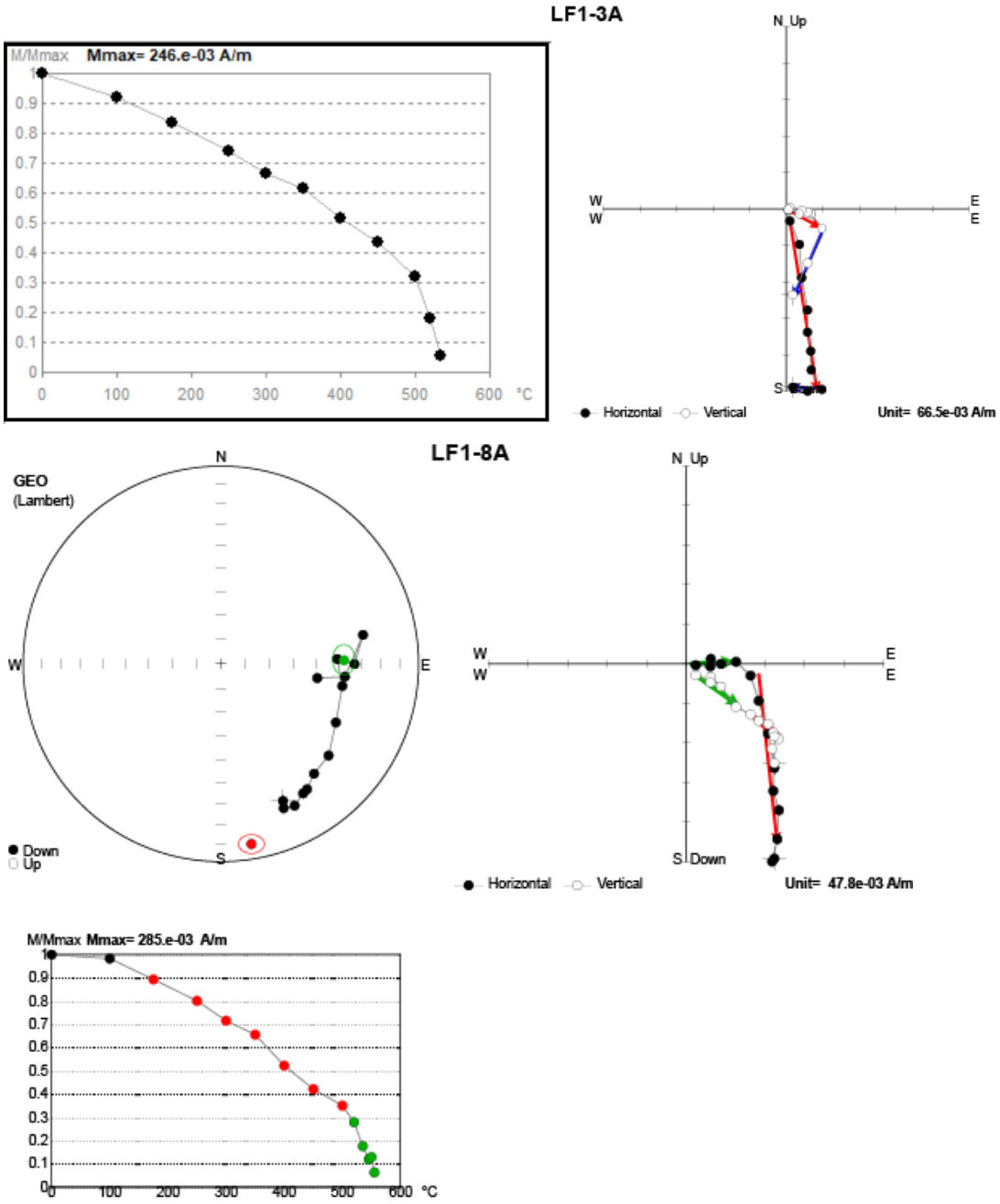

Figure 34: Typical demagnetization behavior and Zijderveld diagram for LF1 samples.

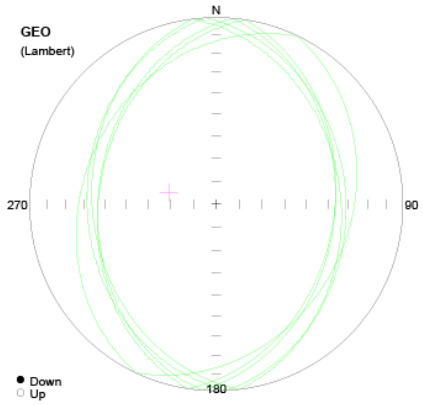

Figure 35: Great circle fits between component B and the highest temperature directions (un-isolated) in samples from LF1.

In Fig. 36 we show the site-level results from LF1. The previously defined A (Blue) and B (Red) components are very similar to those isolated in site RW1, but the third (highest-temperature) component C, which falls to the east at around 30°-35°, was not observed in the Rackwick samples. Note that the distribution of 'intermediate' (component B) directions is streaked and follows the same trajectory as the great circles. This clearly indicates that there is some overlap between the B and C components (i.e. they were not completely isolated). We have excluded the most obvious of these (x's in Fig. 36, middle) from the computation of the mean.

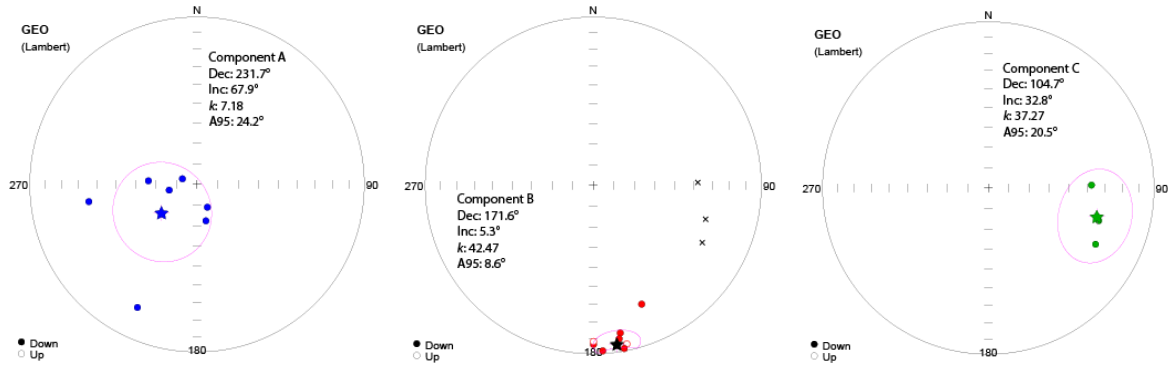

*Figure 36: **Left**: Low stability components. **Middle**: Intermediate and high stability components from LF1, a subset of which forms the basis of the ChRM selected from this site. **Right**: highest-temperature component.*

LF2

The results from the second Lounders Fea locality resembles the first. Most of the specimens show a similar demagnetization behavior, with a slow start and an increased drop at the end down to 535°C-560°C (Fig. 37). As in LF1, the samples from LF2 also exhibit 2-3 component behavior.

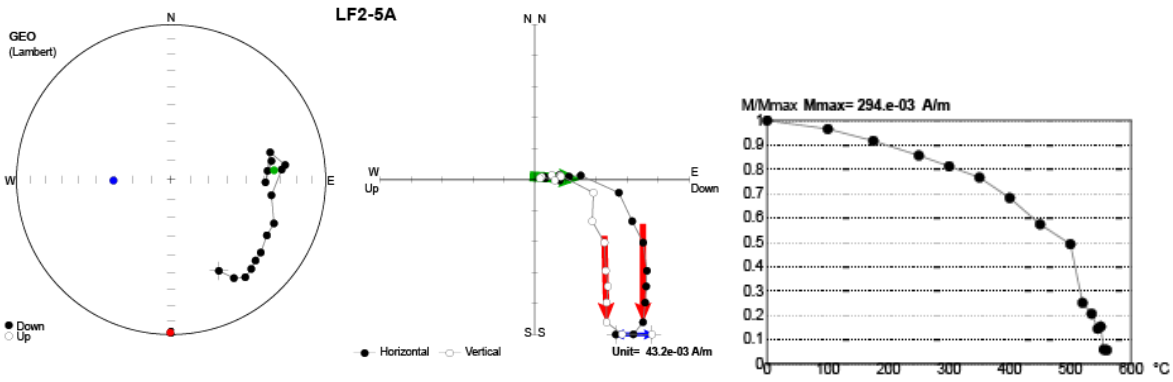

Figure 37: Typical demagnetization behavior of LF2 samples, LF2-5A seen here.

After removal of a weak, low stability component, all specimens show either an intermediate or high stability component falling at a shallow southern angle (Figure 37, red), resembling the B component previously defined. The LF2 specimens 2A, 3A, 4A and 5A all have higher stability components that further track a great circle northward from the intermediate component toward an east-dipping component resembling component C defined in LF1 (Fig. 37). LF2-6B and LF2-7A shows a similar movement, but never make it so far north to fall within the same area.

Fig. 38 shows the site-level results from LF2 by component. Again, note the similarity between these results and those of LF1, as well as the similarity between components A and B and those found at Rackwick (especially site RW1). Note also, as in site LF1, that there is some overlapping of the B and C components, and that the mean for component B was made after the exclusion of some directions that are clearly not fully cleaned of component C (marked as x's).

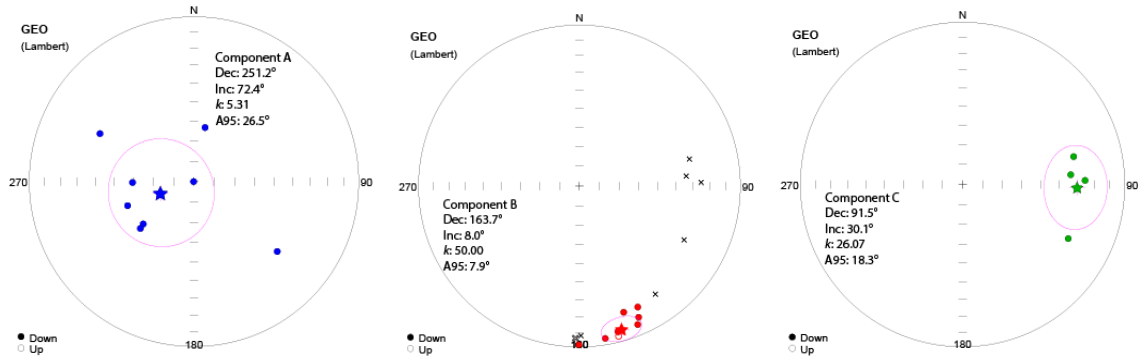

*Figure 38: **Left**: Low stability components. **Middle**: Intermediate and high stability components from LF2, a subset of which forms the basis of the ChRM selected from this site. The de-selected components towards the south are intermediate components were the high stability component is closer to the mean direction. **Right**: highest-temperature component.*

5.1.3 Deerness

Coordinates: 58.920N 2.713W Locality 1 - 4
58.920N 2.712W Locality 5

On the far eastern side of Mainland, the biggest of the Orkney Islands we find another outcrop of the volcanics. Flagstones both below and on top bounds the volcanic rocks here, though the presence of various faults throughout the area makes correlating the top of the different volcanics to the bottom difficult, various samples and measurements were taken to alleviate this. There are three main exposures of lavas (Fig. 39), with the eastern one resembling pillow basalts (DN5). The shape of these however are most likely caused by weathering as they are unusually large for pillow basalts (2-3m in diameter) and contain none of the expected sediments between the pillows. There is a sandstone contact above the second lava flow, which helps define the paleo-horizontal for this area (Fig. 40). The third lava flow is situated above another sandstone contact. This sandstone contact provides an opportunity to conduct a baked contact test, and we therefore collected samples from this unit (site DN2).

Figure 39: Overview of the area at Deerness, samples were collected from dark colored basalts (front), flagstones underneath and from the volcanic outcrops along the beach.

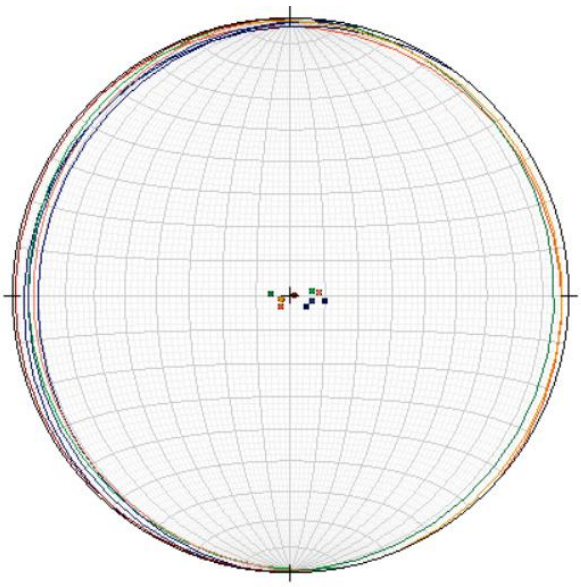

The structural measurements from the entirety of Deerness, for the various sets of samples, the list of measurements was filtered to the relevant set for those samples.

Averages used for tilt correction:

DN1: 200/4 Dipdir/dip

DN2: 231/4

DN3: -

DN4: 194/9

DN5: 263/12

Figure 40: Stereo plot of the Deerness bedding measurements.

From this area we collected five sites: three sites (DN1, DN4 and DN5) were collected from the basaltic flows, and two sites (DN2 and DN3) were collected from the closely associated sedimentary rocks (Fig. 41, 42). Sites DN2 and DN3 were specifically sampled for the purpose of executing a baked contact test, where DN2 was sampled from a baked sediment (immediately below flow DN1), whereas the sediments from DN3 are slightly farther away (stratigraphically) and unbaked. Samples from each site were subjected to both AMS and demagnetization experiments.

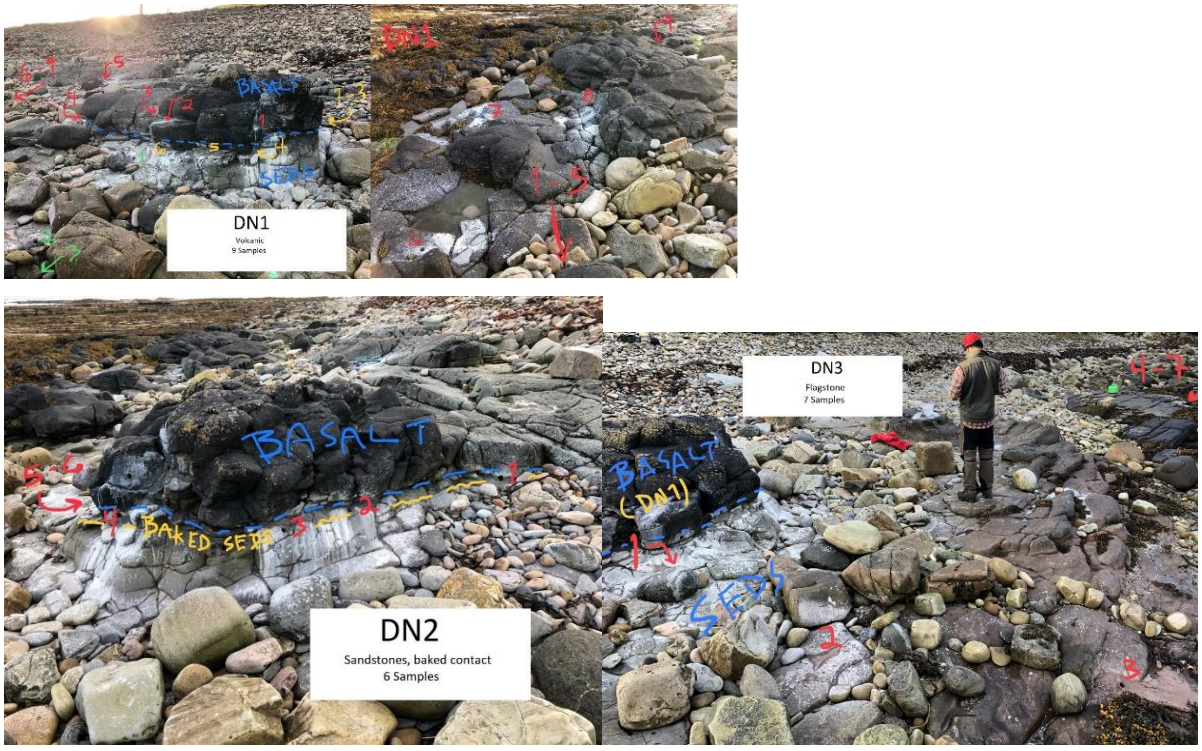

Figure 41: Deerness sampling sites.

Figure 42: Deerness sampling sites

AMS

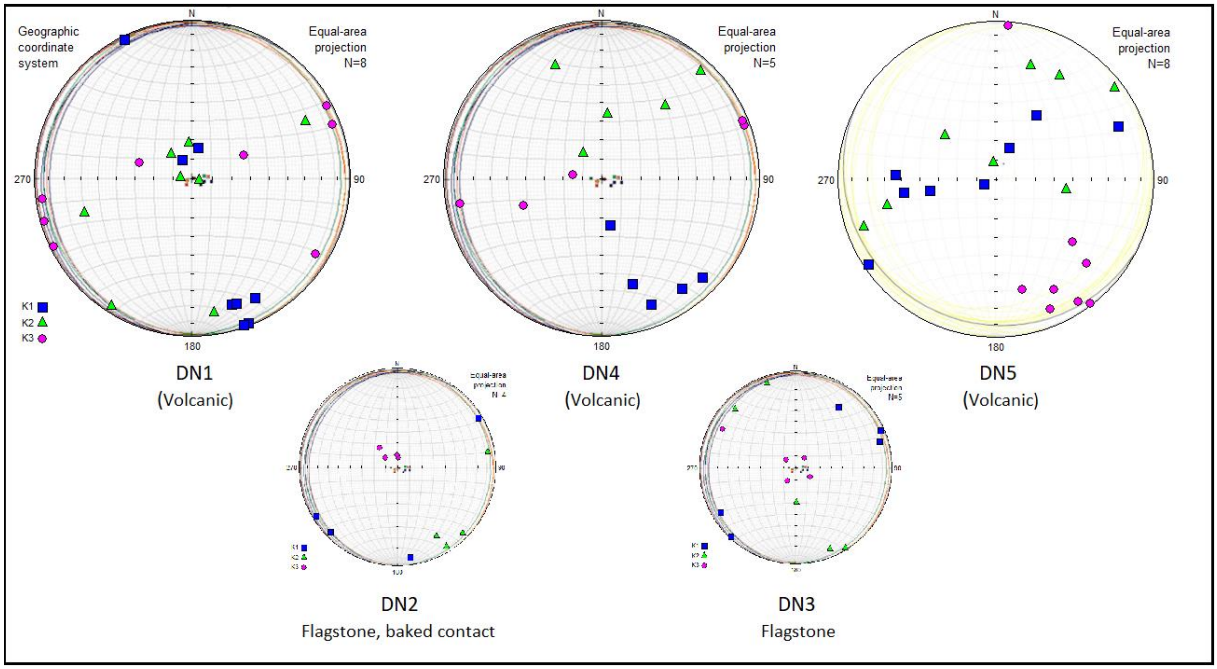

Figure 43: AMS diagrams for the five Deerness collections. The volcanics shows some similarities.

DN1 shows a possible tilting towards the south – southeast, with a shallow angle (Fig. 43). This matches up with the structural measurements taken on site. The DN4 AMS resembles DN1, showing a slight possible tilt to the southeast. AMS from DN5 is similar to DN4, having more specimens

examined to give a clearer image. Possible tilt to the southeast. DN2 Few specimens were measured during AMS, but the ones examined show a possible small tilt to the southeast. The structural measurements were chosen as the tilt correction over the AMS data. The AMS data for DN3 resembles DN1 and DN2 which lies right above in the stratigraphic column.

Demagnetization

DN1 (Basalt)

DN1 consists of eight samples. DN1 is one of the localities where the AF stacking is most apparent from the pilot sample results, so thermal demagnetization was chosen for the set. The specimens generally demagnetize evenly down to 500°C, followed by a rapid drop down to 550°C-560°C, although 25-50% of the remanence loss already occurs before 200°C (Fig. 44). Two components can be recognized in the demagnetization trajectories. The low stability component shows no real pattern, except that it is mostly steep (Fig. 44, blue component), whereas the higher-temperature component is mostly associated with a shallowly-down and south direction (Fig. 44, red component, upper panel). In two samples, however, this high-stability component also appears to be associated with a very steep direction, but is nevertheless distinct from the lower stability component (Fig. 44, lower)

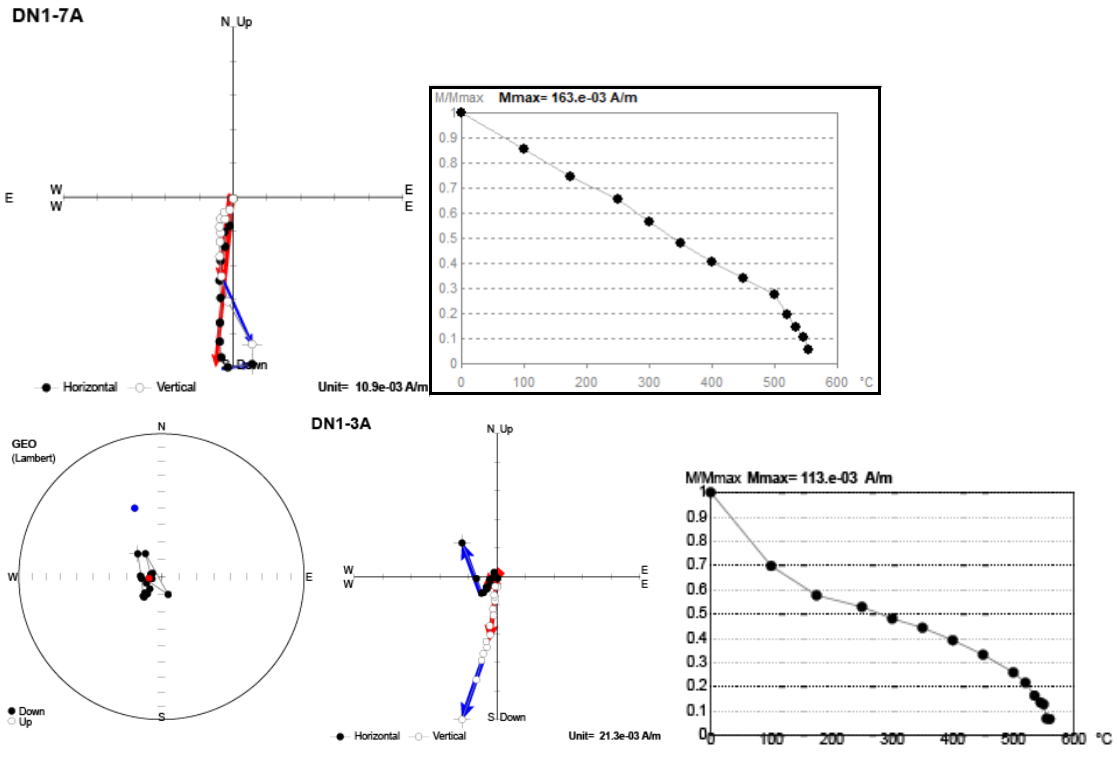

Figure 44: Typical demagnetization behavior and Zijderveld diagram for DN1.

Fig. 45 shows the site-level results. Interestingly, the individual directions of component A cluster very well to the southwest of the vertical when viewed in specimen specific coordinates (Fig. 45, right). This could indicate that this low stability component was imposed during the drilling process. The high stability component shows in six of the specimens a decent clustering to the south, at an angle between 20°-40° (Figure 45, middle), so it is not as shallow as the previously defined B component found in the other volcanics. Among the component B picks, we observe two directions that appear to be directionally dissimilar from the others: DN1-2A and DN1-3A both display high stability components that are almost vertical (x's in Fig. 45, middle). Behaviorally, these two components are identical to the other B component picks, but the direction suggests that they are likely overprints and so we exclude them from the mean calculation.

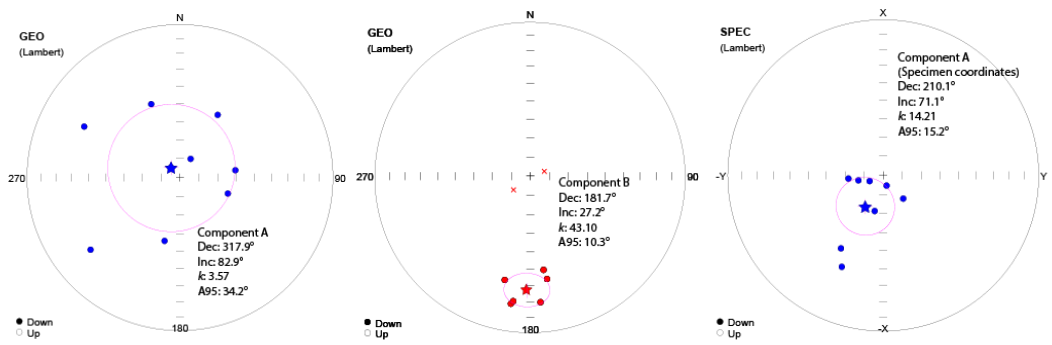

*Figure 45: **Left:** Low stability components. **Middle:** Diagram of the high stability components seen in DN1. The two x-ed out directions around the vertical are rejected from the mean calculations (DN1-2A and -3A**). Right**: low stability components seen in DN1 group up when viewed in specimen specific coordinates.*

DN2

DN2 is the flagstones sitting directly underneath the DN1 volcanics. These samples were collected with the intention of executing a baked contact test. Samples were taken from the contact zone right below the basalts of DN1.

The pilot examination of DN2 showed that thermal demagnetization behaved better than AF, but few specimens were in shape to be examined, so the sample size from this locality is low.
The specimens demagnetize not too differently from the DN1 volcanics. DN2-4A, 5A and 6A lose about 50% of their intensity by 250°C (Figure 46), and then lose very little before hitting 500°C from which the decline is rapid down to less than 10% strength at 550°C-560°C (Figure 47). DN2-3A differs

in that it loses almost 70% strength before 250°C and then hovering between 20-30% strength forever until the process was stopped at 545°C (Figure 47).

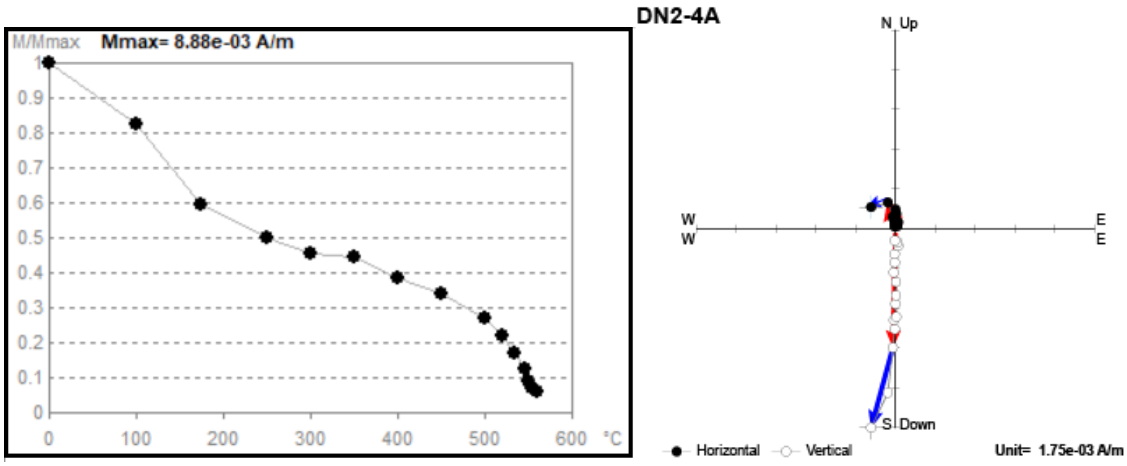

Figure 46: Typical demagnetization behavior and Zijderveld diagram for DN2.

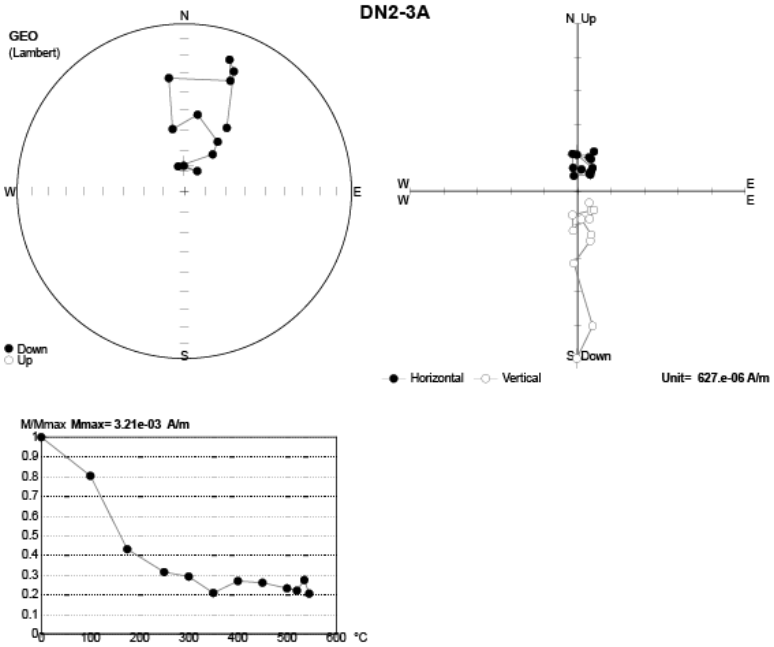

Figure 47: Demagnetization behavior of DN2-3A, the intensity drops rapidly before 250°C.

All specimens resemble the few samples with the vertical (possibly overprinted) component seen in the previous site (DN1). DN2-3A does wander northwards erratically once the intensity has stabilized at 250°C (Figure 47, top left). There are two components visible in DN2-4A, 5A and 6A, with a low stability falling scattered to the west of the vertical, with the high stability component being well clustered just north of the vertical.

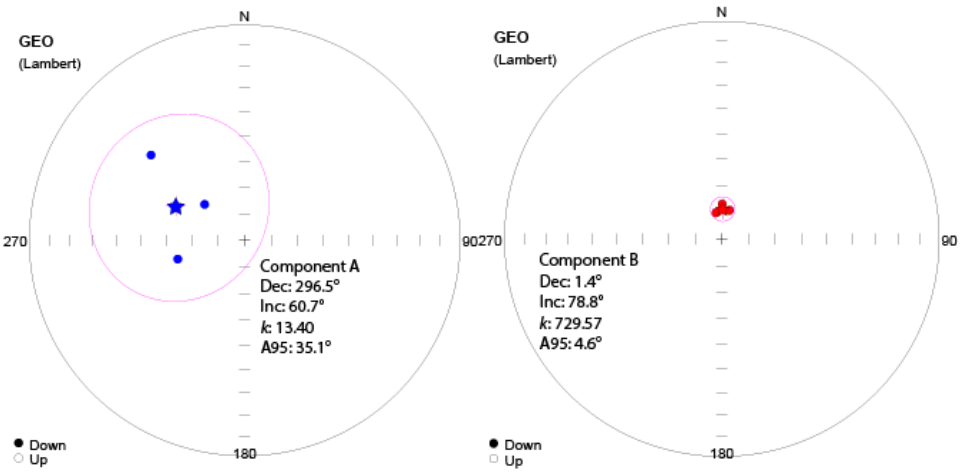

Figure 48: ***Left:*** *Low stability components.* ***Right:*** *high stability component pointing at an almost vertical direction, DN2*

Because the only high stability components seen in these samples are similar to the vertical component seen in the two dissimilar samples from DN1, the baked contact test fails (Fig. 48, right). The three samples in DN2 that exhibit this vertical direction are the samples DN2-4A, -5A and -6A, which were drilled almost directly underneath the two samples in DN1 with the same behavior (Figure 41, left image. Red samples numbered 2 and 3 are from DN1, yellow samples numbered 4 to 6 are from DN2).

DN3

The third set of samples from Deerness was taken from the flagstones beneath DN1 and DN2. The strategy behind this set of samples were to provide a reference for the unbaked sediments beneath the DN1 set of samples. The samples were taken along a stratigraphic profile going further away and downwards from the DN1 and DN2 set of samples (Figure 41, bottom right, red numbered samples). Sadly, the results from the demagnetization were of little use due to highly erratic behavior, consequently, no site mean was calculated for this site, but two samples showed some potential and will be covered below.

Two sets of pilot samples were examined from DN3, and while two specimens (DN3-3A and DN3-4A, figure 49) resembles some of the results found in the previous Deerness samples from DN1, the rest proved to be highly erratic and unusable (Fig. 49, 50) or overwritten giving a vertical component. The DN3-3A has a low stability component falling around the vertical, like the previously defined *A* component, while the high stability component here points at a shallow southern direction just like the *B* component from before (Figure 49, left). This is the only specimen however from DN3 where

this is apparent. DN3-4A on the other hand starts off just to the east of -3A and moves towards the south-east (Figure 49, right).

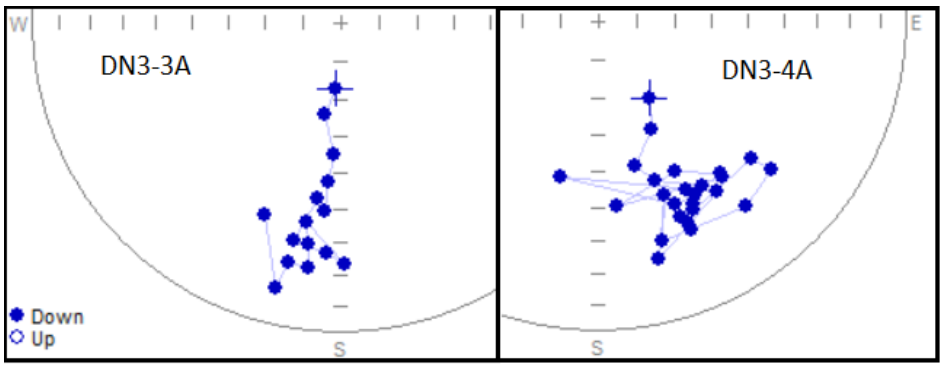

Figure 49: Erratic movement of the NRM, but possibly trending towards a southern component. Not possible to identify in Zijderveld.

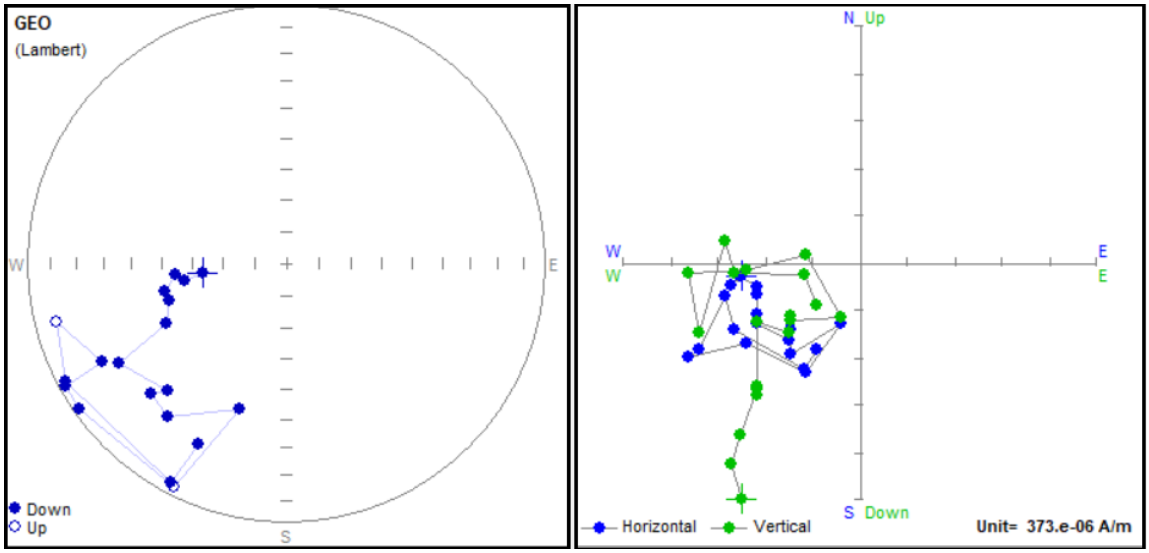

Figure 50: Erratic movement seen in DN3-7B and Zijderveld diagram.

DN4

The DN4 specimens consists of six samples taken from a basalt layer above DN1, on top of the beach. DN4 is mostly thermally demagnetized except for DN4-3A which is taken from the pilot sample and is demagnetized using alternating field demagnetization (Fig. 53).

Both thermal and AF demagnetization gave results, with thermal being chosen as the method for the rest of the specimens due to the fear of AF stacking.

DN4 continues the trend of the Deerness samples of demagnetizing similarly. The intensity drops quickly before 200°C, which is followed by a slow decrease down to 500°C from which the decay drops rapidly down to 550°C (Fig. 51, left). DN4-5A and 6A differs in that they drop 50-60% of their

intensity before 175°C and dips below 10% strength at 500°C and thereby never experiences the rapid decline after this point (Fig. 51, right).

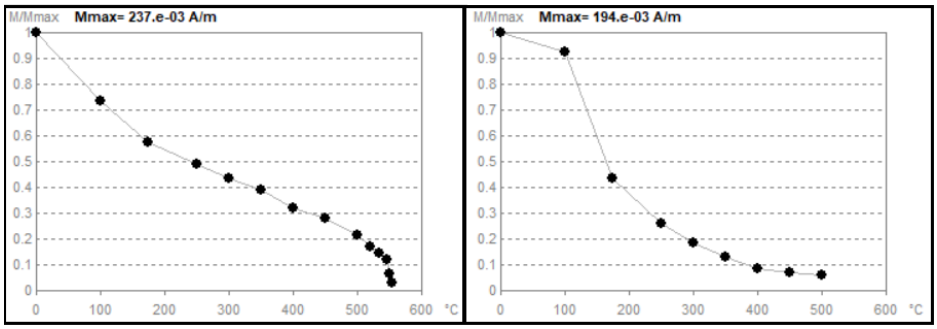

Figure 51: The two typical demagnetization behaviors seen in DN4 specimens

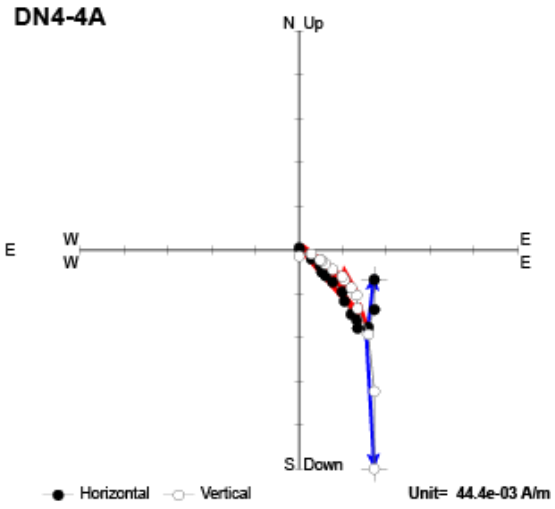

Figure 52: Demagnetization behavior for DN4-4A

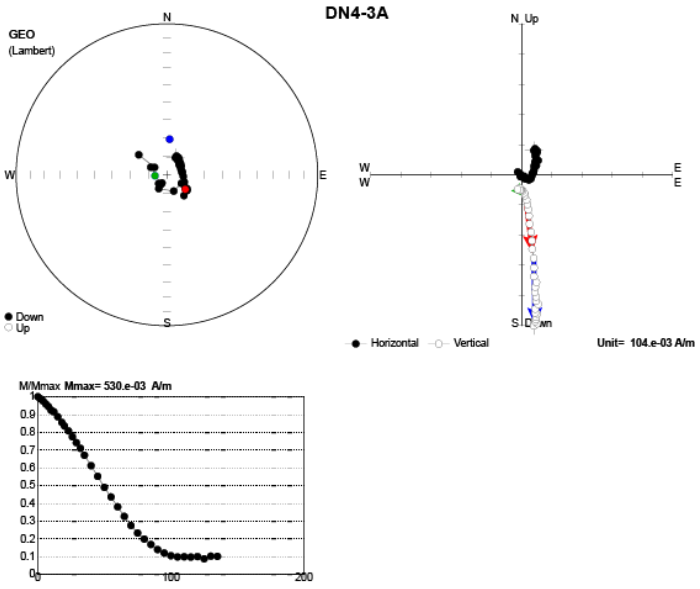

Figure 53: Demagnetization behavior of DN4-3A. The NRM moves towards the southeast (Red) from the initial position (Blue), before turning towards the west (Green).

All specimens have a low stability component falling at a steep angle just north of the vertical (Fig. 54, left), and a direction that travels towards the southeast (Fig. 54, right). This higher stability component is similar to the one seen in DN3-4A (Fig. 49, right). The distance the direction travels before full demagnetization varies, giving a scattered set of high stability components, all in the southeast. The three furthest south is the closest to the B component and has been grouped with these in the main table. Figure 53 shows a good example of the three samples where the high stability component does not make it far towards the southeast, this behavior is seen in all three samples (-1A, -2A and -3A; 3A is the one shown in the figure)

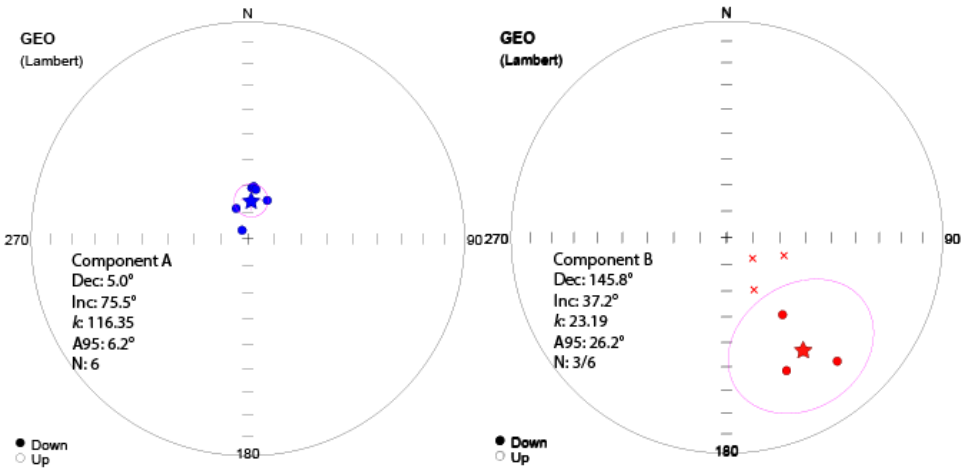

Figure 54: Low and high stability components seen in DN4.

DN5

The DN5 sample set consists of eight specimens who were all thermally demagnetized. DN5 is located just ~25m to the northeast of DN1-DN4.

Both thermal and AF demagnetization gave reasonable results, so thermal demagnetization was chosen for this locality just as the others from Deerness.

The DN5 specimens all demagnetize evenly down to around 535°C-555°C. These do not exhibit neither the rapid drop in intensity as seen in the other Deerness volcanics nor the big decline before 175°C-250°C (Fig. 55, 56).

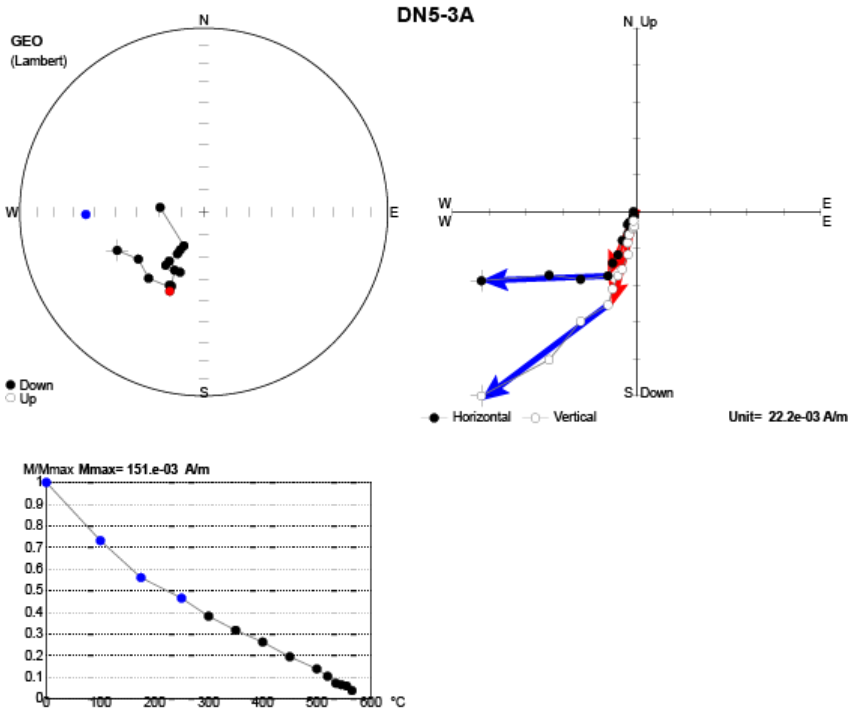

Figure 55: Typical demagnetization behavior and Zijderveld diagram for DN5 samples with two identifiable components.

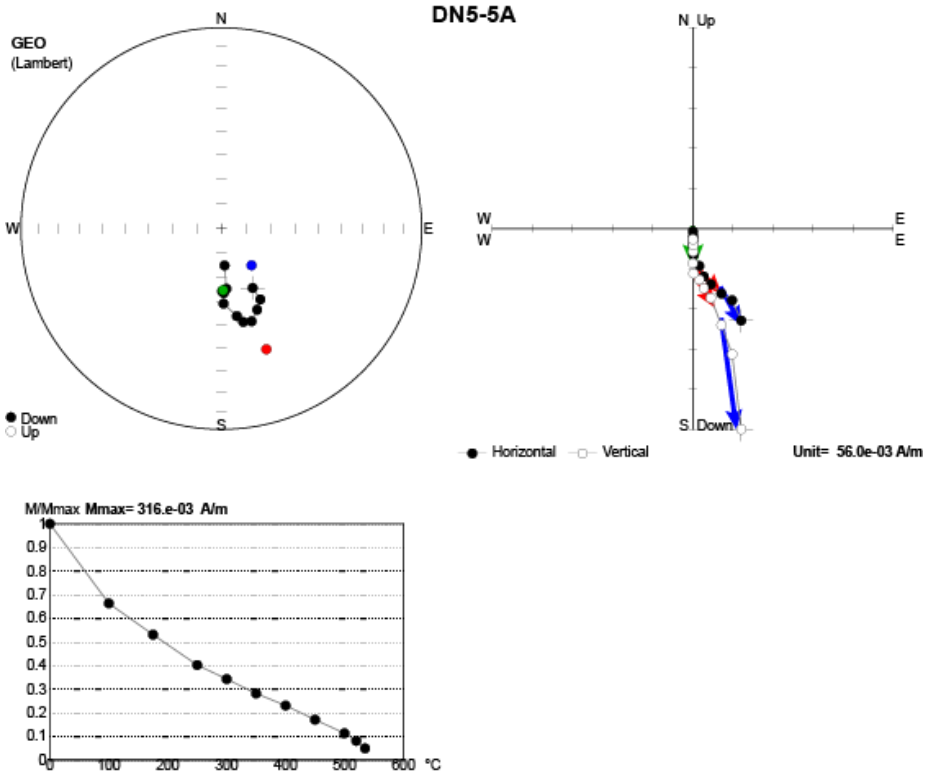

Figure 56: Demagnetization behavior of DN5 samples where the third component (green) is available for identification from the Zijderveld diagram.

All samples exhibit a low stability component which is removed by 250°C during the demagnetization process (Fig. 55, 56; bottom panels). This component is scattered but gives a nearby mean (Fig. 57, **a**). These group up when viewed in specimen coordinates and could be an artefact from the drilling

(Fig. 57, **b**). Above the low stability component are 1 to 2 additional components. In figure 55 and 56 we see two different samples where the first intermediate component is seen, but only in the case of DN5-5A (Fig. 56) were we able to define this component in the Zijderveld. The movement of the NRM in figure 55 suggests that a third component is present due to the continued movement northwards, but it was not possible to see it in the Zijderveld diagram.

As we can see in figure 56 and a little in figure 55, the higher stability component moves the NRM northwards towards the vertical. The result of this is seen in figure 57, **d)**, with the mean falling just north of the intermediate (Fig. 57, **c**).

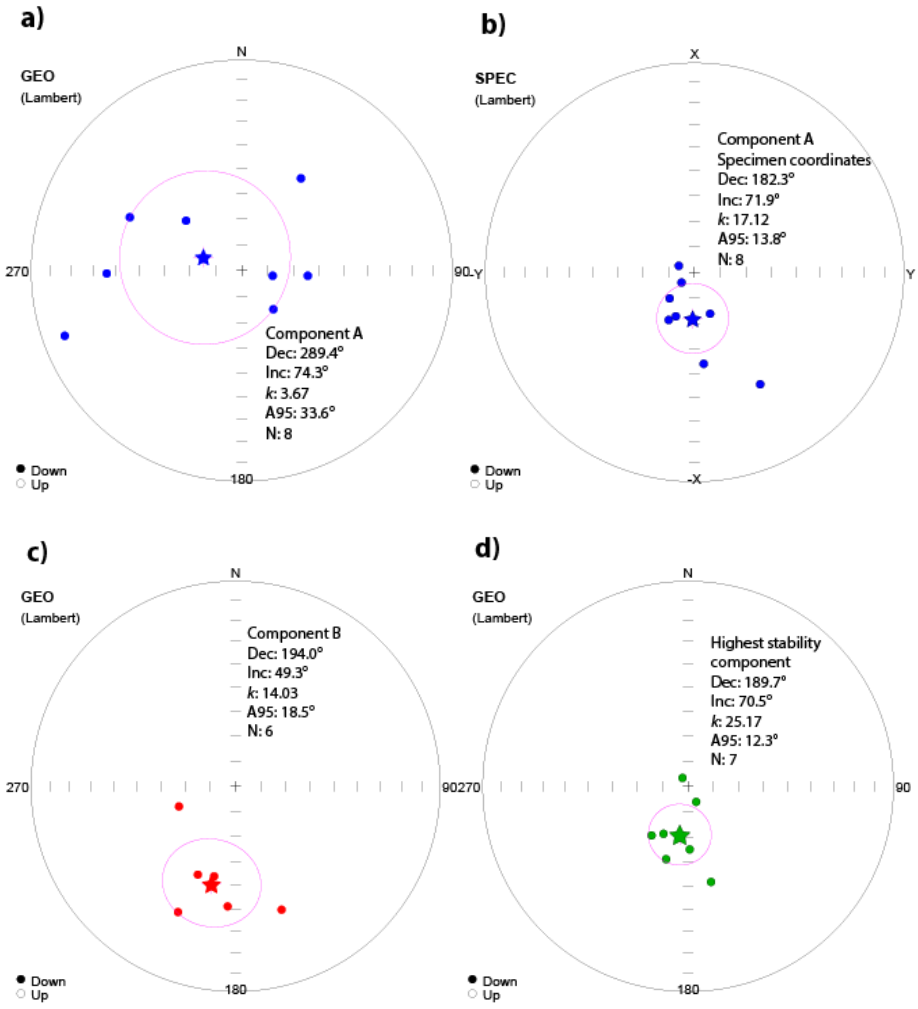

*Figure 57: **a):** Low stability components. **b):** low stability components when viewed in specimen coordinates. **c):** Intermediate stability components. **d):** High stability components*

The three Deerness volcanics (DN1, DN4 and DN5) has an intermediate or high stability component that points south, though at a steeper angle than at Rackwick and Lounders Fea. The Deerness

volcanics are ever so slightly younger than the Hoy volcanics which Rackwick and Lounders Fea are a part of, so a little difference in the vector component is not unusual. The Deerness samples have a greater degree of overprint than the Rackwick and Lounders Fea volcanics, but the high stability components from Deerness is still pointing close to the same general area previously defined as the B component.

5.1.4 Melsetter

Coordinates: 58.778N 3.273W

Situated on the south side of the island of Hoy, the Melsetter locality takes its name from the nearby Melsetter farm and House. This locality consists of a deep volcanic outcrop situated between sandstones on either side and above (Fig. 58). To the west the sandstone contact is lost to a wide beach with no outcrops, while to the east the contact is obscured due to a fault. The volcanic rocks are vascular and amygdaloidal and looks heavily altered. The volcanic topography is sub horizontal and shows no sure contact with the overlying sandstone. Moving south away from the hill the volcanics turns more undulating, most likely caused by surface erosion.

Figure 58: Overview of the Melsetter volcanics

Figure 59: Sampling sites at Melsetter.

The Melsetter samples consisted of eight samples (Fig. 59) with just one specimen from each core, four were demagnetized thermally and four with AF demagnetization.

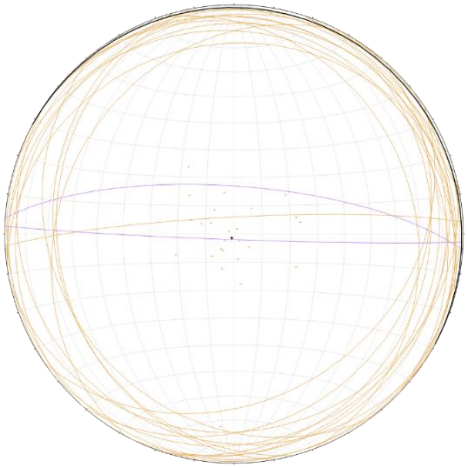

Figure 60: Stereo plot of the Melsetter bedding measurements.

The bedding measurements (Fig. 60) here is taken from the volcanics themselves, since no flagstones are in immediate contact with the volcanics. These have then been averaged using Fisher (1953) statistics like at the other locations.

Average used for tilt correction: 28/4 Dipdir/dip

AMS

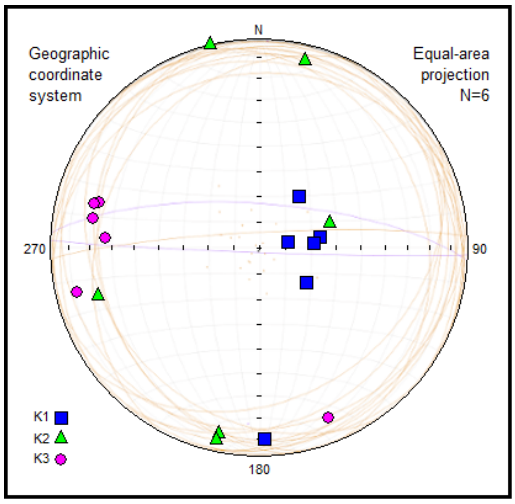

Figure 61: AMS results from Melsetter.

The Melsetter samples group decently with a slight tilt towards the west (Fig. 61).

Demagnetization

The Melsetter samples were subjected to two sets of pilot examinations, and due to the lack of specimens the results were four specimens demagnetized thermally and four using AF.
The demagnetization behavior varies quite a bit between the specimens, MS1-1A, 6A and 7A demagnetize evenly, with a few fluctuations down to a plateau reached at 500°C-535°C from which there is no real further drop (Fig. 62).

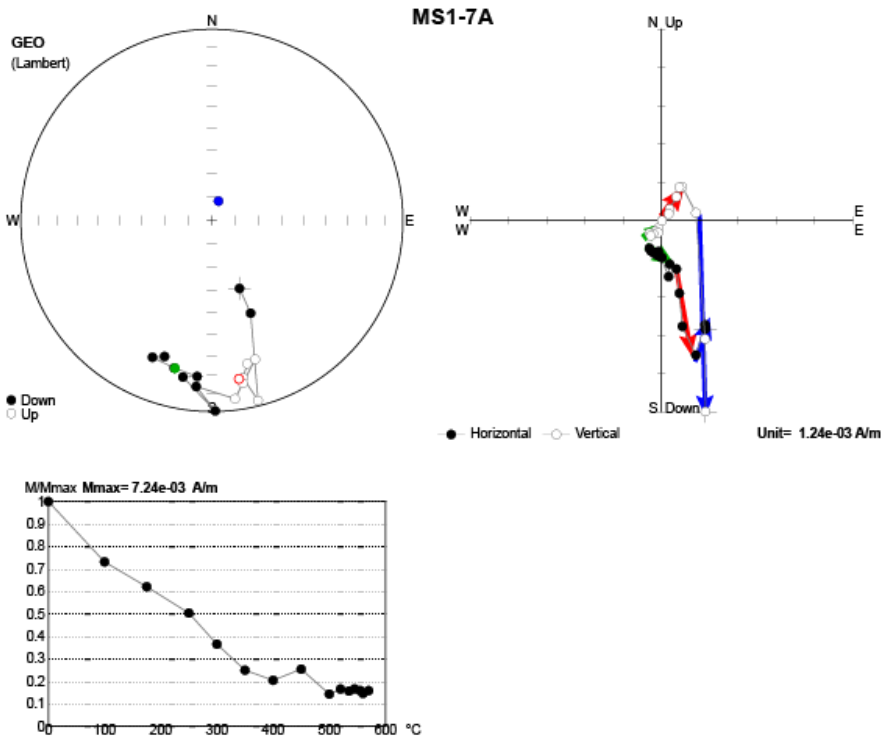

Figure 62: Demagnetization behavior for some of the Melsetter samples

MS1-3A, 4A and 8A are almost identical in the way they demagnetize, even with MS1-4A being demagnetized thermally and the two others using AF. All three specimens drop evenly down to 30mT or 300°C before they start to plateau (Fig. 63).

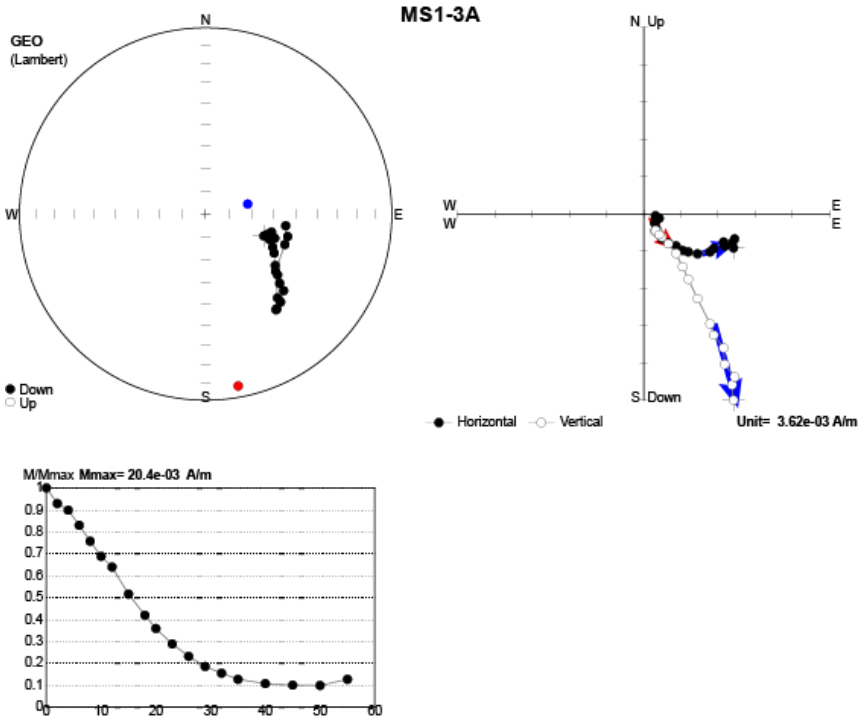

Figure 63: Demagnetization behavior for some Melsetter samples.

The last two specimens, MS1-2A and 5A do not fall in these categories. Both specimens were demagnetized using AF, and still had intensity left in the sample when the measurements were halted at 150mT (Fig. 64). MS1-2A starts with a quick 50% drop in intensity by 24mT, from which the intensity increases and reaches the NRM levels of intensity at 150mT. MS1-5A on the other hand loses almost 75% of its strength by 24mT. This is followed by a very slow decline to 10% intensity reached at 90mT, and from here, the intensity stays at 10% all the way to 150mT.

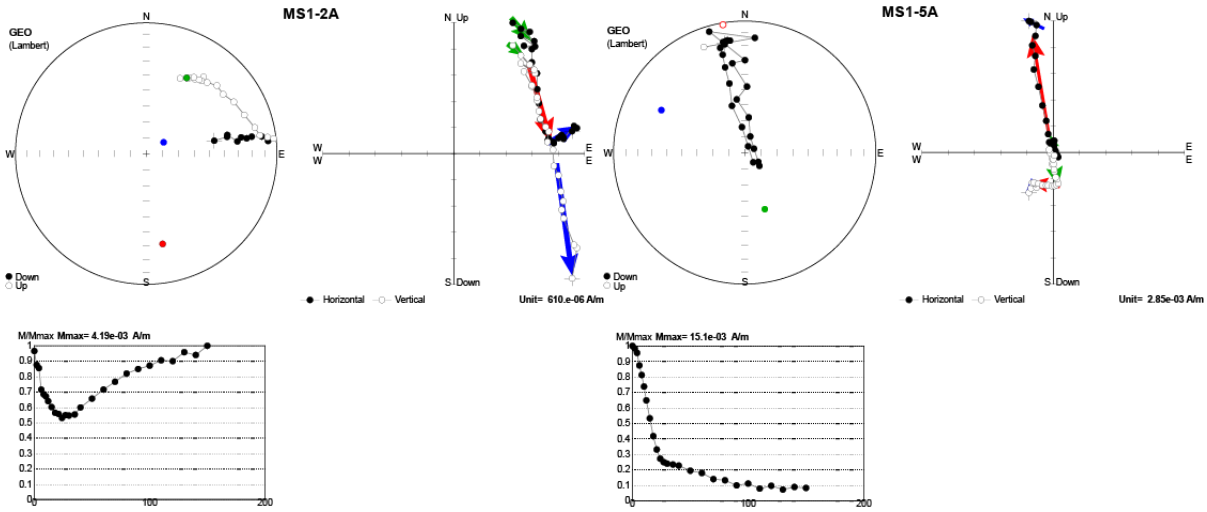

Figure 64: The two outliers in demagnetization behavior, Melsetter

These two behave oddly, the Zijderveld diagram for MS1-2A does not travel towards the origin, with the NRM seemingly moving along a great circle upwards. The NRM movement in MS1-5A starts in the north, moves to the vertical, then turns back and moves back to the start in the north again.

The directions seen at Melsetter is highly varied. There seems to be a lot of overlap between the different components, making the directions move around a lot during demagnetization and giving directions that differs a lot between the different specimens.

The low stability component however is similar between the samples, falling just to the north of the vertical, resembling the previously defined A component (Fig. 65).

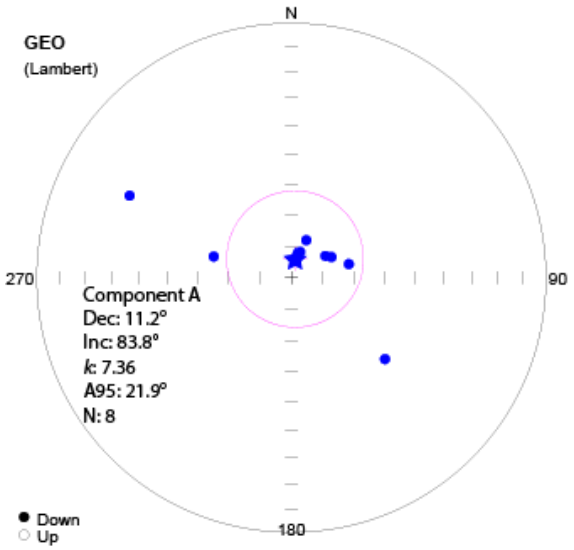

Figure 65: Low stability component seen at MS1.

The following intermediate component seen in the samples falls towards the southeast (Fig. 66)

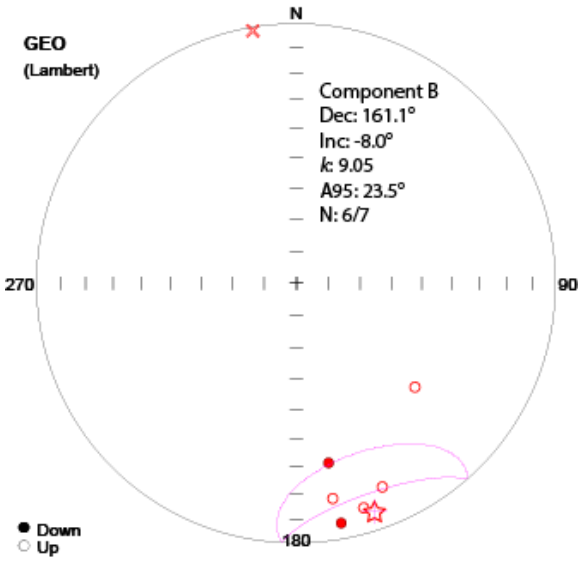

Figure 66: Intermediate stability components seen in the MS1 samples. The x-ed out sample towards the north is MS1-5A (Fig. 64, right).

Above the intermediate component some specimens have a higher stability component. Of these three samples have a southern direction, while the other two lies at a northeastern direction, at an upwards facing direction (Fig. 67).

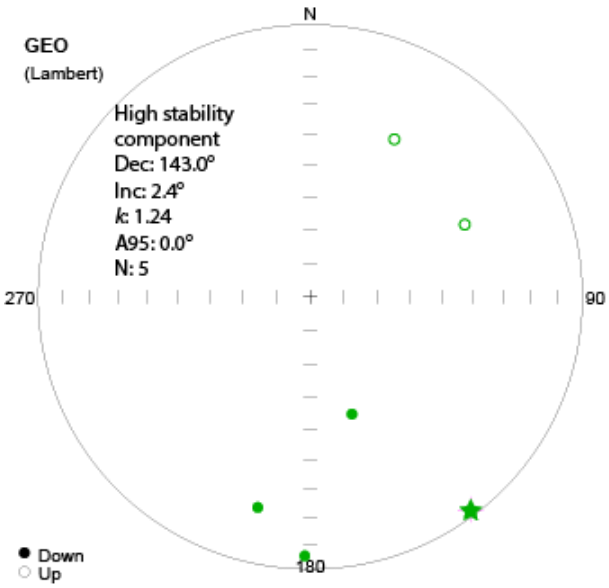

Figure 67: High stability components seen in the MS1 samples.

The great circles the directions in all specimens seem to move along however, has a common intersection point at a shallow southern direction, close to where the previous B component is situated in the other volcanics (Fig. 68). This is the best candidate seen for an old high stability component found at this locality.

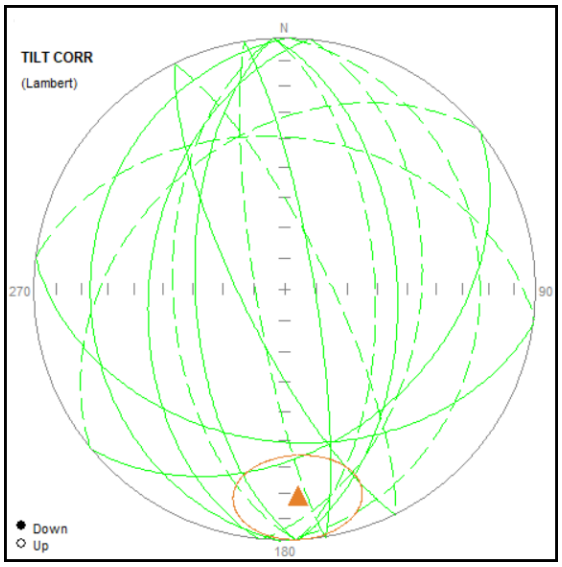

Figure 68: Great circles from the Melsetter samples. Intersection point to the south.

Due to the scattered directions and wide means when looking at the intermediate and high stability components, this site has been disregarded from any calculations regarding the VGP.

5.2 The dikes

5.2.1 Birsay

Coordinates: 59.138N 3.307W Locality 1 - 3

Situated at the northwestern edge of Mainland. The dike here trends towards 70°N and is slightly tilted towards the north. The sandstones on either side shows a similar tilt, so the contact looks vertical. The dike does several jumps as it travels towards the east.

Samples were collected from two sites on along the dike and a contact test was taken from the sandstones on the northern side (Fig. 69).

Figure 69: Overview of the dike at Birsay. The dike is the BR1 set of samples, BR2 is the baked contact test taken from the sediments next to the dike, and BR3 is from the flagstones situated a few meters north of the dike.

The Birsay locality consisted of eight samples taken from the dike, and two sets of samples taken from the sandstones lying to the north, with BR2 being the closest to the dike and BR3 some meters away (Fig. 69).

The flagstones lying to either side of the dike forms the basis for the bedding correction (Fig. 70).

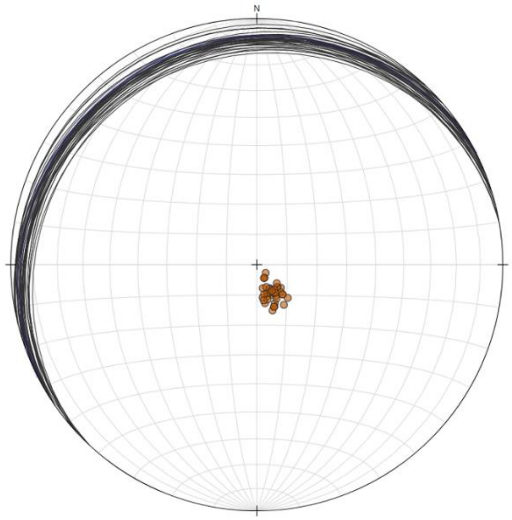

Average used for tilt correction: 332/11 Dipdir/dip

Figure 70: Stereo plot of the bedding measurements from Birsay.

AMS

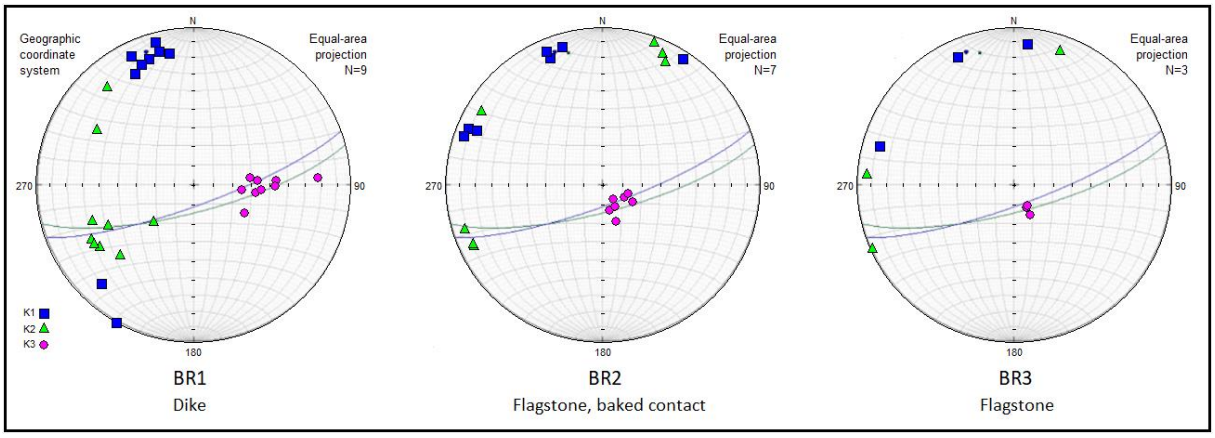

Figure 71: AMS results from the three Birsay sites. Two axes seem to align with the dike orientation

The main samples from Birsay is decently well grouped and show a slight tilt towards the west /Fig. 71).

Birsay 2 and 3 shows the same grouping, with the weak axis slightly towards the south-east and the two main axes distributed along a shallow great circle. These are typical sedimentary measurements.

Demagnetization

BR1

The dike at Birsay, samples were taken from two places along the exposed dike, with about 30 meters between them (Fig. 72).

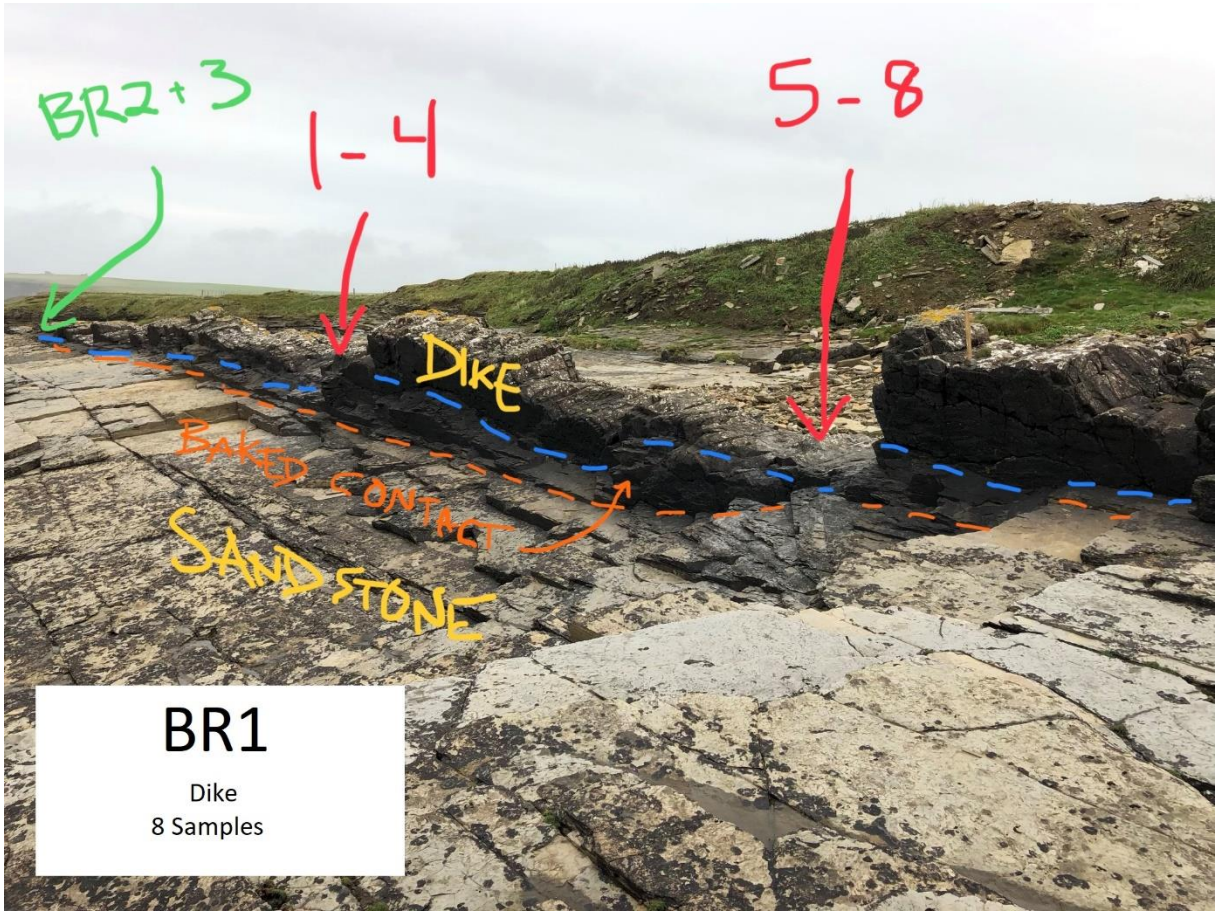

Figure 72: Sampling sites for BR1, with a diagram of the surrounding area, Birsay.

Following the pilot examination, it was found that the Birsay dike responded best to AF demagnetization.

The specimens all demagnetize the same way, quickly losing 80 to 90% of their intensity by 10mT then flattening out and staying at around 5% intensity from there (Fig. 73, left). Due to the low amount of remanent intensity and exhibited erratic behavior in some specimens most of the measurements were stopped between 15 and 23mT. BR1-8A held onto its remanence better than the rest and gave good results up to 45mT (Fig. 74).

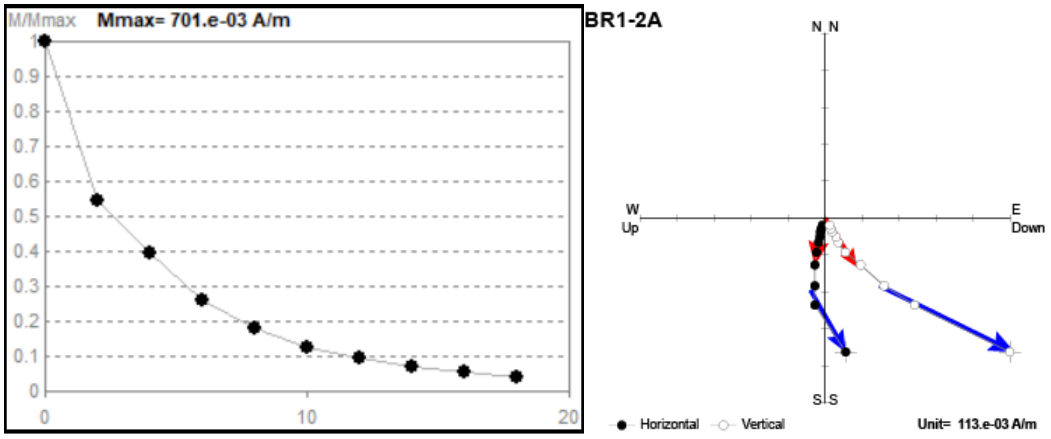

Figure 73: Typical demagnetization behavior and Zijderveld diagram, BR1. The vertical plane has been changed from the W-E plane to the N-S plane for visibility.

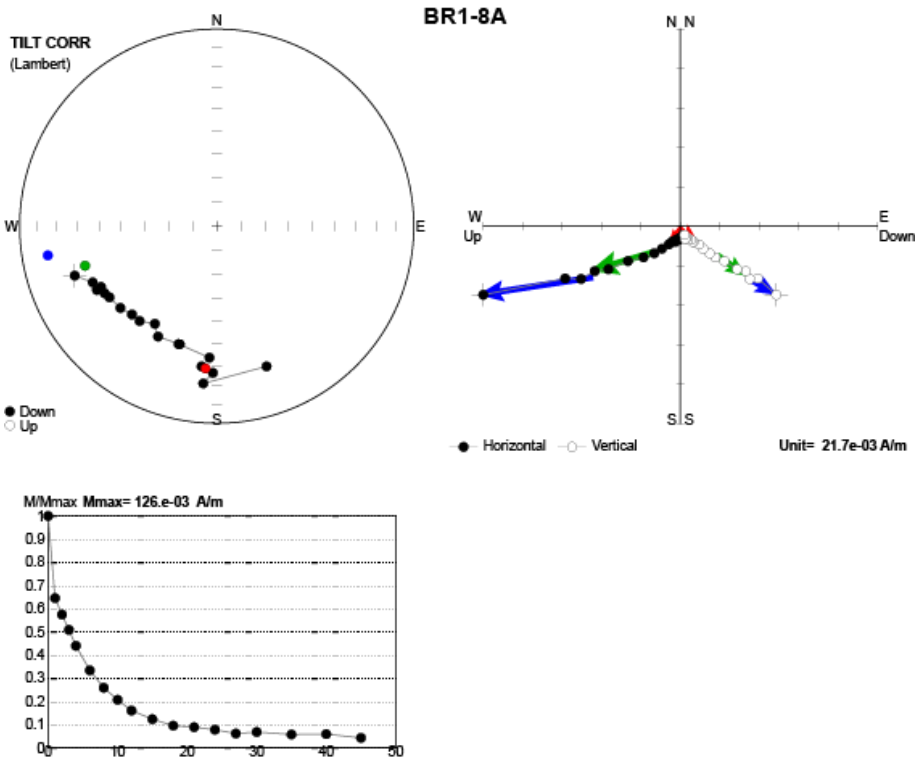

Figure 74: BR1-8A holds onto the remanent magnetism until around 45mT where the process was halted. The vertical plane in the Zijderveld is changed from WE to NS for visibility.

The high stability components at BR1 seem to fall into three categories, BR1-1B, -2A, -5A and 7B has a movement that in general travels southwestwards from the initial NRM (Fig. 75). They all end up towards the southwest in the same area and forms the biggest part of the mean calculation for this set of samples.

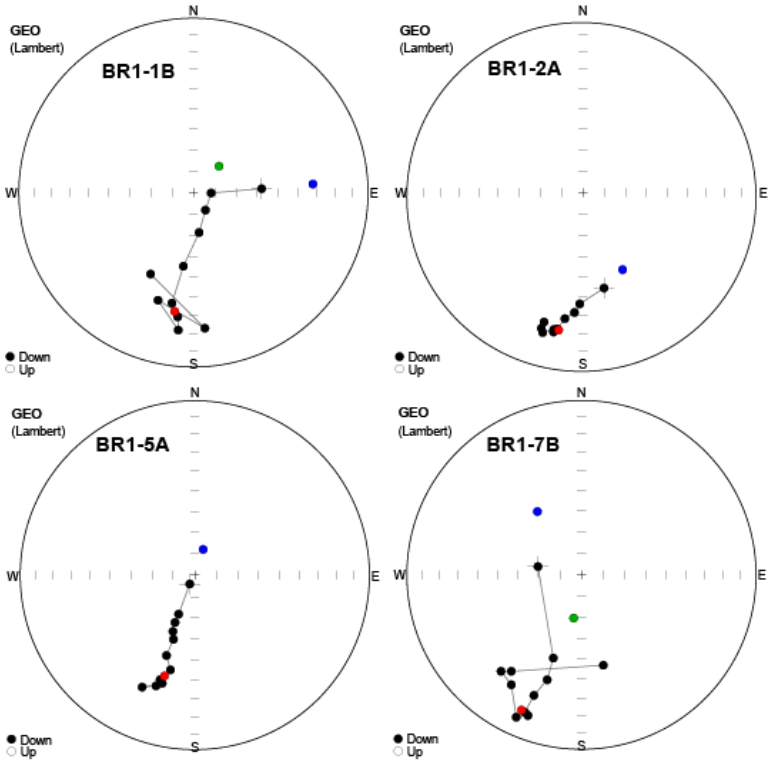

Figure 75: Four samples from BR1 exhibit a similar behavior during demagnetization.

The second set that resembles one another consists of the samples BR1-3A and BR1-8A (Fig. 76). These two have an initial NRM towards a western direction and both travels towards the south along a great circle. The BR1-3A specimen runs out of magnetic intensity before the vector reaches as far south as the other high stability component and is therefore the westernmost component at this locality.

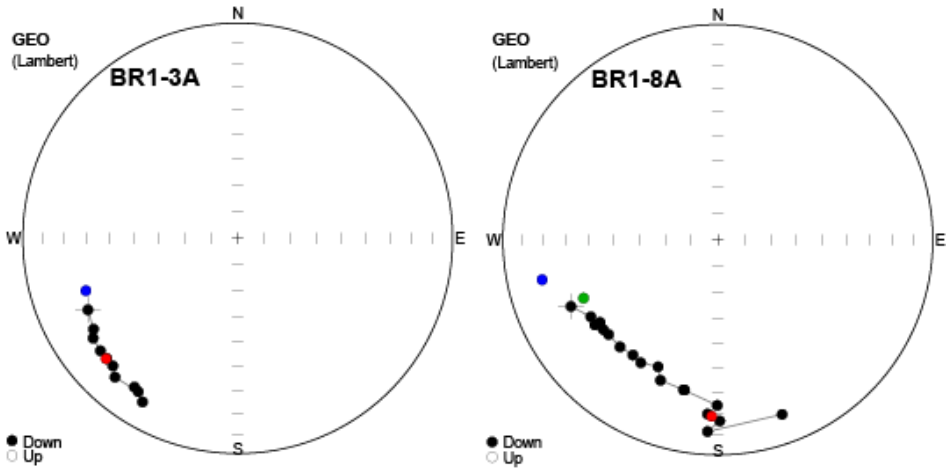

Figure 76: Second set of similar specimens follows a great circle towards the south.

The last two specimens are the two disregarded components seen in the overview of the high stability components (Fig. 80). These are BR1-4A and BR1-6A, which does not resemble any of the other seen at this site. BR1-4A starts at a shallow southeastern direction and clusters just to the east of the starting point (Fig. 77, left). The BR1-6A specimen travels southwards from its initial eastern direction and runs out of magnetic remanence after a short travel (Fig. 77, right).

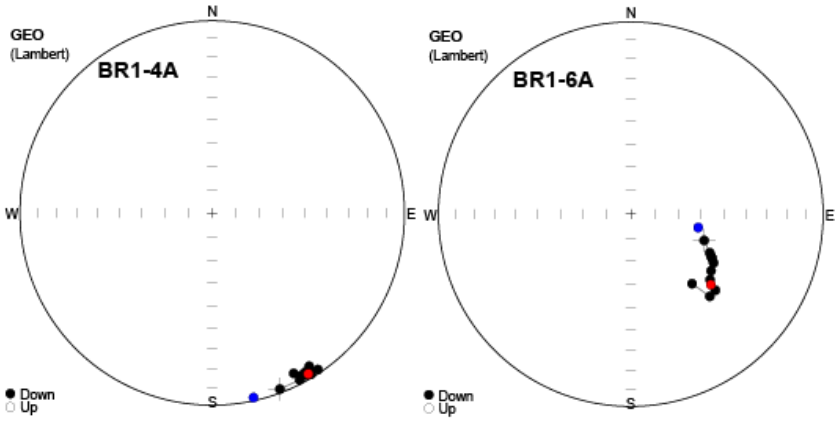

Figure 77: The last two specimens does not resemble any other behavior seen in the Birsay dike.

The directions seen at the Birsay dike are decently separable, with a low (Fig. 78) and intermediate (Fig. 79) component both being scattered around the vertical when viewed in geographic coordinates. These are much better grouped in specimen specific coordinates falling around the vertical.

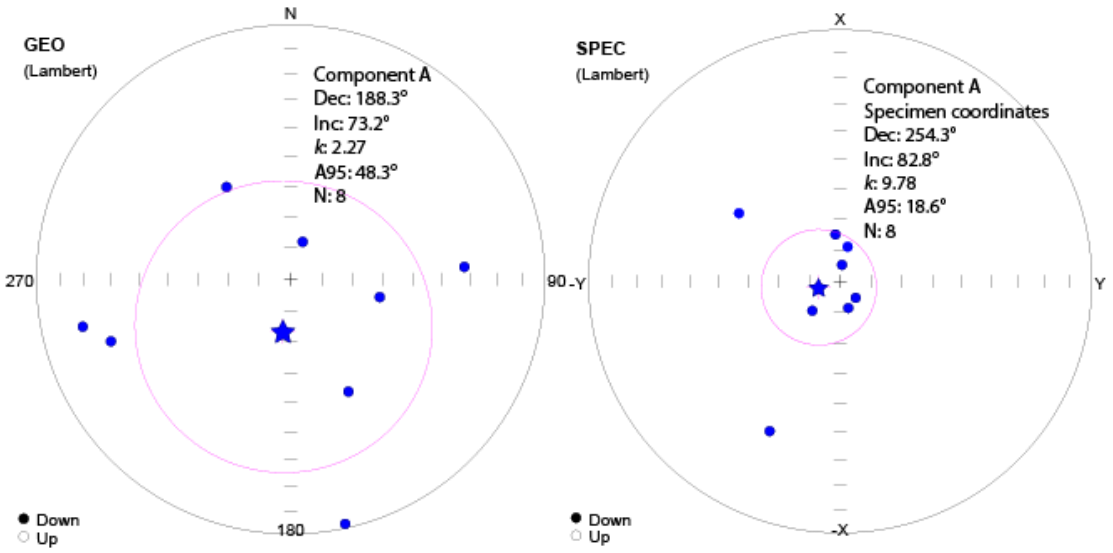

*Figure 78: **Left:** Low stability component in BR1. **Right:** Same low stability component viewed in specimen specific coordinates.*

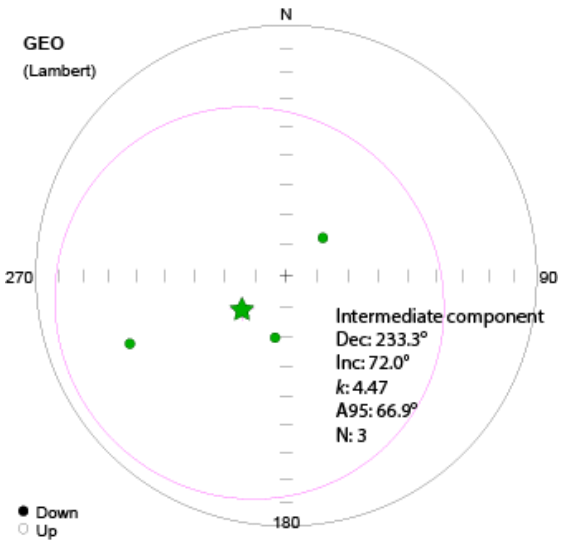

Figure 79: Intermediate stability component seen in a few specimens from BR1.

Above the low and intermediate component all specimens exhibit a high stability component. This high stability component in five out of the eight specimens group at a semi-shallow southern angle, with three specimens differing (Fig. 80). Two of these end up in the south-east at a medium steep angle, resembling the southeast high stability component seen at volcanic localities like Deerness (DN4 especially) and Lounders Fea. The last outlier is BR1-3A, which falls to the west of the others, it resembles BR1-8A (Fig. 74, 76) in NRM movement during demagnetization but does not travel quite as far towards the south before being demagnetized to the point the measurements were stopped.

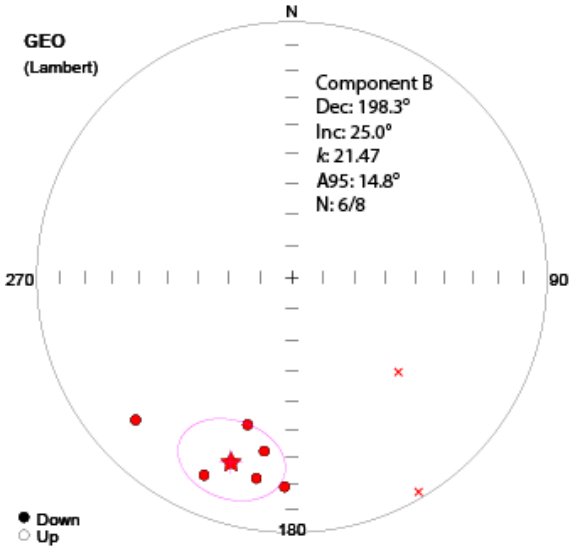

Figure 80: High stability components seen in the BR1 set of samples. The two x-ed out specimens in the east are BR1-4A and BR1-6A.

BR2

The second locality at Birsay was planned as a baked contact test from the flagstones to the north of the dike. Samples were taken from the baked contact and along a profile around 3 meters away from the dike (Fig. 81).

Figure 81: Sampling sites for BR2.

After the pilot sample, it was decided to use a combination of thermal and AF demagnetization on these specimens. The AF produced better results, but were unable to completely demagnetize the specimens, so for the rest of the specimens they were first demagnetized using AF to 100 mT then subjected to thermal demagnetization, starting at 100°C.

The resulting demagnetization curve is marked by a brief increase in intensity at low mT followed by an even drop down to around 30-50% intensity reached at 100mT. Once thermal demagnetization begins the intensity stays at mostly the same level until the temperature passes 250°C from which the strength drops and reaches 5% remaining intensity at 350°C and measurements stop (Fig. 82).

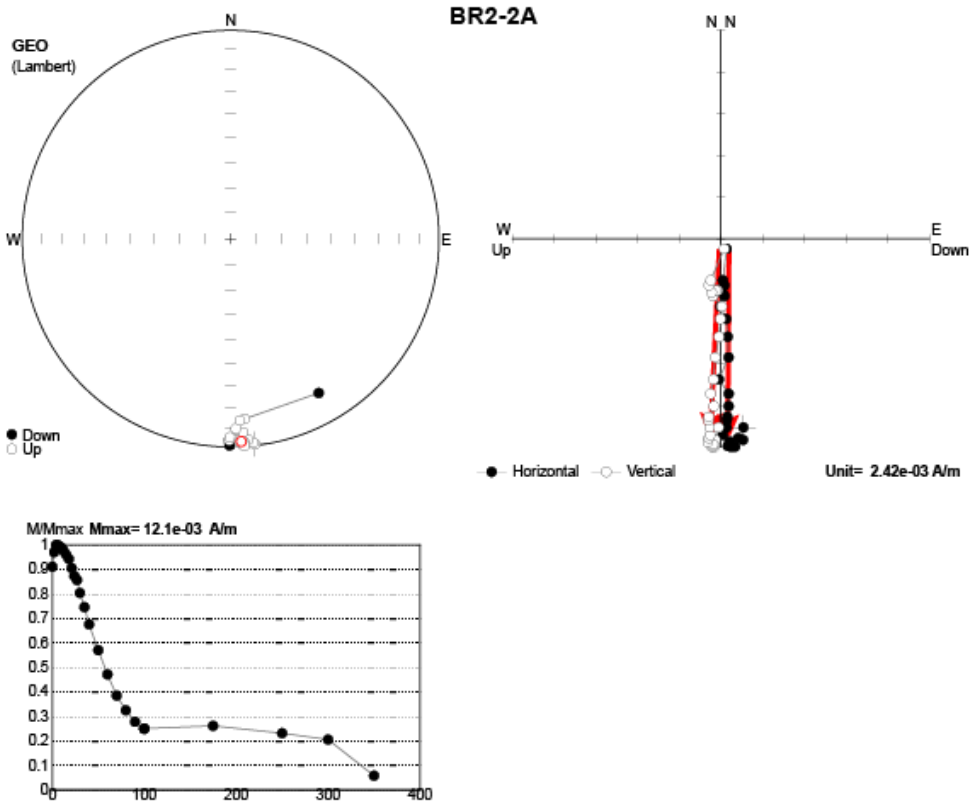

Figure 82: Typical demagnetization behavior, AF to 100mT then thermal to 350°C. The vertical plane in the Zijderveld is N-S for visibility of the components.

There seems to be a low stability component in the samples when you view the Zijderveld, but trying to select and define this component gives a component situated at a shallow north-eastern direction with a wide angle of confidence (Fig. 73). This is the case for nearly all the specimens, and though the resulting low stability component in some specimens seem to fall more towards a western direction, the angle of confidence is always wide. The distance between this proposed component and the NRM clustering on a whole might be a result of the dual demagnetization process.

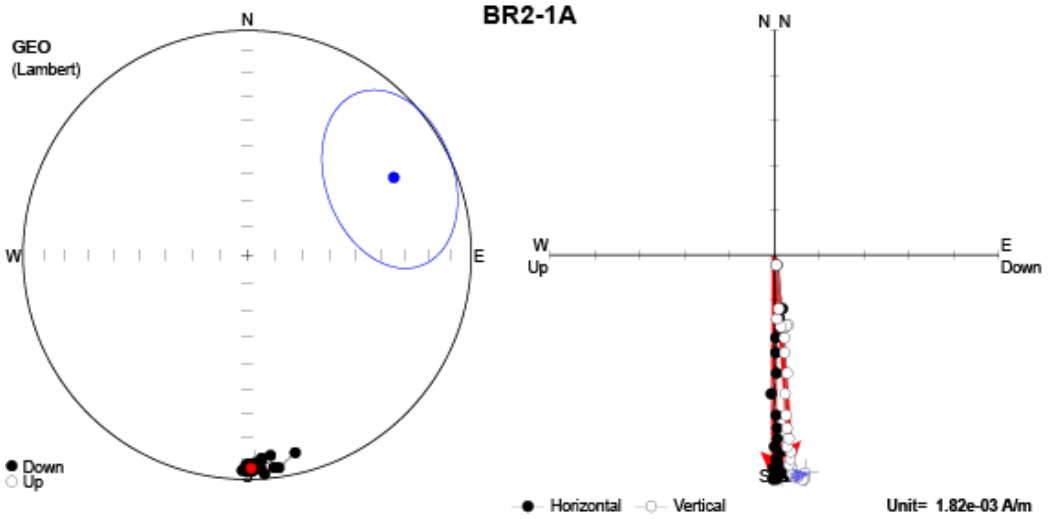

Figure 83: BR2-1A with a low stability component selected (blue).

The direction seen in all specimens is a mostly univectorial component pointing at a shallow, almost horizontal southern direction (Fig. 84). This southern direction is seen in all samples from the baked contact zone next to the dike and is still there a few meters away from the dike. The baked contact test fails since the direction does not match the dike, nor does it change as the samples move away from the dike.

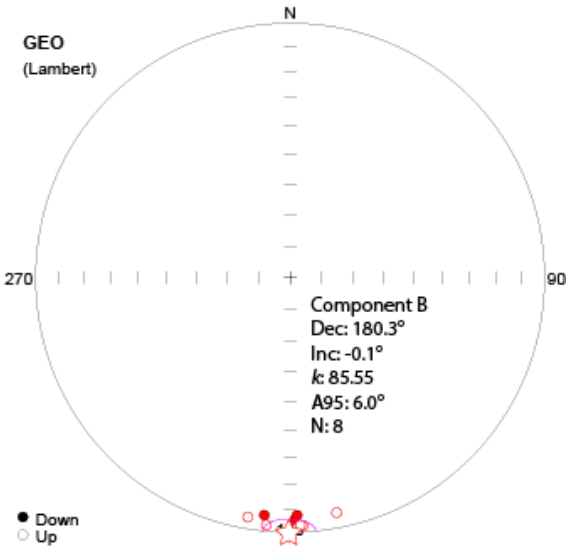

Figure 84: High stability component seen at BR2.

BR3

The last sampling locality at Birsay, taken from the flagstones several meters north of the dike (Fig. 85). This was taken as a reference to the baked contact test of BR2, to see if there were any change further out from the dike.

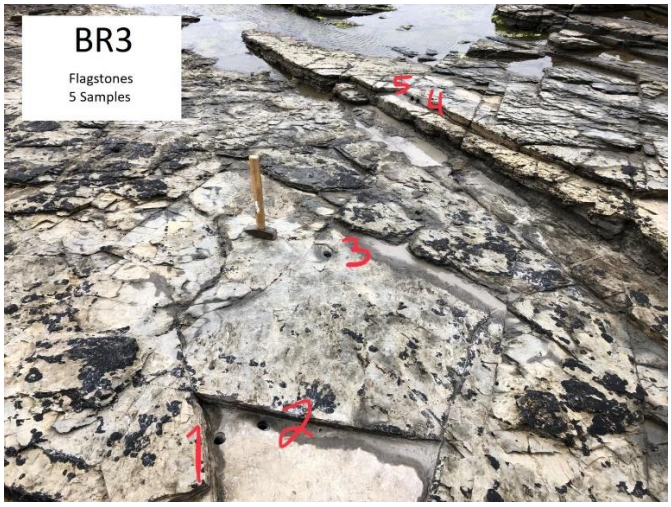

Figure 85: Sampling sites for BR3.

The BR3 specimens did not respond well to neither thermal (Fig. 86) nor AF (Fig. 87) demagnetization, so the last few samples from this set did not get further examined after the pilot.

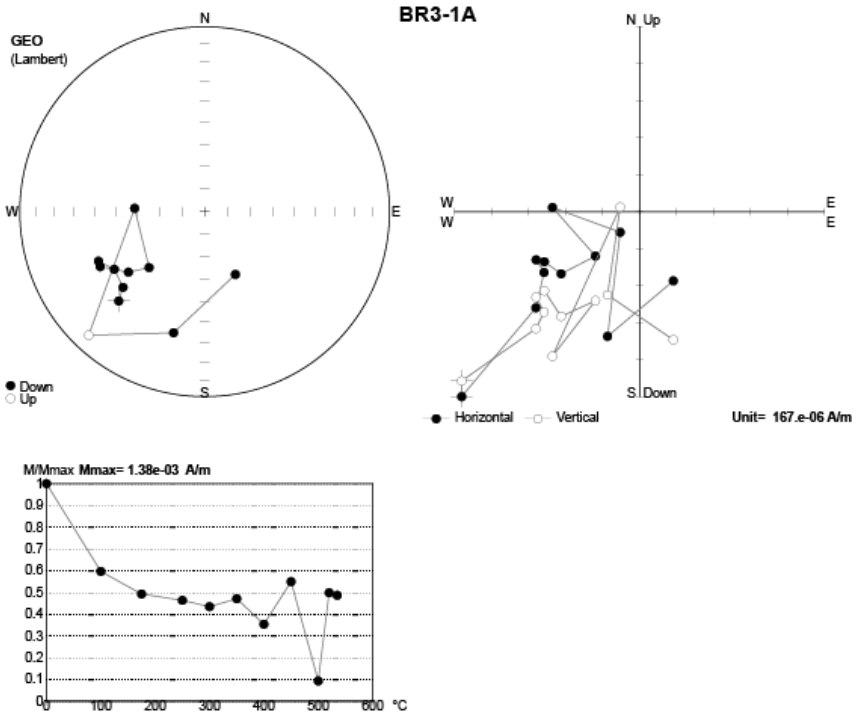

Figure 86: Demagnetization behavior during thermal demagnetization, BR3-1A.

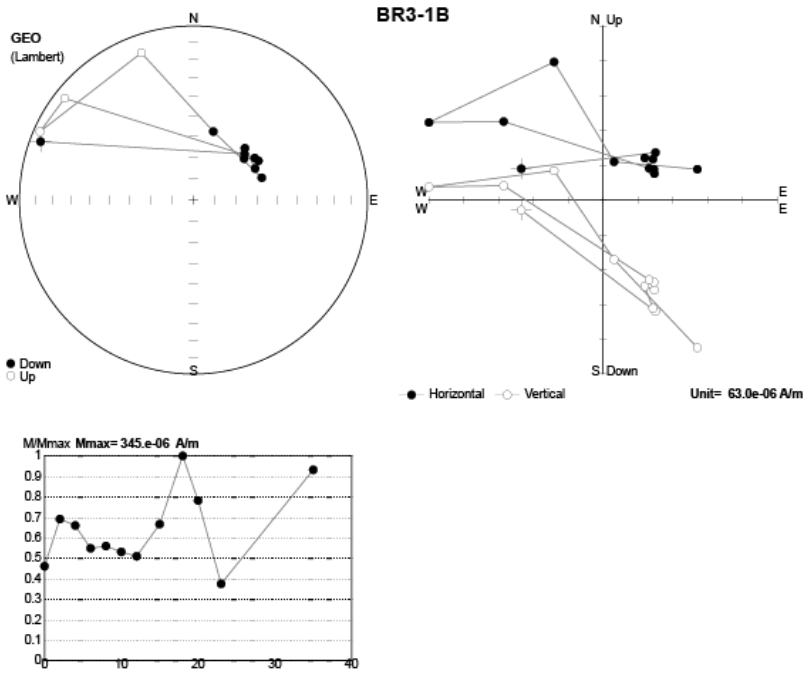

Figure 87: Demagnetization behavior during AF demagnetization, BR3-1B.

5.2.2 Nethertown

Coordinates: 58.952N 3.319W

Nethertown is located on the southwestern side of Mainland, close to Stromness. The dike here looks to be connected to a dike found just outside of Stromness on a map view, so this locality was chosen to be less intrusive. It is also not as inaccessible due to the tides as the exposure outside of Stromness was. The dike is cutting through the flagstones on either side and shows signs of erosion (Fig. 88). The orientation is about 70° N, the same as the dike at Yesnaby and the Bay of Skaill. The dike looks vertical and does a little 2m jump to the northwest. Samples were collected along a few meters of dike then carefully filled in and covered up after we were done.

Figure 88: The Nethertown dike and surrounding flagstones.

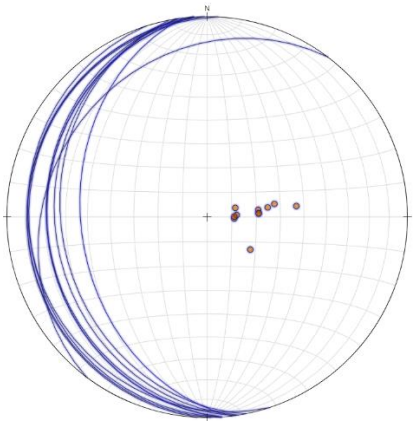

Figure 89: Stereo plot of the Nethertown bedding measurements

The Nethertown dike sample set consists of seven specimens as one of the eight cores was too broken to be made into specimens. The dike is surrounded by flagstones, which forms the basis for the bedding corrections (Fig. 89).

Average used for tilt correction: 272/17 Dipdir/dip

AMS

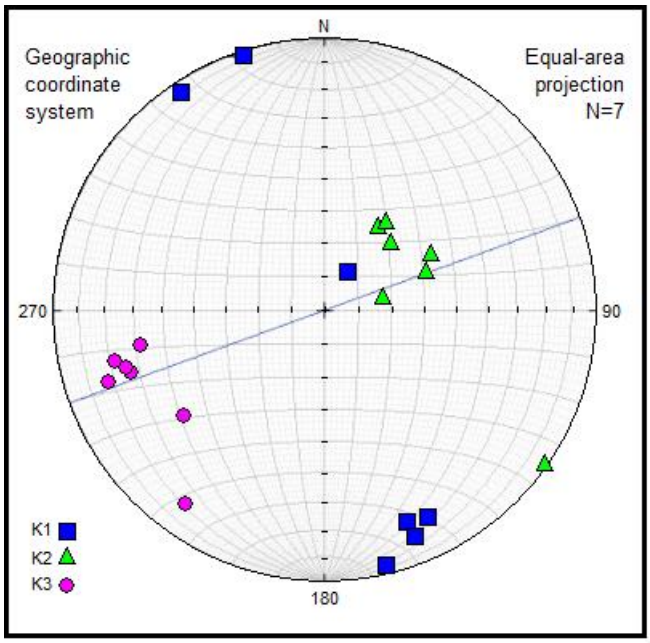

Figure 90: AMS results from Nethertown. Two axes seem to align to the dike orientation, marked in light blue

Good grouping with a slight tilt towards the south-west (Fig. 90), similar to Yesnaby and some of the volcanics like Lounders Fea.

Figure 91: Sampling sites from Nethertown.

Demagnetization

Following the pilot, it was determined to demagnetize this set of samples using AF demagnetization, since it seemed to give slightly clearer results in contrast to the thermal demagnetization.
All specimens drop about 20-30% intensity right away, between the NRM and 2mT. From here the drop is mostly regular and starts to flatten out after 20mT, with most specimens reaching 5% intensity remaining at 40mT (Fig. 92).

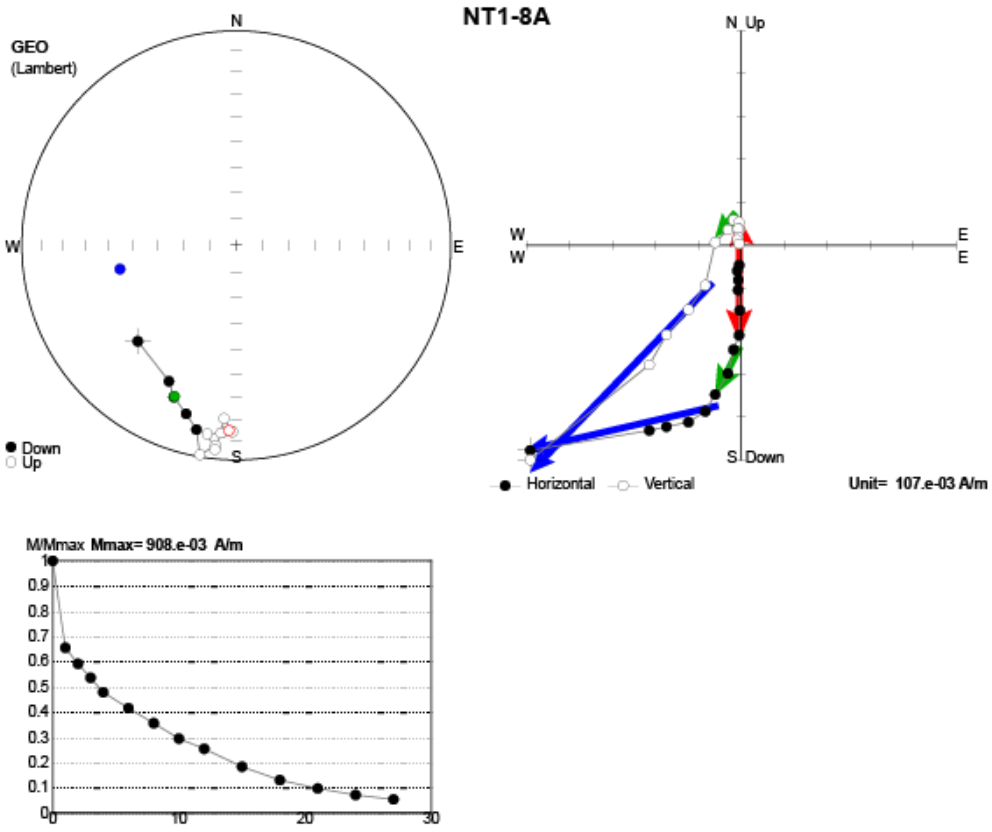

Figure 92: Typical demagnetization behavior and Zijderveld diagram, NT1.

The demagnetization behavior seen at Nethertown seem to fall into two categories (Fig. 93). In NT1-2A, 3A, 4A and 8A the NRM moves towards the final southern direction from a northwestern direction (Fig. 93, top four panels), while NT1-1A, 5A and 7B starts from the northeast and moves southwest to the final resting place (Fig. 93, bottom three panels).

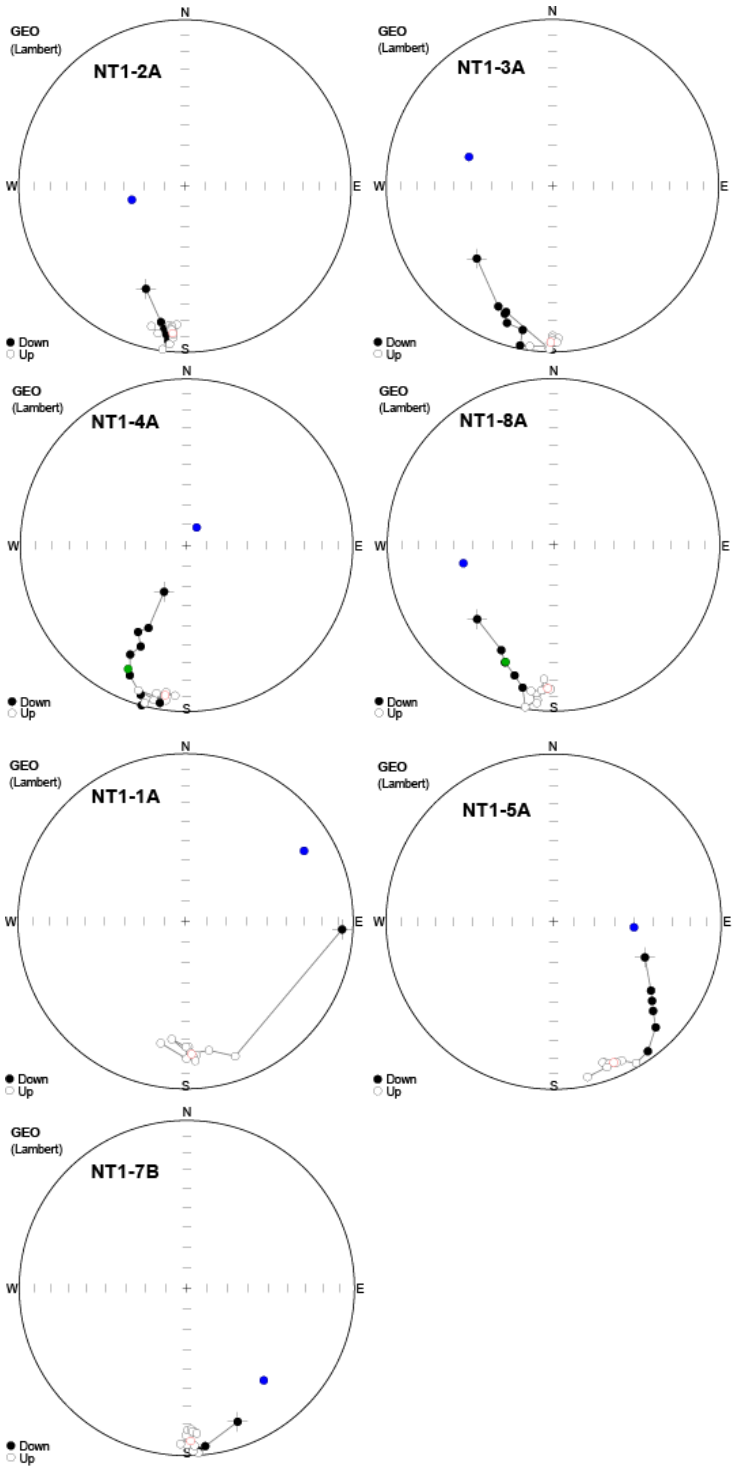

Figure 93: The movements seen in the NT1 samples seem to fall into two categories.

All specimens have a low stability component falling scattered around the vertical (Fig. 94, left). This is also a set of samples where this low stability component seems to group up when viewed in specimen specific coordinates (Fig. 94, right).

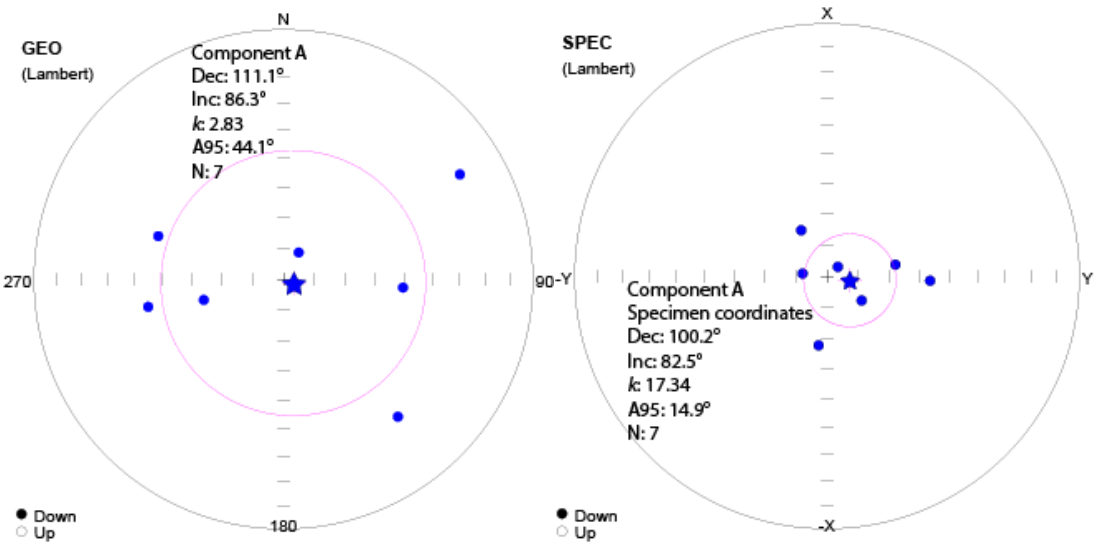

*Figure 94: **Left:** Low stability components. **Right:** Same low stability component seen in specimen specific coordinates.*

Two specimens have what appears to be an intermediate component, falling at a medium shallow southwestern direction (Fig. 95).

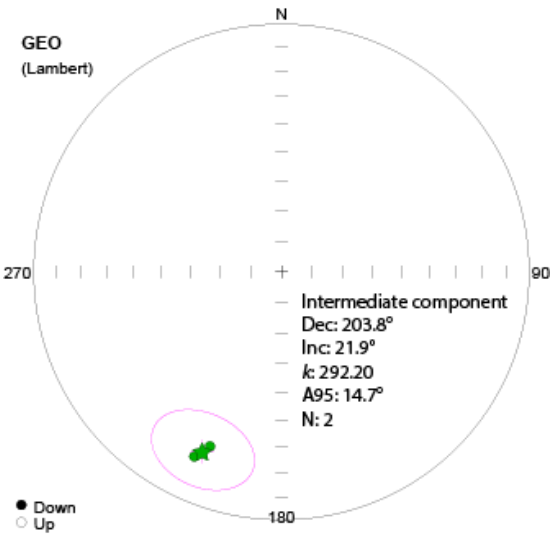

Figure 95: Intermediate component seen in NT1-4A and NT1-8A.

The high stability component in all specimens points at a shallow, upwards facing direction directly south (Fig. 96). The component has a *k* value of 53.34 and an A_{95} value of 8.3°. This component resembles the high stability component seen in the baked contact test from BR2, although at a higher angle above the horizon.

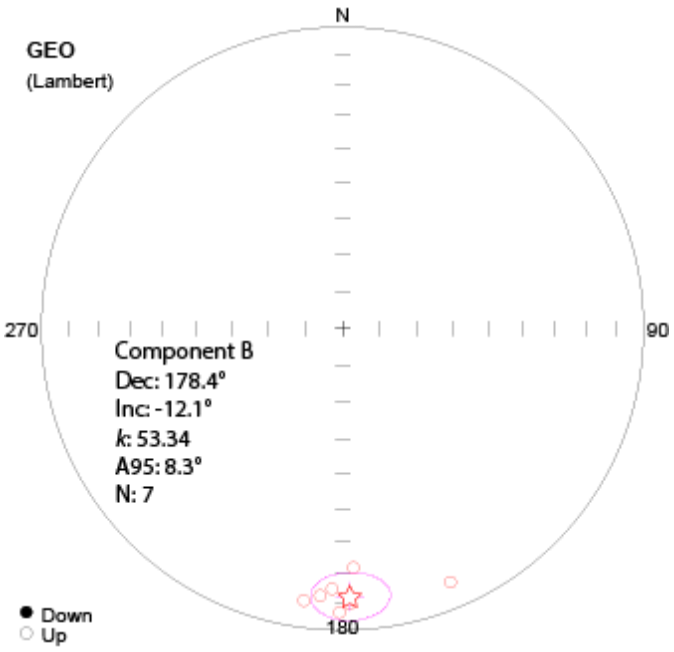

Figure 96: High stability components seen at the Nethertown dike.

5.2.3 Tingwall

Coordinates: 59.087N 3.039W

North on Mainland, the dike here is situated about 400m east of the ferry terminal at Tingwall. The location is right outside the Fernvalley Wildlife Centre. The dike here is a camptonite, about 140cm wide and an apparent vertical contact with the sandstones is cuts through (Fig. 97). The dike has a little jump in the western end before it disappears. The exposure is similar in size to the one found at the Bay of Skaill, and we did our best to get a good spread of the samples drilled.

Figure 97: The Tingwall dike and surrounding flagstones.

The dike at the Tingwall ferry landing, eight cores were drilled and made into specimens. The flagstones lying to either side of the dike forms the basis of the bedding correction here as well (Fig. 98).

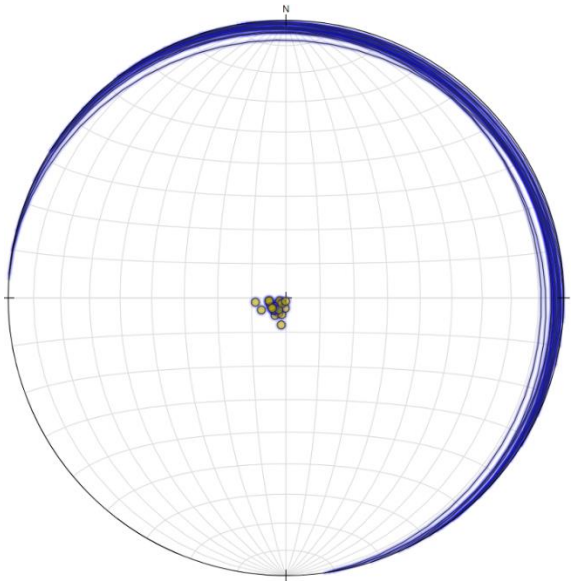

Figure 98: Stereo plot of the bedding measurements at Tingwall.

The flagstones that forms the basis of the tilt correction has a very low spread, even across hundreds of meters on either side of the dike.

Average used for tilt correction: 050/04 Dipdir/Dip

AMS

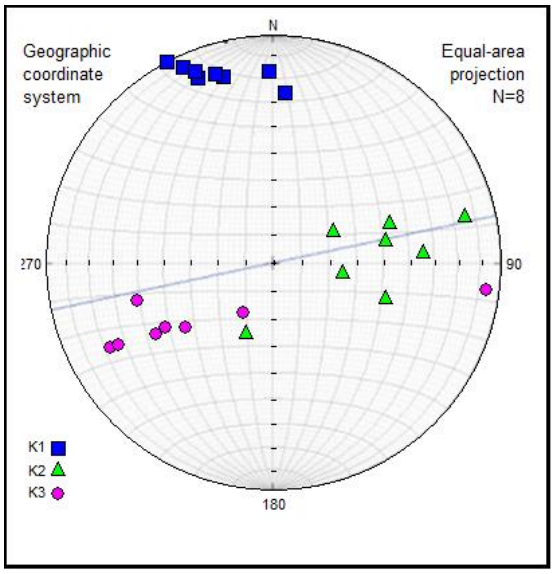

Figure 99: AMS results for the Tingwall dike, two axes of anisotropy aligning close to the dike orientation, marked in light blue.

Showing a possible tilt towards the north west, the K2 and K3 axes are a bit scattered in comparison to K1, but still showing a good trend. The K2 and K3 axes might follow the trend of the dike itself (Fig. 99).

Figure 100: Sampling sites at Tingwall.

Demagnetization

Not unsurprisingly it was AF demagnetization which proved the best for this dike as well.

The specimens from Tingwall drop their intensity incredibly quickly, with some specimens losing 90% or more of their strength by 6mT (Fig. 101, left), and most being done by around 20mT. One specimen, TW1-6A, differs in that it took until 140mT before it dropped below 10% strength (Fig. 101, right), the sister sample TW1-6B was also examined and behaved in the same way.

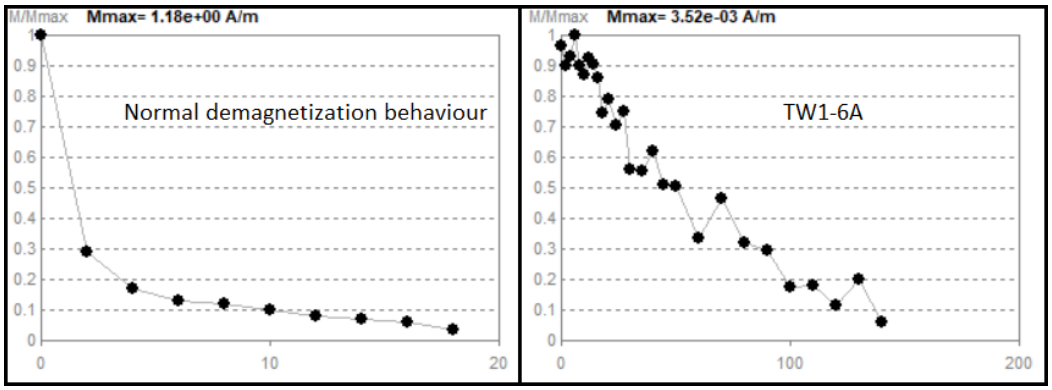

Figure 101: Normal and outlier, demagnetization behavior seen at Tingwall.

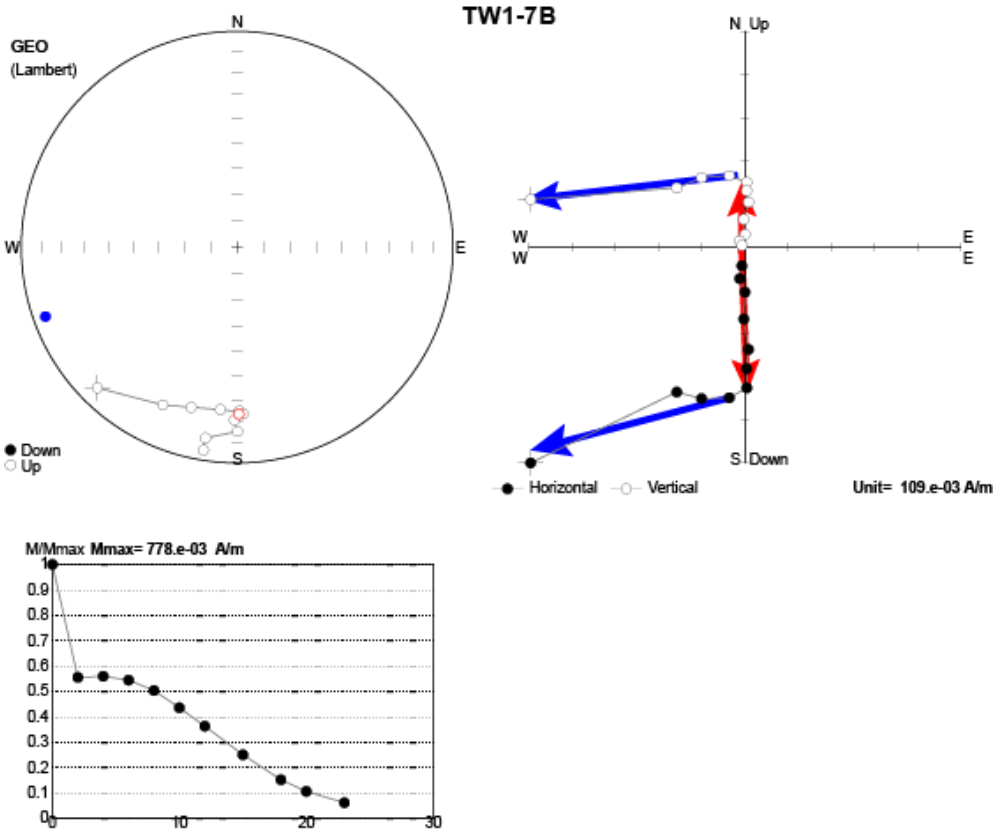

Figure 102: Typical Zijderveld diagram for TW1

Three specimens from Tingwall differ from the rest and are marked as x-ed out specimens in the mean figures (Fig. 105). These three all have a similar demagnetization intensity curve as the other specimens from this site, but the NRM direction does not match up with the others (Fig. 103).

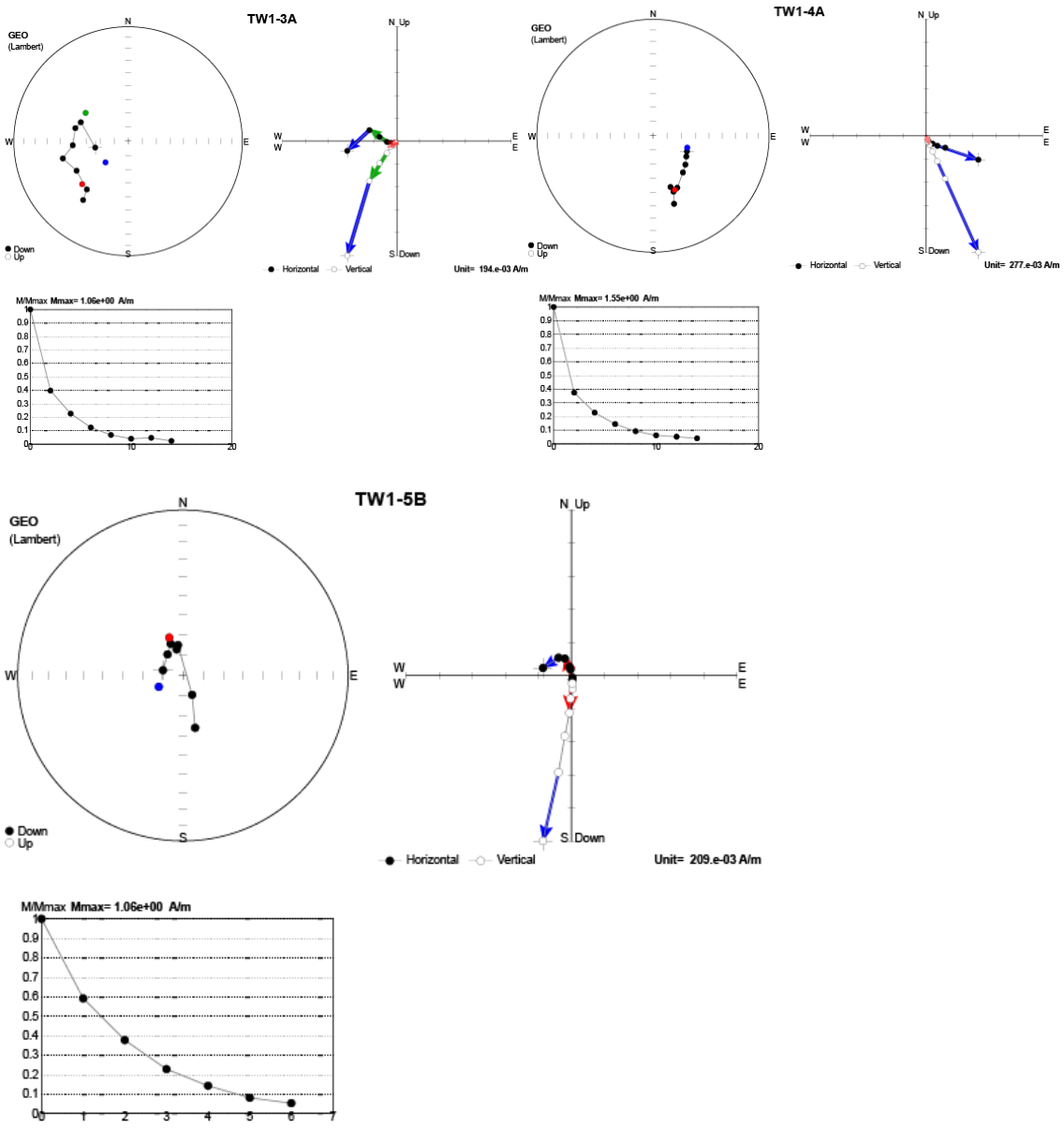

Figure 103: The three outliers from TW1.

The Tingwall dike has a low and intermediate component that generally seem to fall in the same general area. Both components are quite scattered to the west of the vertical (Fig. 104).

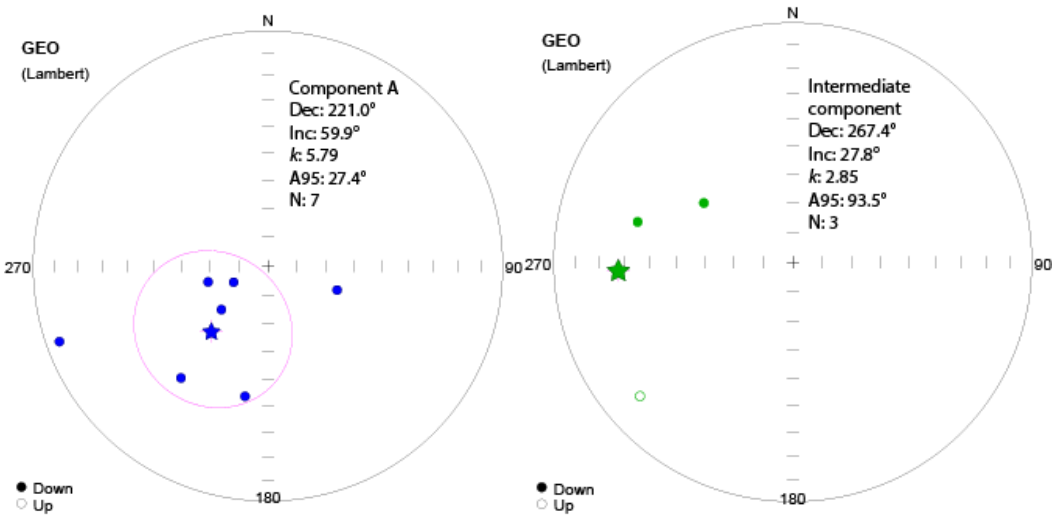

Figure 104: ***Left:*** *Low stability component.* ***Right:*** *Intermediate stability component.*

The high stability component has three specimens falling closer to the vertical, while the remaining five specimens all group at an upwards facing southern direction (Fig. 105). This is close to where the high stability component from Nethertown pointed at (Fig. 96). The cluster of high stability components has a *k* value of 64.50 and an A_{95} value of 9.6°. Of the three that are more scattered, two resembles slightly steeper southern directions seen elsewhere (BR1 and DN4 respectively), while the last is pointing close to the present earth field. These three differing specimens are all pointing downwards while the other five which forms the base for the mean calculations point upwards.

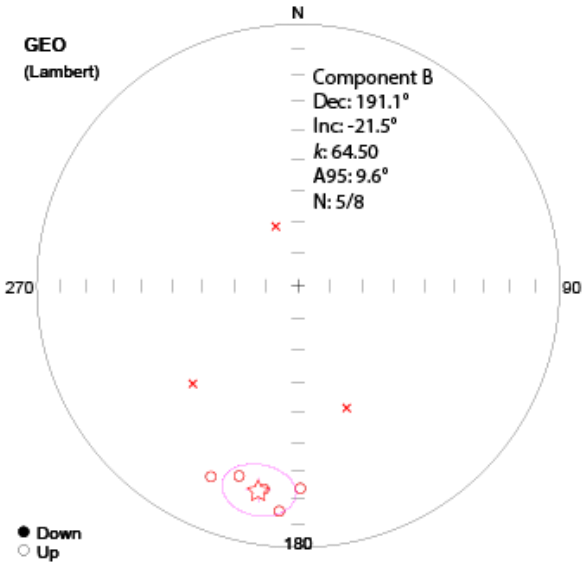

Figure 105: High stability components seen in the Tingwall dike. The three x-ed out specimens are TW1-3A, 4A and 5B (Fig. 94).

5.2.4 Yesnaby

Coordinates: 59.025N 3.359W

The fourth of the dikes is at Yesnaby, this is a spectacular location on the western side of Mainland, a little south of the Bay of Skaill. The stratigraphy of the area is cut through by a 2m wide dike running towards 78° N (Fig. 106). The dike takes a series of turns and steps in this area (Rian, 2018). Samples were collected from both the southern and northern side as well as on top of the dike. Drilling locations were carefully selected to be as least conspicuous as possible since this dike runs through a strongly protected site of stromatolite fossils. The dike cuts the sandstones on either side, and there seems to be no vertical displacement of the sandstones across the dike. The Stromatolites are highly concentrated within one layer, and functions as a good measurement tool for any possible vertical displacements. There were ample evidences of earlier paleomagnetic samples having been taken from this dike, and we chose to drill our samples as far out and away from these as possible to not destroy the area any further.

Figure 106: The dark Yesnaby dike and surrounding flagstones.

The Yesnaby set consists of just four measured specimens due to poor conditions of the drilled cores. The flagstones of Yesnaby, found on either side of the dike forms the basis for the bedding correction (Fig. 107).

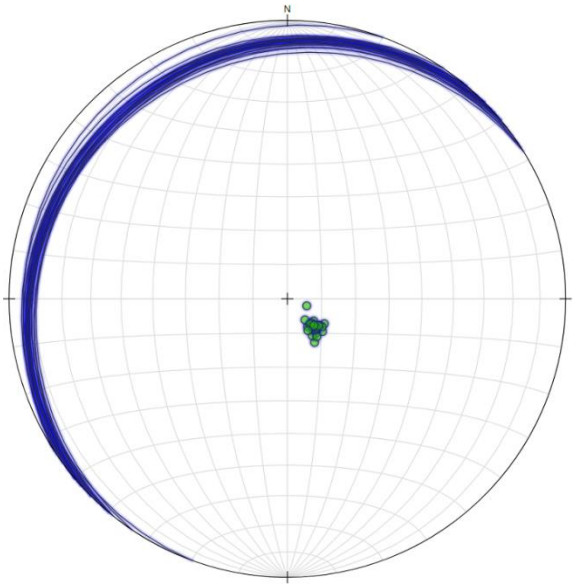

The beddings on either side of the dike has a very low spread.

Average used for tilt correction: 317/11 Dipdir/dip

Figure 107: Stereo plot of the Yesnaby bedding measurements.

AMS

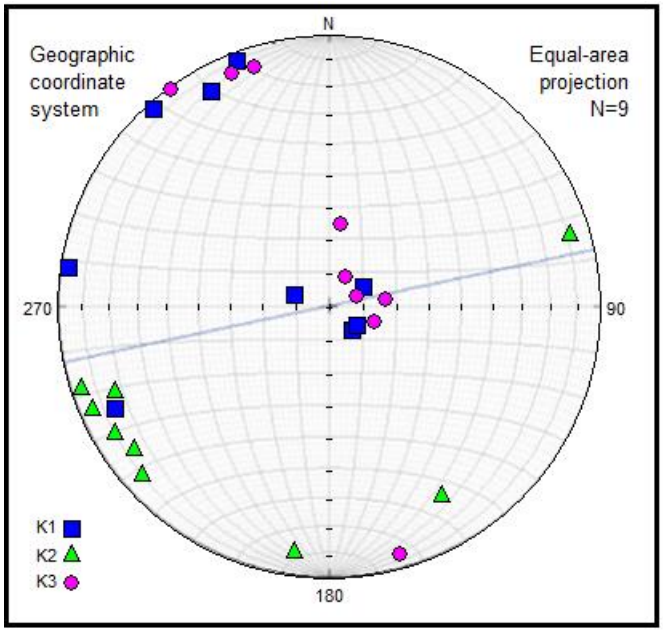

Figure 108: AMS results for the Yesnaby dike. Possible alignment to the dike orientation, marked in light blue.

The Yesnaby samples are well grouped with a very slight tilt towards the south-west. The outlier seen right above the 270° line is YB1-6B, and a sister sample (YB1-6A) was measured as well to see if the difference persisted throughout the entire core. YB1-6A fell alongside the rest of the samples (Fig. 108).

Figure 109: Sampling sites from Yesnaby.

Demagnetization

The pilot examination showed that the Yesnaby specimens responded best to AF demagnetization, but the number of viable specimens were low due to cracks in the sample cores.

The specimens behave a bit differently during demagnetization. YB1-2B and 5B demagnetize regularly down to 29mT and 40mT, with a rapid 30% drop in intensity between the NRM and 2mT (Fig. 111).

YB1-3A was demagnetized thermally and looks similar, with a quick drop to below 40% strength at 175°C, followed by little change until 500°C from which the decline is steep (Figure 110, right).

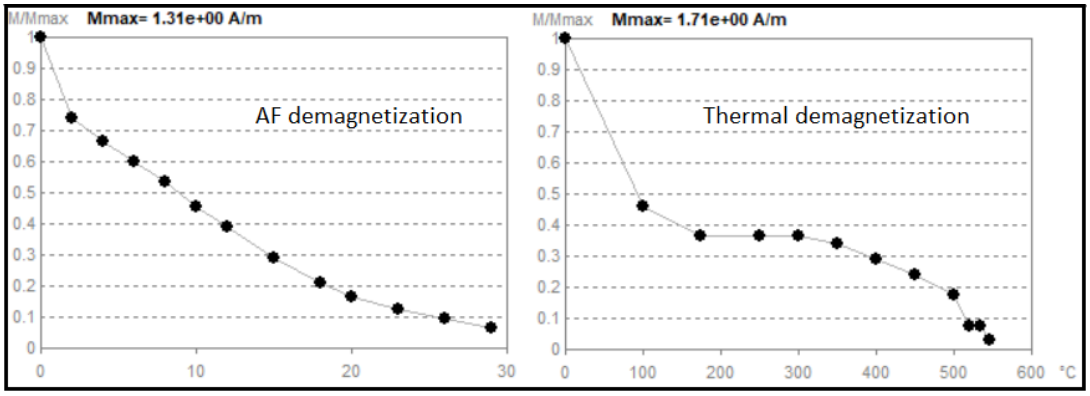

Figure 110: Demagnetization behavior for AF demagnetization (Left) and thermal demagnetization (right).

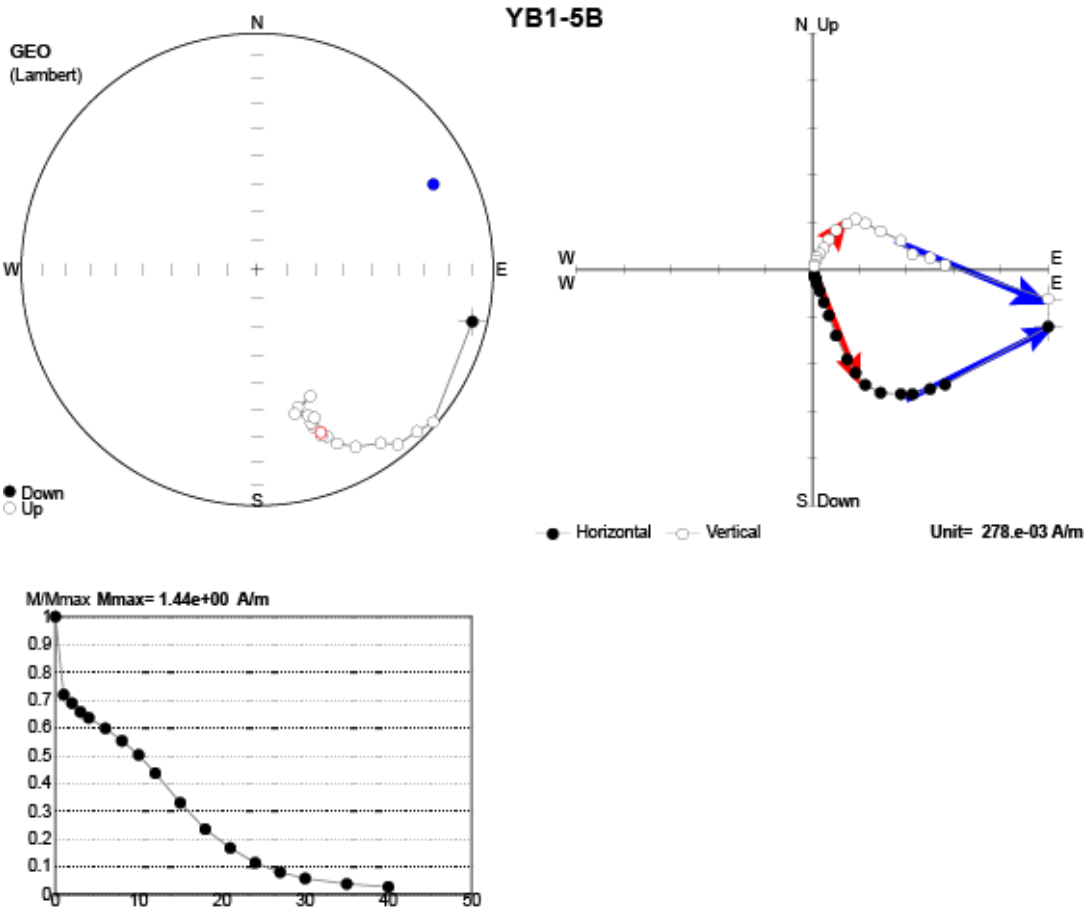

Figure 111: Typical Zijderveld diagram for YB1

The last specimen is YB1-7C, which does not lose any intensity before 10mT, but then have an even descent to about 20% intensity at 40mT (Fig. 112). From here, the intensity starts increasing again and the direction observed begins moving quickly. YB1-7C was not a part of the pilot examination, but due to very evident AF stacking seen in the YB1-7B specimen (Figure 113), its sister specimen was examined as well using the countermeasures proposed. The resulting direction looks fine for the first steps but seems to also be influenced by the AF process once passed a certain point in the

process. The picked component from this is therefore selected from the points before 30mT before where it looks like the direction starts to veer off.

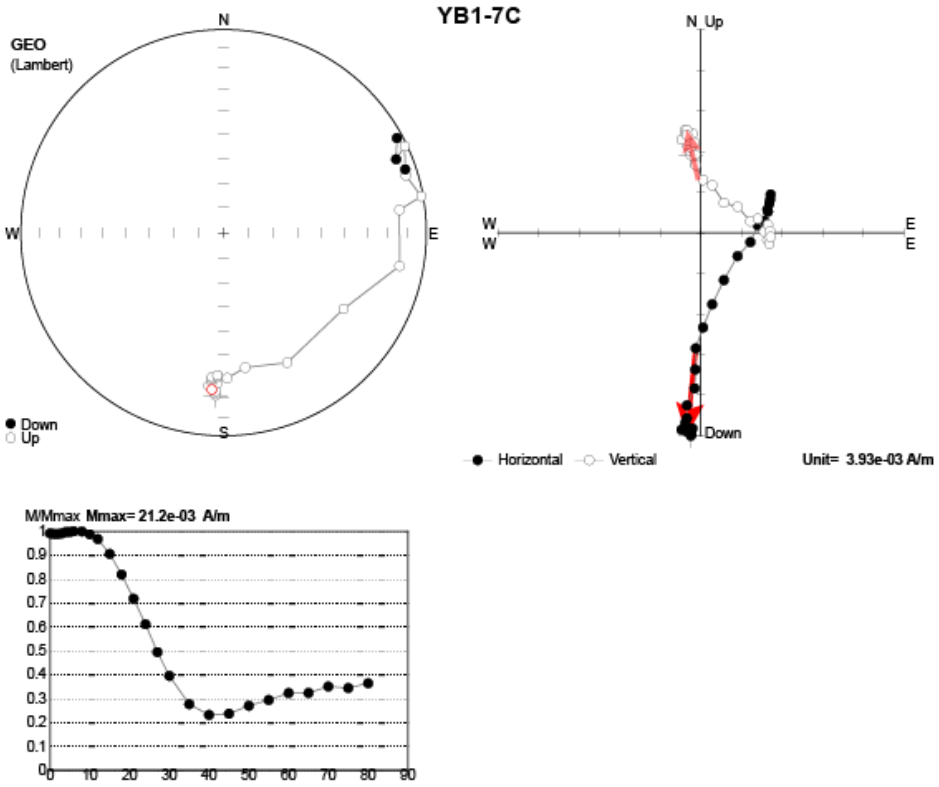

Figure 112: The sample YB1-7C has an NRM that starts at a shallow southern angle before it veers off rapidly.

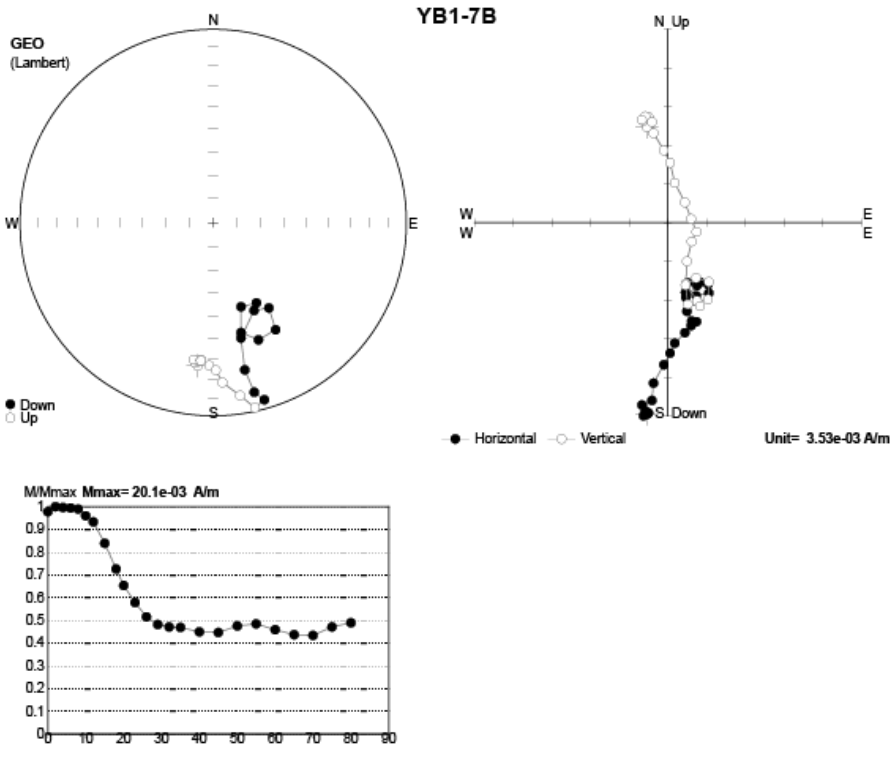

Figure 113: The YB1-7B specimen starts to spiral around a single point after some time during the AF demagnetization process. When viewed in specimen coordinates this is around the vertical.

The low stability component can be seen, but is too scattered to be of any use, also in specimen coordinates (Fig. 114).

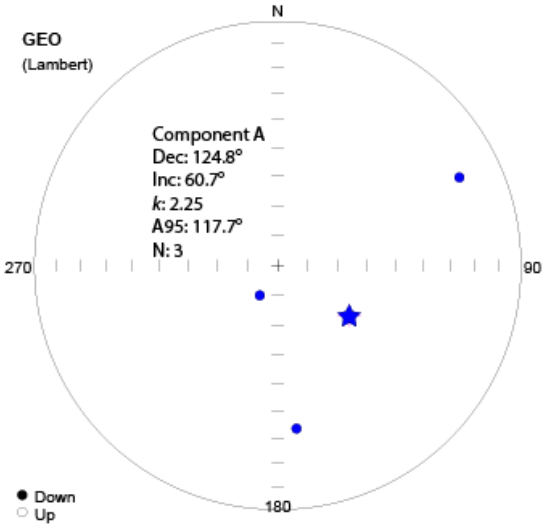

Figure 114: The low stability components seen in the three Yesnaby specimens.

The high stability component on the other hand is well grouped and points at a shallow angle upwards to the south as seen in the other dikes (Fig. 115).

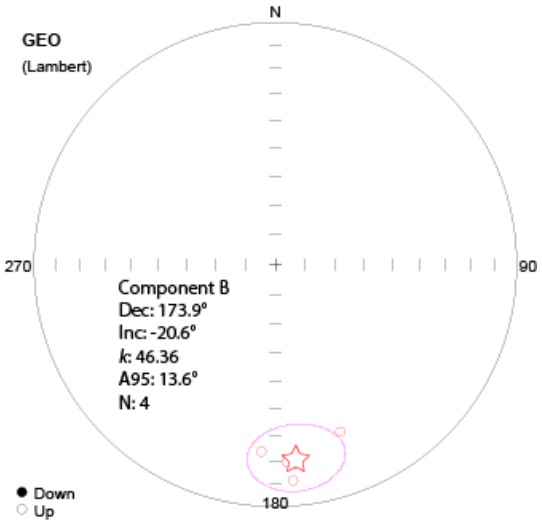

Figure 115: High stability components seen in the Yesnaby dike.

The direction seen in the high stability component at Yesnaby is well defined, but the number of specimens is low due to the poor coherence of the samples.

5.2.5 Bay of Skaill

Coordinates: 59.057N 3.338W

The Bay of Skaill dike is located on the west coast of Mainland. The exposed dike here is small, only 140cm wide and a few meters long buried in the loose rocks of the bay amongst the flagstones (Fig. 116). The dike is oriented at 70°N. Samples were collected and structural measurements were taken from the flagstones below and above the dike. To get a better spread of sampling we removed a good amount of rocks to expose more of the dike, which was later placed back to further conceal evidences of our drilling.

Figure 116: Sampling sites at the Bay of Skaill.

AMS

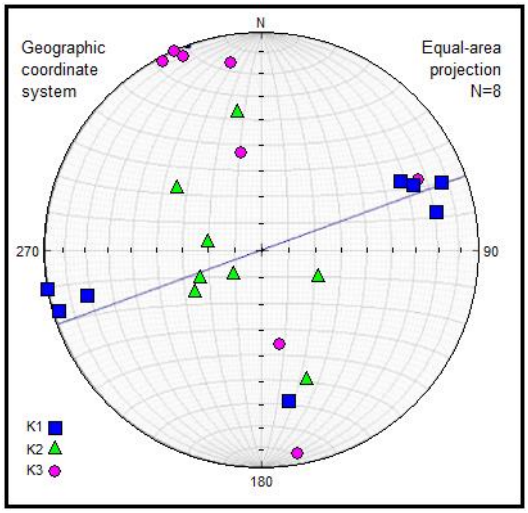

Figure 117: AMS results, Bay of Skaill dike, one axis along the dike orientation, the other two forming a possible inverted fabric.

The Bay of Skaill measurements shows a possible inverted fabric for the AMS data, the K_1 axis falls along the dike orientation, with K_2 and K_3 forming what looks like a perpendicular plane (Fig. 117).

The paleomagnetic data from Bay of Skaill proved far too chaotic following the pilot examination and was not examined further (Fig. 118).

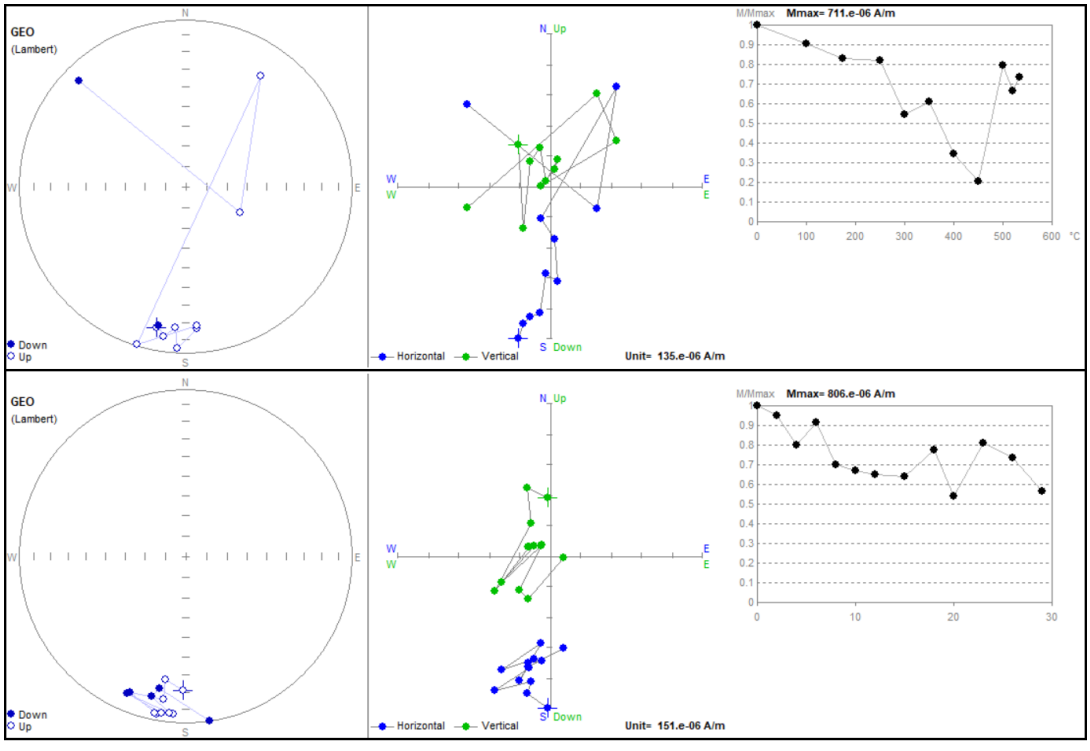

Figure 118: Erratic NRM behavior at the Bay of Skaill dike, some tendency towards a southern direction.

While there does seem to be a trend for the NRM to cluster at a shallow upwards facing southern angle, there was no opportunities to find and identify any specific component in the Zijderveld diagram. This component would fit well with the other dike localities, but that is only an observation.

Site	Slat	Slong	Lithology	Dip Dir.	Dip	N/n	D/GC	GDec	GInc	k	A95	Gplat	Gplon	Tdec	Tinc	Tplat	Tplon
Melsetter																	
Lounders Fea																	
LF1	58.917	-3.366	Basalt	261	10	8/8	8/-	171.6	5.3	42.47	8.6	-28.1	6.2	172.7	5.1	-28.2	5.0
LF2	58.919	-3.369	Basalt	261	12	8/8	8/-	163.7	8.0	50.00	7.9	-25.7	14.7	165.5	9.3	-25.3	12.6
Rackwick																	
RW1	58.869	-3.399	Basalt	312	13	8/8	8/-	187.7	-4.5	287.33	3.3	-33.1	-12.6	187.5	2.8	-29.4	-12.1
Deerness																	
DN1	58.920	-2.713	Basalt	200	4	6/8	6/-	181.7	27.2	43.10	10.3	-16.7	-4.5	182.3	23.4	-18.9	-5.1
DN4	58.920	-2.713	Basalt	194	9	3/6	3/-	145.8	37.2	23.19	26.2	-5.5	29.2	150.2	30.9	-10.6	26.3
DN5	58.920	-2.713	Basalt	263	12	6/6	6/-	194.0	49.3	14.3	18.5	-0.2	-14.8	205.4	43.8	-2.9	-25.5
											VGP	-18.7	3.2			-20.1	0.1

Site	Slat	Slong	Lithology	Dip Dir.	Dip	N/n	D/GC	GDec	GInc	k	A95	Gplat	Gplon	Tdec	Tinc	Tplat	Tplon
Birsay																	
BR1	59.138	-3.307	Camptonite	332	11	6/8	6/-	198.3	25.0	21.40	14.8	-16.2	-21.8	202.8	32.3	-11.1	-25.4
BR2	59.138	-3.307	Sandstone	332	11	8/8	8/-	180.3	-0.1	85.50	6.0	-30.9	-3.6	180.7	9.6	-26.0	-4.1
Nethertown																	
NT1	58.952	-3.319	Camptonite	272	17	7/7	7/-	178.4	-12.1	53.34	8.3	-37.2	-1.4	175.0	-10.6	-36.2	2.8
Tingwall																	
TW1	59.087	-3.039	Camptonite	50	4	5/8	5/-	191.1	-21.5	64.50	9.6	-42.3	-17.8	192.0	-18.4	-40.5	-18.7
Yesnaby																	
YB1	59.025	-3.359	Camptonite	317	11	4/4	4/-	173.9	-20.6	46.36	13.6	-41.4	4.6	172.0	-11.7	-36.5	6.5
											VGP	-34.1	351.5			-30.7	351.7

Table 2: Site-means of the ChRM component, component B. Abbreviations: Slat/Slon: Sampling location latitude and longitude. Dip dir/Dip: Structural measurements used for tilt correction. N/n: Number of samples used in the mean/Number of samples measured. D/GC: Number of linear/Great circle fits used to find the ChRM mean. Gdec/Ginc: Site-mean inclination and declination of the ChRM in geographic coordinates. k: paleomagnetic precision parameter. A_{95}: Angular cone of 95% confidence. Gplat/Gplon: Virtual geomagnetic pole (VGP) calculated from GDec/Ginc. TDec/TInc: Site-mean inclination and declination of the ChRM in tectonic coordinates. Tplat/Tplon: VGP calculated from TDec/Tinc

6. Discussion

6.1 Summary of components

6.1.1 The volcanics

Samples

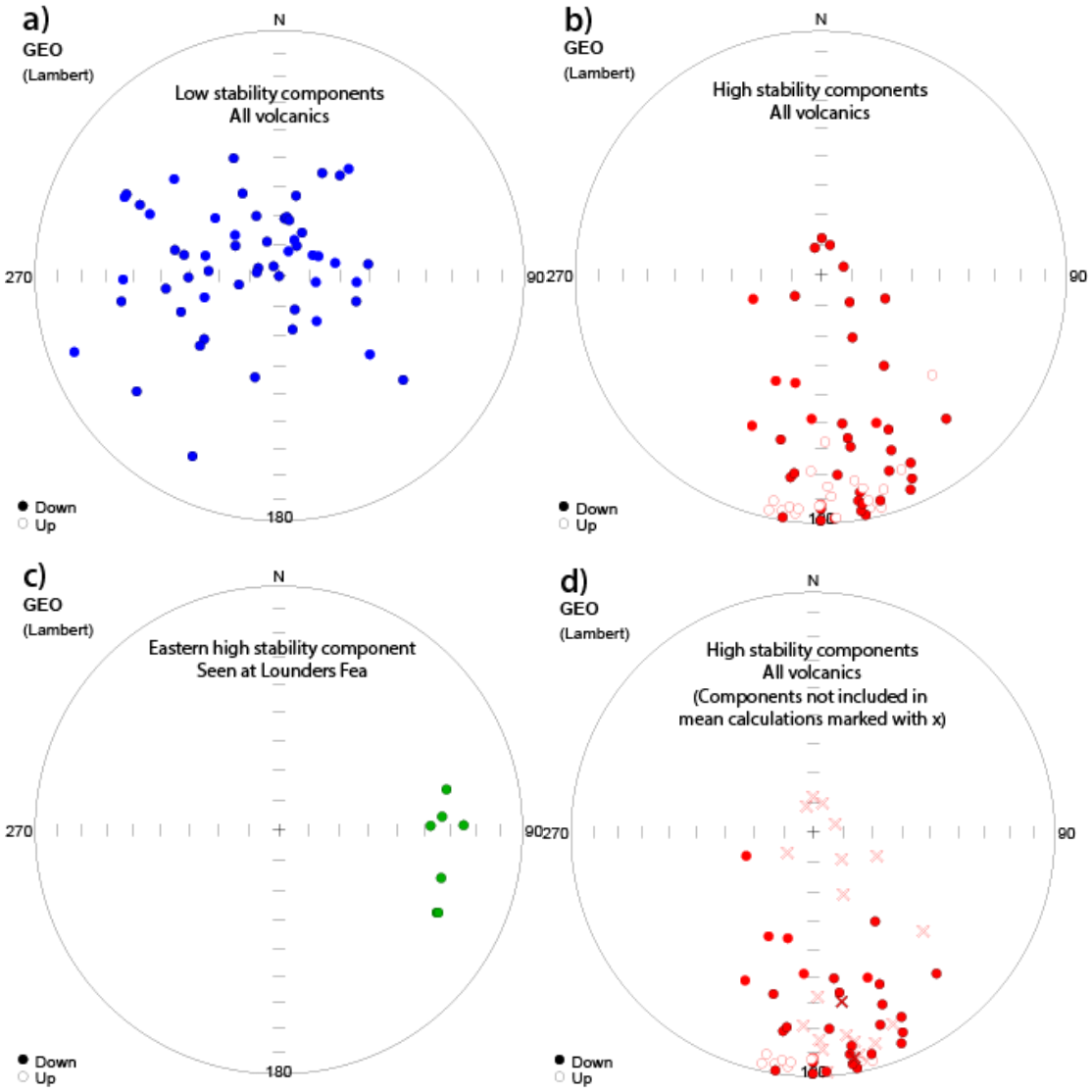

Figure 119: Component maps of all samples from the volcanics. ***a)*** *low stability components.* ***b)*** *high stability components.* ***c)*** *high stability, eastern component seen at Lounders Fea.* ***d)*** *High stability components, sites and components not included in mean calculations marked with x's.*

Low stability component

The low stability components (Fig. 119, **a**) scatter mostly around the vertical, favoring the western side.
Some of these samples group together around the vertical when viewed in specimen specific coordinates, suggesting the low stability component may be a result of the drilling process giving such a uniform vertical direction. Few samples have low stability components lying close to the present earth magnetic field, so the rest may be of an older date, but still more recent than the high stability components seen in the same samples.

High stability component

The high stability components (Fig. 119, **b**), while most showing a southern direction, seem to group into either pointing below the horizon, or above it. Some localities have higher stability component lying closer to the vertical, but these are usually outliers when the sample set is viewed as a whole and disregarded for the mean calculations. The resulting subset are all situated at a southern direction, usually within 45° of the horizontal.

The high stability components seem to favor a slightly more south-eastern direction overall, both with the downwards facing components and the upwards facing ones.

A lot of the upwards facing components seen that lies directly south and southeast are found in the Rackwick volcanic tuffs, as well as from Melsetter, these are not included in the mean calculations due to low sample numbers or high erratic movement during demagnetization (Fig. 119, **d**).
The more downwards facing vertical components all come from the Eday volcanics collected at Deerness, the Hoy Volcanics all group up close to the horizon.

Eastern component

At Lounders Fea, 3 samples from the southern LF1 locality and 4 samples from the northern LF2 locality had a well-defined eastern component (Fig. 119, **c**). The components all start close to the south-eastern cluster that's seen in the other volcanic localities before it travels along a great circle towards the east. This eastern component may be of the same origin as the reverse polarity component seen by Storetvedt and Meland (1985; Fig. 6, right) in the results from the Old Man of Hoy which is situated just to the south-west of Lounders Fea on the western coast of Hoy. The end

points towards the east seen in this study may be due to the intensity of the remanence dropping off before the end point is reached during demagnetization.

Means

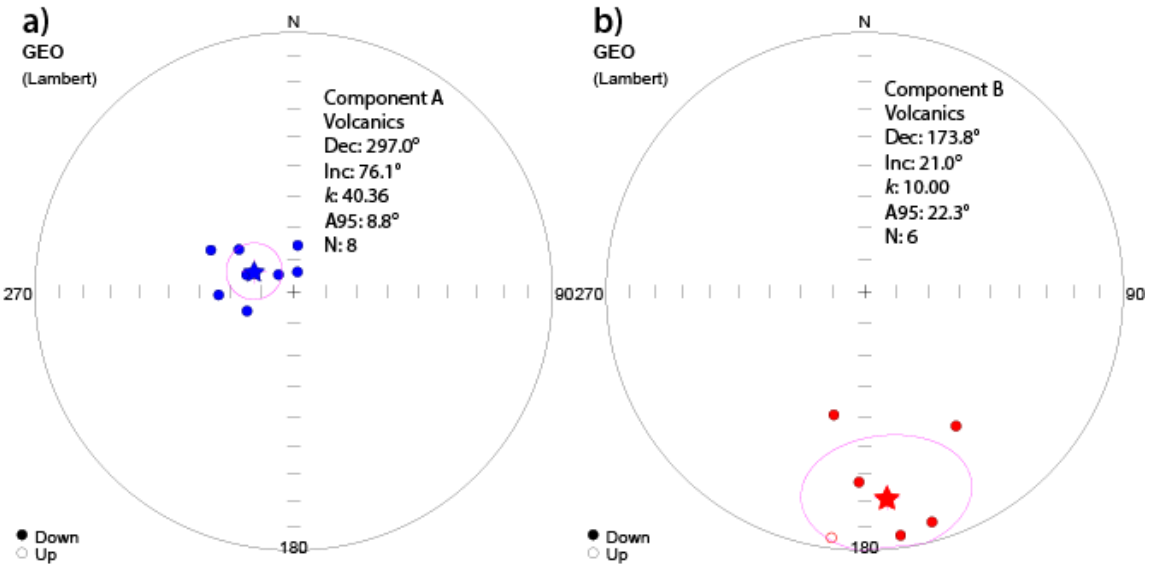

*Figure 120: Component means from the volcanics. **a)** Low stability A components. **b)** High stability B component.*

Low stability component

Looking at the means (Fig. 120, **a**) we see that the localities cluster close together just west of the vertical. The scatter we see in the sample figure translates into means with broad angle of confidences (seen in the individual localities) due to the large dispersion of individual components at each site. The resulting means on the other hand all group up with a low A_{95} value when calculating the overall mean for all volcanic low stability components.

High stability component

The means from the high stability components distill down into 5 downwards facing components, and one upwards facing one (Fig. 120, **b**). The overall mean of these fall slightly to the east of a direct southern direction and have an A_{95} angle of confidence of 22.3°. This spread is caused by the

disparity between the three localities from the Hoy Volcanics and the three representing the Eday Volcanics.

The biggest change from the sample map to the means map is the removal of most of the upwards facing components. Apart from the RW1 samples, most of the upwards facing components are seen in sample sets that did not get included in the mean calculations due to low sample numbers or unclear/erratic behaviors (RW2 and RW4, MS1). Some few are also from sites where the mean ended up under the horizontal.

6.1.2 The Dikes

Samples

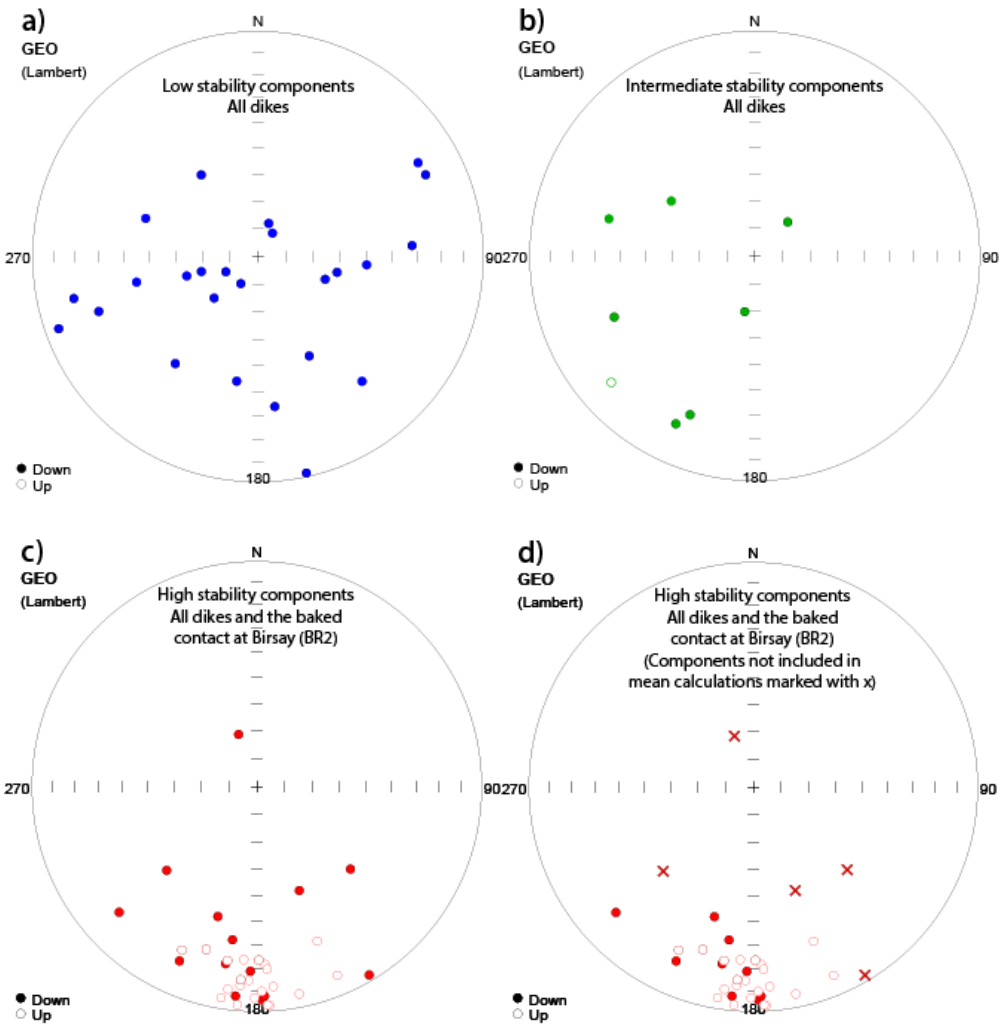

Figure 121: Component maps of all samples from the dikes. ***a)*** *Low stability components.* ***b)*** *Intermediate stability components.* ***c)*** *High stability components.* ***d)*** *High stability components, components not included in mean calculations marked with x's.*

Low stability component

A similar scatter is seen in the samples collected from the dikes (Fig. 121, **a**) as from the volcanics (Fig. 119, **a**), though for the dikes most seem to favor a slightly more southern direction than the westerly one seen in the volcanics. No discernible dominating direction is seen, mostly marking these as overprints.

Intermediate stability component

The intermediate components are showing a similar spread as seen in the low stability components (Fig. 121, **b**). These favor a more southwestern direction, but little differentiates them from the low stability components.

High stability component

The high stability components (Fig. 121, **c**) all lie towards the south with one outlier close to the present earth magnetic field. The upwards facing components are all within 30° of the horizontal, with a wide spread between southwest and southeast, though favoring a direct southern direction. The downwards facing directions seem more scattered, having a wider spread than the upwards facing components both in a horizontal and vertical direction.

The upwards facing components resembles many of the upwards facing components seen in the high stability components from the volcanics. These components in the volcanics are mostly connected to localities where the results are difficult to extract due to erratic behavior. The same directions are much clearer in the dikes, causing them to be carried over to the mean calculations. The downwards facing components is mostly seen in the dike at Birsay, while the other dikes are more uniformly upwards facing, this is reflected in the means.

Means

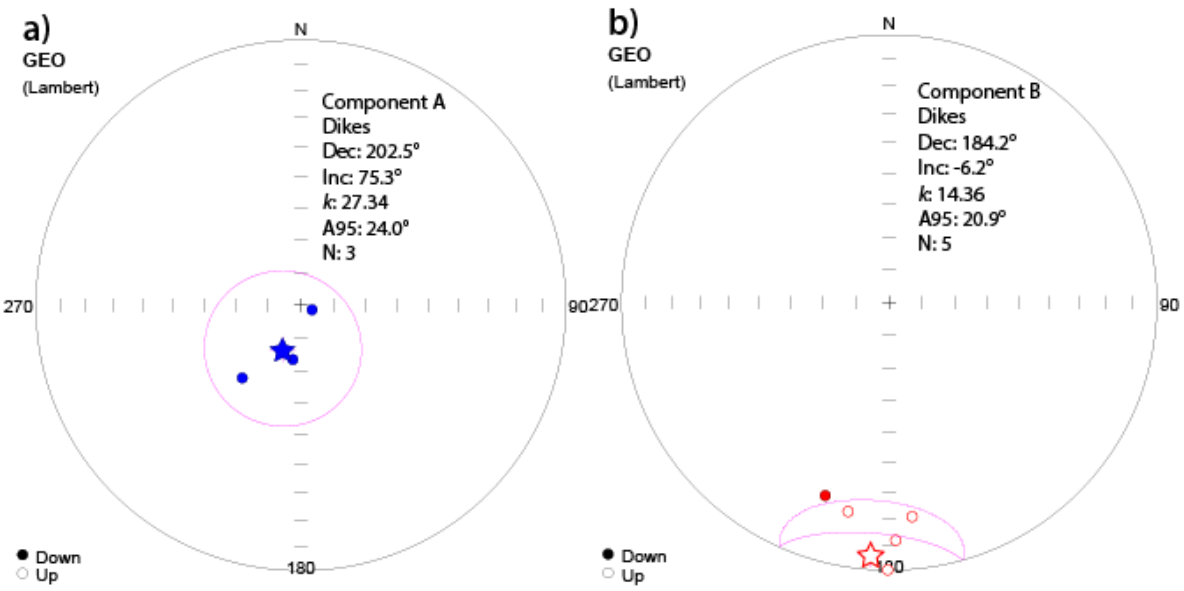

Figure 122: Component means from the dikes. ***a)*** *Low stability A component.* ***b)*** *High stability B component.*

Low stability component

The favoring towards a slight southern direction seen in the sample map (Fig. 121, **a**) is also evident in the mean calculations (Fig. 122, **a**). The wide array of scattered components coalesces into three means just south of the vertical. Between the four dikes and the contact test at Birsay, only three of the dikes had discernible low stability components, giving us the three that is left as the basis of the overall mean. The Yesnaby dike had too few results and the contact test was univectorial towards the south.

High stability component

The high stability components seen in the dikes (Fig. 122, **b**) are mostly upwards facing, slightly to the southwest close to the horizontal. The one downwards facing component (from BR1, the Birsay dike) causes the A_{95} angle to widen to 20.9° and pushes the mean towards a more horizontal direction.

The dike means preserves the upwards facing directions from the sample map to the means map, thanks to clearer results during the demagnetization process in comparison to the volcanic samples with similar directions. The overall mean calculation for the dikes is close to the high stability component seen at Rackwick (RW1),

6.2 Virtual Geomagnetic Pole (VGP)

6.2.1 Calculating the VGP

Calculating the Virtual Paleo pole given the site means gives the following table for the volcanics:

Site name	Gplat	Gplon	Tplat	Tplon
LF1	-28.1	6.2	-28.2	5.0
LF2	-25.7	14.7	-25.3	12.6
RW1	-33.1	-12.6	-29.4	-12.1
DN1	-16.7	-4.5	-18.9	-5.1
DN4	-5.5	29.2	-10.6	26.3
DN5	-0.2	-14.8	-2.9	-25.5

This was done using the Remasoft 3.0 software, which takes into account the site latitude and longitude as well as the site means for the chosen component.

The Fisher (1953) averaged VGPs is calculated and gives the following paleo pole:

Paleo pole: Volcanics - in geographic coordinates:

Plat	**Plon**	**n**	**r**	**k**	**A_{95}**	**csd**
-18.6	3.2	6	5.6708	15.2	17.8	20.8

Paleo pole: Volcanics - in tilt corrected coordinates:

Plat	**Plon**	**n**	**r**	**k**	**A_{95}**	**csd**
-20.1	0.1	6	5.6819	15.7	17.4	20.4

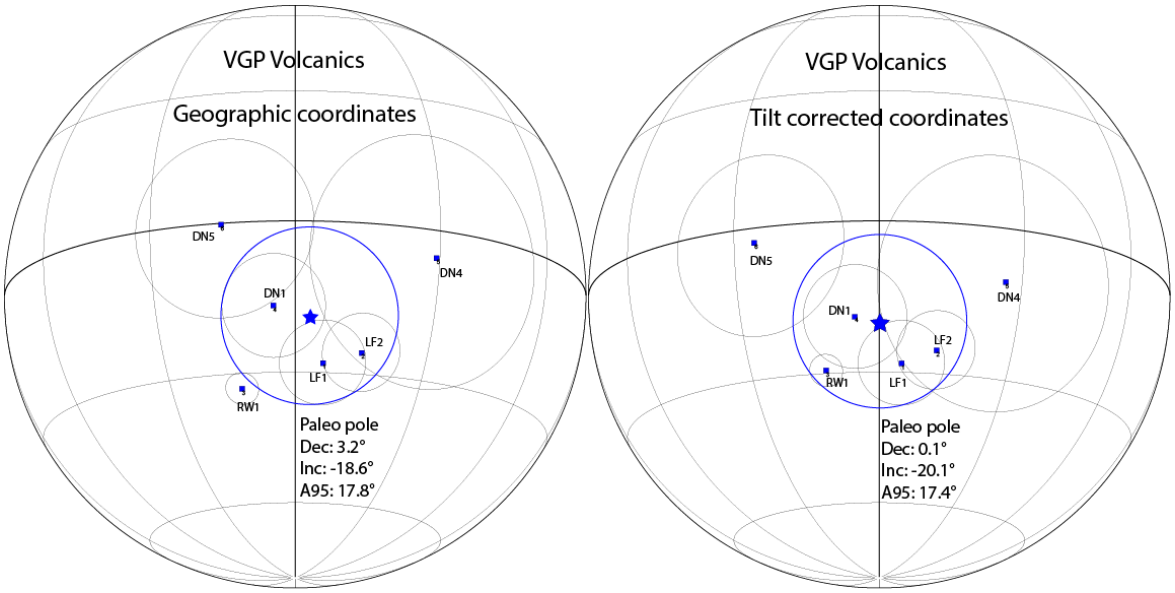

Figure 123: Calculated VGPs for the volcanics, given the site means and site latitudes and longitudes. ***Left****: Geographic coordinates.* ***Right:*** *Tilt corrected coordinates.*

The VGPs for the volcanics group to the south of the equator, with an overall mean and paleo pole falling just to the east of a direct southern direction (Fig. 123). The two sites from Lounders Fea, the one from Rackwick and the first from Deerness lies close to the overall mean marked with a blue star in figure 123. The two furthest away with larger A_{95} cones are the DN4 and DN5 sites.

When correcting for the bedding the VGPs moves closer together, and the new paleo pole is now almost directly south (Fig. 123, right).

And then for the dikes:

Site name	Gplat	Gplon	Tplat	Tplon
BR1	-16.2	-21.8	-11.1	-25.4
BR2	-30.9	-3.6	-26.0	-4.1
NT1	-37.2	-1.4	-36.2	2.8
TW1	-42.3	-17.8	-40.5	-18.7
YB1	-41.4	4.6	-36.5	6.5

Paleo pole: Dikes - in geographic coordinates:

Plat	Plon	n	r	k	A_{95}	csd
-34.1	351.5	5	4.8770	32.5	13.6	14.2

Paleo pole: Dikes - in tilt corrected coordinates:

Plat	Plon	n	r	k	A_{95}	csd
-30.7	351.7	5	4.8284	23.3	16.2	16.8

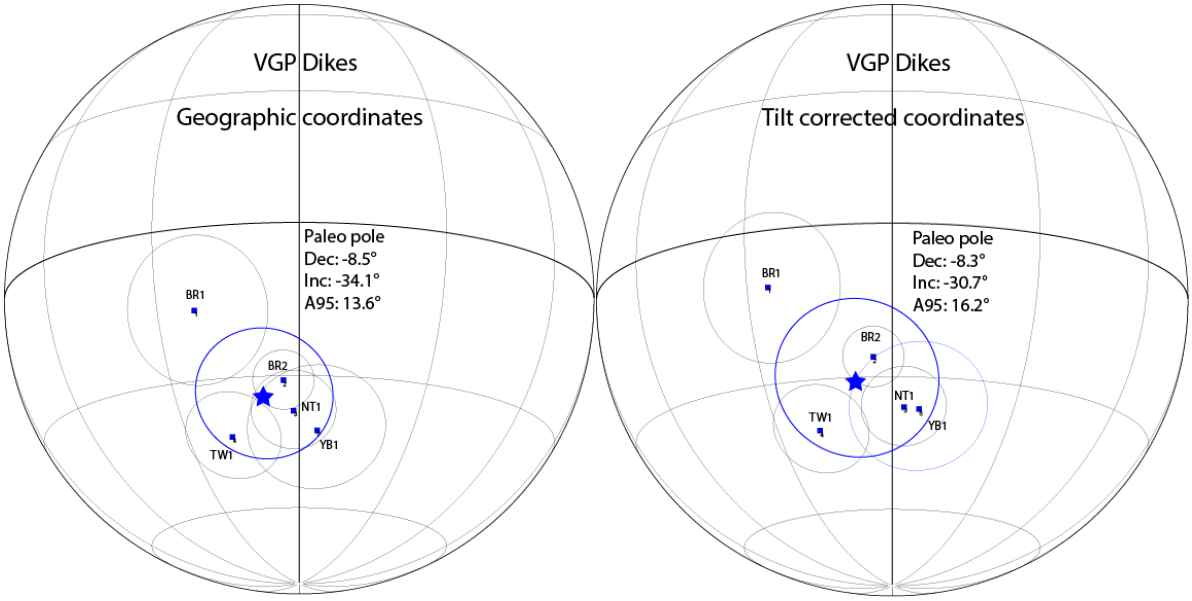

Figure 124: Calculated VGPs for the dikes, given the site means, site latitudes and longitudes. ***Left****: Geographic coordinates.* ***Right****: Tilt corrected coordinates.*

The VGPs for the dikes have four which clusters close together, with the BR1 dike falling further to the northwest than the rest (Fig. 124). This correlates with the site component means, where the BR1 is also further away from the other 4 localities (Fig. 122, b). The resulting paleo pole is still well situated close to the four closest sites.

The paleo pole is placed towards the south-southwest, with an inclination of -34.1°, declination -8.5°.

When correcting for the bedding tilt the mean moves slightly northwards, with almost no change in declination.

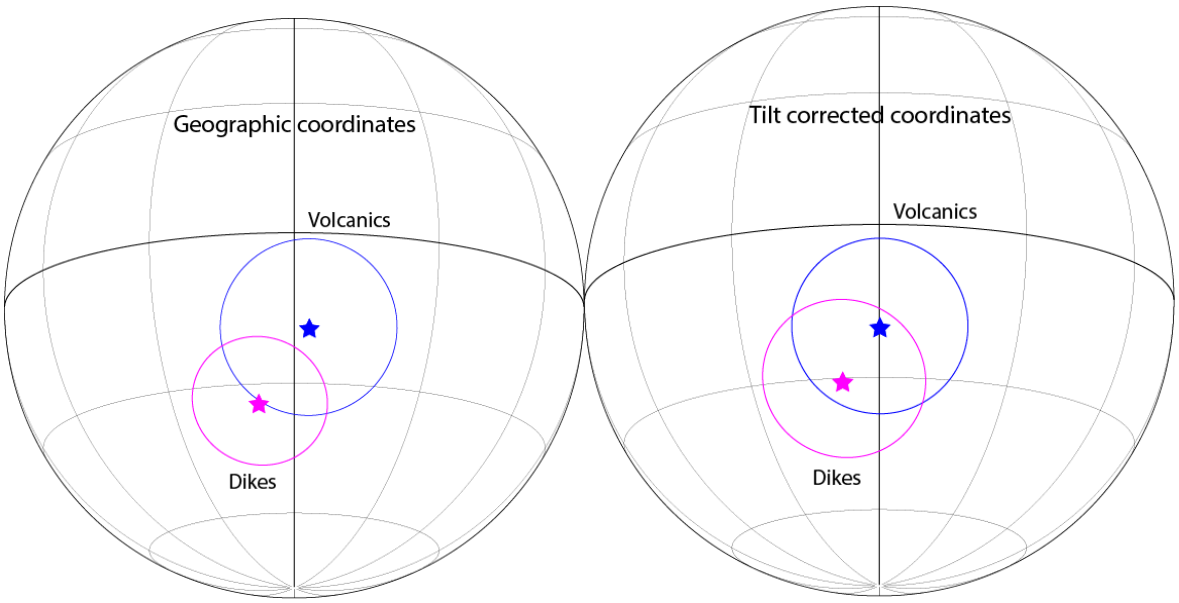

Figure 125: The two paleo poles. The paleo pole for the volcanics is marked in blue and the pole for the dikes is marked in purple.

Comparing the two calculated paleo poles, we see some overlap between their angle of 95% confidence, so we can not with certainty say that these are two distinctly separate components (Fig. 125). The overlap increases when correcting for bedding tilt due to the volcanics moving slightly westward and the dikes moving north.

The degree of overlap can be calculated statistically using the common_mean function, a part of the pmagpy python library. The inclination and declination of the various site means is compared between the volcanics and the dikes, and the degree of statistical overlap is calculated and displayed (Fig. 126).

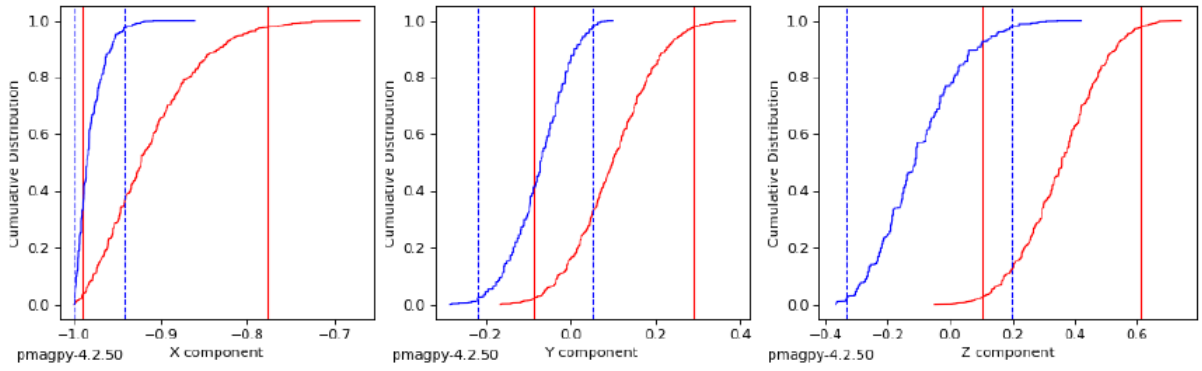

Figure 126: Statistical calculation of common mean between the volcanics and the dikes in x, y and z components. Geographic coordinates used in the list of inclinations and declinations.

There is some statistical overlap between the two populations, with varying degree between the three components.

6.2.2 The Apparent Polar Wander Path (APW)

The Devonian Volcanics

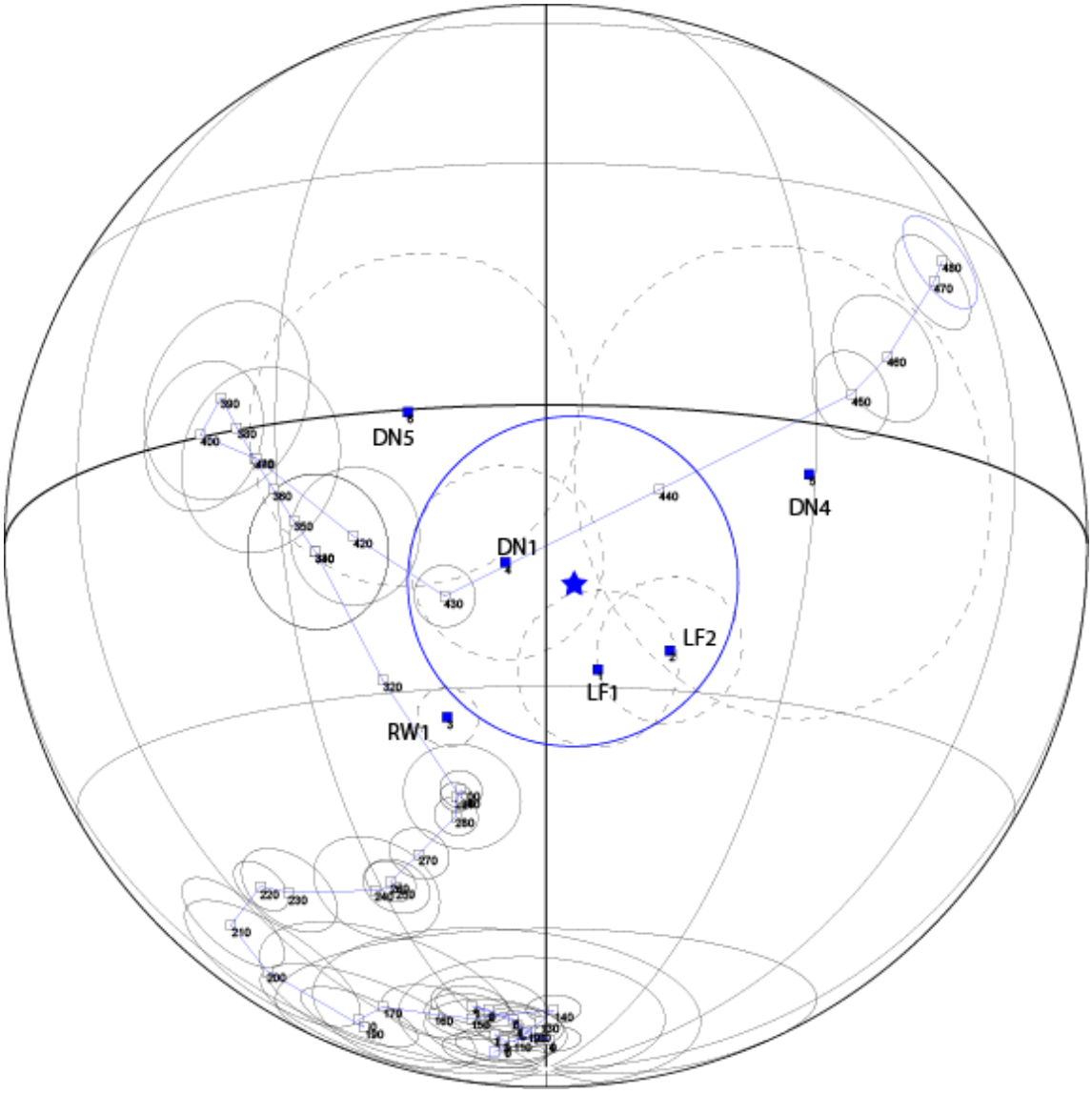

Figure 127: The paleo pole for the volcanics (blue) in comparison to the current APW reference for northwestern Europe. Site VGPs marked with blue boxes, A95 in dashed lines. The 380 Ma reference is situated at the equator, ca. 32° W.

We can compare our VGPs and the corresponding paleo pole to the current reference and expected paleo pole for northwestern Europe (Fig. 127).

Our volcanics, which are 378 Ma old, should have a paleo pole close to the equator, over 30° further west than what is observed in the Orkney volcanics. Our paleo pole is much closer to the expected paleo pole for western Europe between 440 Ma and 430 Ma, but there is no geological basis for this being a true Silurian paleo pole.

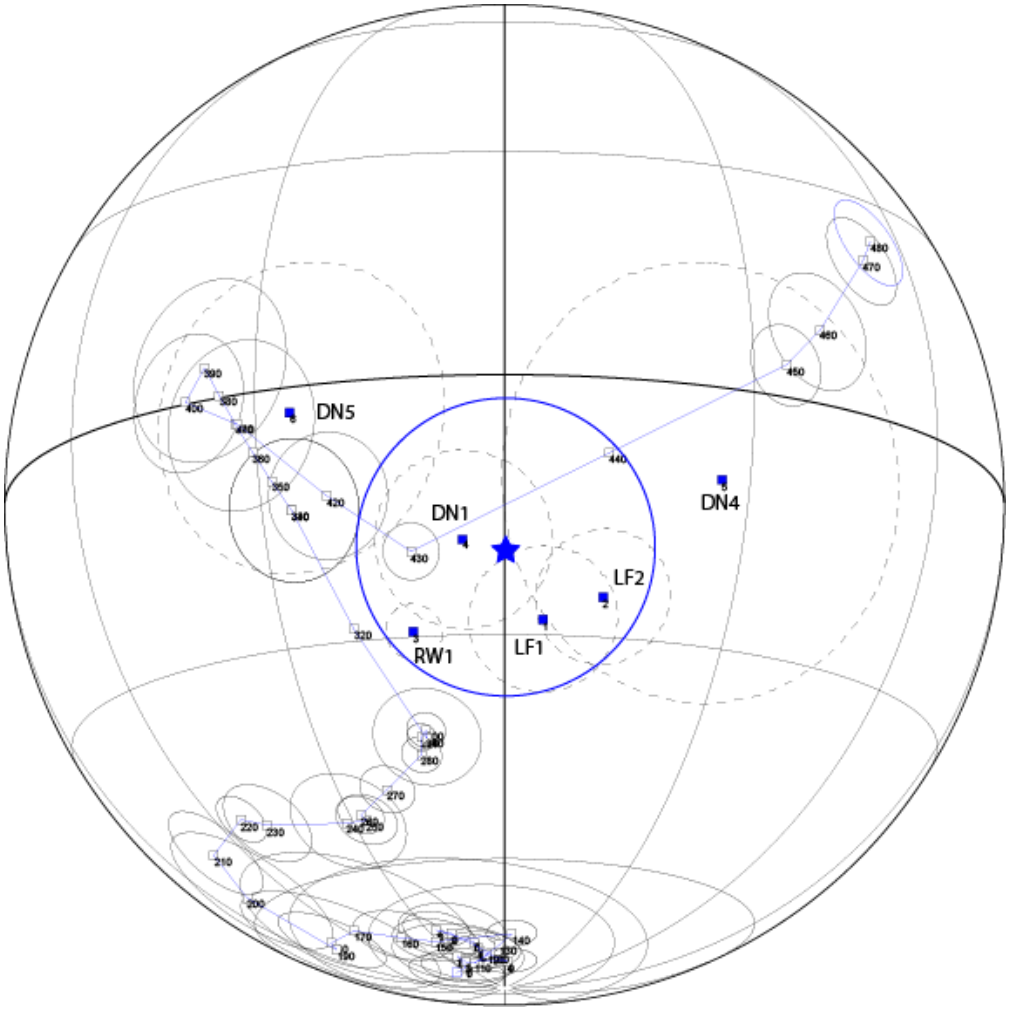

Figure 128: Tilt corrected paleo pole and reference APW.

With tilt correction, the volcanic paleo pole moves a little closer to the reference line between 430 Ma and 440 Ma (Fig. 128). It is interesting to note that the DN5 VGP falls close to the expected 380 Ma reference, while DN4 is way off towards the east (Both with quite large A_{95} cones).

The dikes

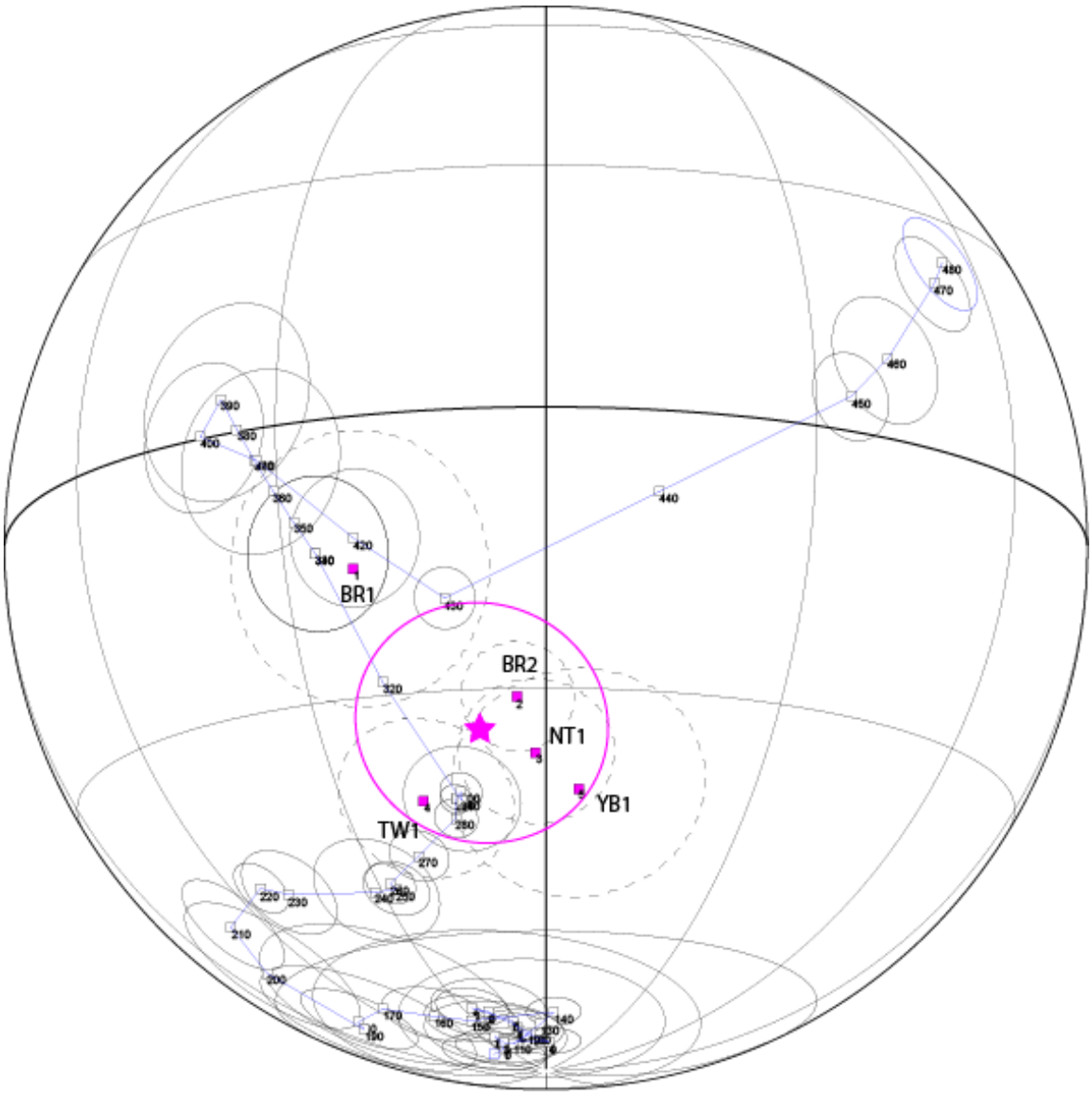

Figure 129: The paleo pole for the dikes (purple) in comparison to the current APW reference for northwestern Europe. Site VGPs marked with purple boxes, A_{95} in dashed lines. The 300 Ma reference is situated just to the south-southwest of our paleo pole, the 310 Ma to 280 Ma poles lies close together.

The paleo pole calculated from the dikes however is closer to the expected reference (Fig. 129). The 300 Ma reference for northwestern Europe is situated just to the south-southwest of our pole. The Birsay dike pulls the paleo pole northwestwards, while the baked contact test (BR2) falls close to the other dikes and the reference pole.

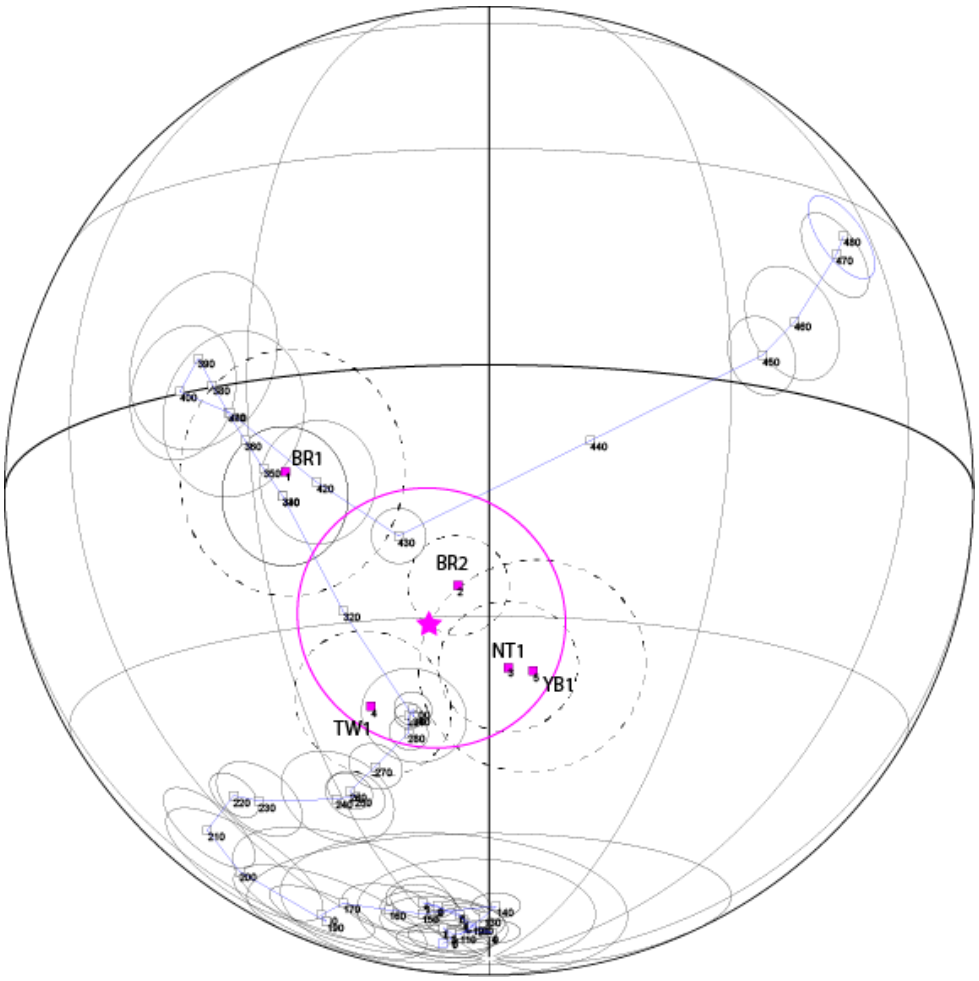

Figure 130: Tilt correction moves the paleo pole a little further away from the reference pole.

When correcting for bedding tilt the paleo pole moves northwards, away from the reference at 300 Ma (Fig. 130). The Nethertown and Yesnaby dikes also moves closer together.

Looking at the sites that lies close to our paleo pole and reference, it looks like they have been shifted east-northeast from the expected position at 304 Ma. The TW1 dike lies to the west of the reference, but this site was defined by very low strength of the remanence, which may have led to the slight shift westwards. The BR1 results are harder to interpret, lying so far away from the other dikes, and its own baked contact test. The BR1 dike was internally consistent, with six out of eight specimens falling within the same area, so whatever has affected the remanent direction here has managed to affect the whole dike.

6.2.3 Comparison with previous results

The Hoy Volcanic member

From the set of 60 specimens collected in Storetvedt and Petersens study in 1971, 7 specimens showed a slightly southwestern direction, just below the vertical at declination 205°, inclination 8.4°. They observed a demagnetization behavior where the lavas would lose 50% intensity by 200°C, and the tuffs did not reach a similar level until 600°C.
This demagnetization behavior was not observed in the same volcanic samples from this thesis. In the lavas from RW1 the stability remained stable close to 100% intensity for all samples demagnetized thermally until the 200°C step was reached, from which the stability started to drop. The tuffs of RW2 and 4 on the other hand does match up with the previous studies, holding on to their intensity until 600°C and above.

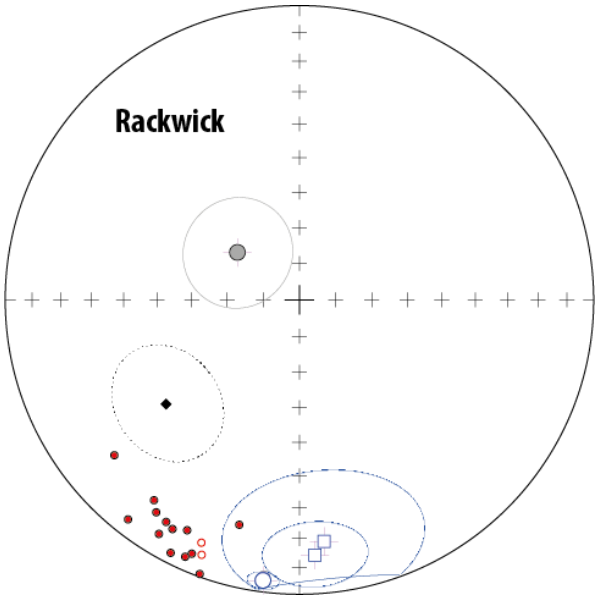

Figure 131: Old and new studies on the Rackwick basalts and tuffs. Diamond: Morris et al., 1973. Red circles: Storetvedt and Meland, 1985. Grey circle: Overprint, this study. Blue circle: B-component, this study. Blue squares: B-component, Rackwick tuffs, this study.

During the 1985 study by Storetvedt and Meland, they also sampled the sediments below the Old Man of Hoy. In these sediments they saw another magnetization directed almost directly south with an upwards inclination of around 30° (Storetvedt and Meland, 1985). This behavior resembles the components observed in the Rackwick tuffs in this study (Fig. 131), and from the dikes of Nethertown, Tingwall and Yesnaby (NT1, TW1 and YB1).

The Rackwick lava samples from that study gave 15 specimens with a stable end point in the southwest, similar to the samples from the same locality in this study (Fig. 131).

Storetvedt and Meland also observed a movement towards the northeastern quadrant in a few of the thermally demagnetized specimens, suggesting a presence of the two-polarity magnetization seen in the 1971 study. This northeastern movement was not observed in the basalts in this study, but it did show up in the volcanic tuffs.

Morris *et al.* 1973, collected and studied samples from Orkney, among which were rocks sampled from Lounders Fea and Melsetter. The Lounders Fea specimens were not demagnetized, and the reported NRM is the initial state of the rocks (Fig. 132; Morris *et al.,* 1973). The Melsetter samples were demagnetized using AF, and the end point seen is close to the starting NRM (Morris *et al.,* 1973). Both components are at a medium steep south-southwestern angle. Resembling some of the results from Deerness seen in this study.

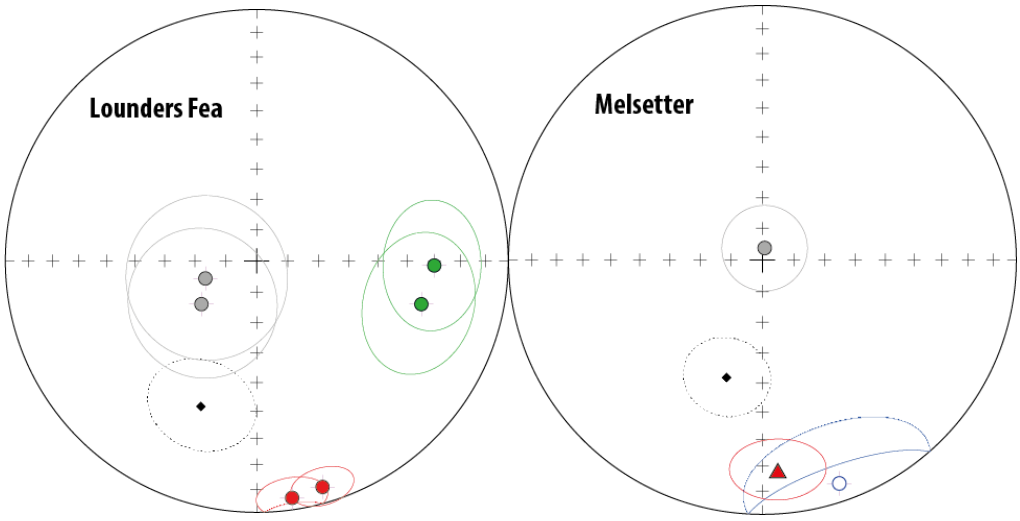

Figure 132: The old study by Morris et al. 1973 is marked with a black diamond. ***Left:*** *Grey circles are the low stability; red circles are high stability and the green circles are the eastern component.* ***Right****: the red triangle is the suggested great circle intersection point; blue is the intermediate stability component seen at Melsetter.*

<u>The Eday volcanics</u>

There seem to be better similarities between the Robinson (1985) study and this thesis (Fig. 133). The contact test in Robinson's study beneath the Deerness lavas showed a low stability component close to the present earth's magnetic field, and a higher stability component falling downwards towards the south (Fig. 9, top left; Fig. 133; Robinson, 1985). The baked contact zone, as far away as 20cm from the volcanics shows a noteworthy agreement with the mean directions seen in the above-lying lavas (Robinson, 1985).

The baked contact test in this study show a similar direction to the lava above, but sadly in my case the direction seen in both the lava and baked contact is an almost vertical direction, falling close to the present earth's magnetic field (Fig. 133, grey square).

The direction around the present earth's magnetic field seen in the baked contact test in this thesis and in a few specimens in the lava, is also seen by Robinson in specimens from South Ronaldsay

from the Upper Eday Sandstone (Robinson, 1985). This component is found at both low stabilities and high and is believed to be a viscous remanent magnetism (VRM) and a chemical remanent magnetism (CRM) respectively in origin (Robinson, 1985). Morris *et al.* 1973 also saw a similar component falling just to the west of the vertical. In a few samples an upwards facing southern direction is seen in the intermediate stability range, similarly in direction to the component seen in the Rackwick tuffs and in the dikes in this study.

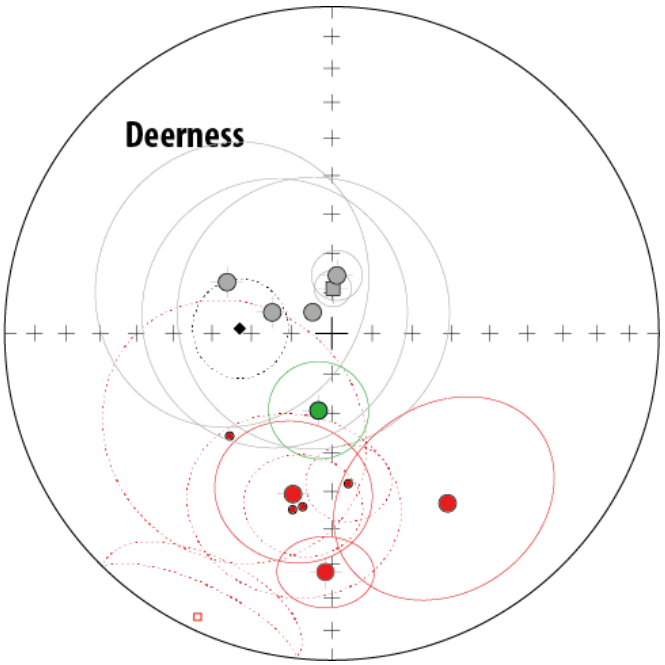

Figure 133: The old and new studies from the Eday Volcanics. Morris et al., 1973 marked with a black diamond. The small red circles and squares are Robinson, 1985, and the bigger grey (overprint), red (ChRM) and green (Highest stability) circles are from this study.

Overall the directions seen in this study corresponds decently well with what Robinson found, although the DN4 set of samples does veer off towards the east in comparison to the rest.

The Dikes

The components seen in the dikes are a little different from the earlier study by Storetvedt and Otterå (1987). The lack of overlap between sampled dikes may explain why the directions seen in this study does not correspond well with the earlier study. The Birsay dike is the only dike sampled by both studies, and while one specimen from my study does fall in the *B* category defined by Storetvedt and Otterå (BR1-4A), the rest of the specimens favor a more southern to southwestern direction. The closest evidence of the *A* component defined by the earlier study, with a more steep upwards facing southeastern direction, is present in the samples collected from the Nethertown and Yesnaby dikes, though these two fall just on the southern side of where Storetvedt and Otterås specimens seem to group. The dike at Billia Croo, numbered 7 in Storetvedt and Otterås study, is close to the Nethertown dike from this study, and displays similar behavior.

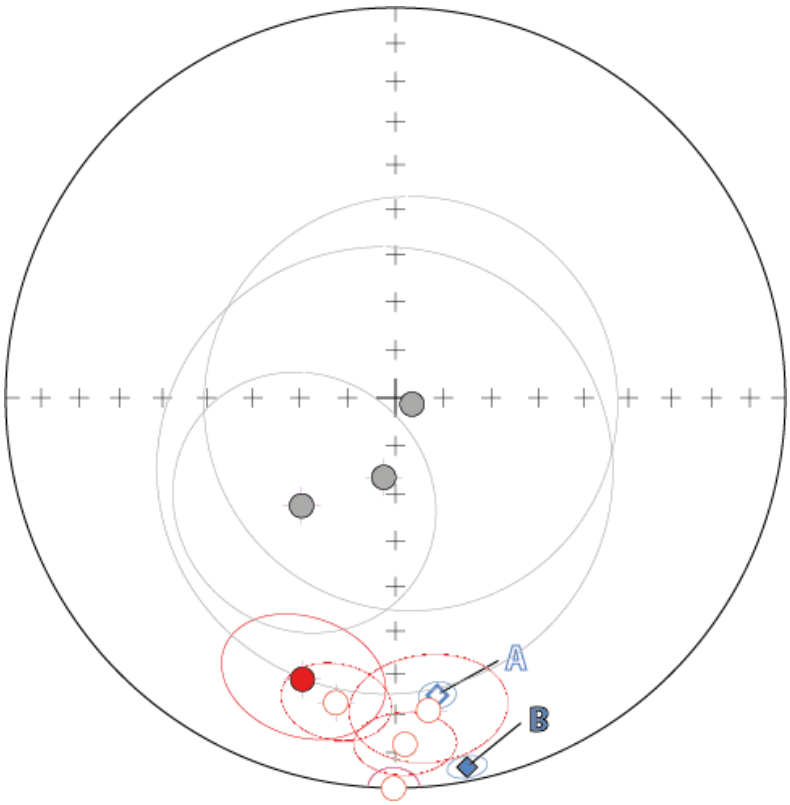

Figure 134: The components seen in the dikes. The two diamonds are from Storetvedt and Otterå (1987). B component is believed to be the older of the two.

6.3 The big picture

There seem to be the possibility to divide the components seen in the Devonian volcanics into two categories, called 'B1' and 'B2' in figure 135. The B1 components are mostly pointing towards a south-southeastern direction, above the horizontal. This set is seen in the Rackwick volcanics and tuffs, as well as in the Melsetter samples. This set of components resembles the dike components and are possibly a Permo-Carboniferous overprint acquired at the same time as the emplacement of the dikes.
The B2 set is all downwards facing, south-southeast. These mostly come from Lounders Fea and Deerness, as well as the possible great circle intersection from Melsetter.

Looking at the components in the APW comparison (Fig. 127 and 128) the 'B2' set of components is most likely our closest representation of a Devonian magnetic remanence, but they have been moved counterclockwise from the expected reference at 380 Ma.

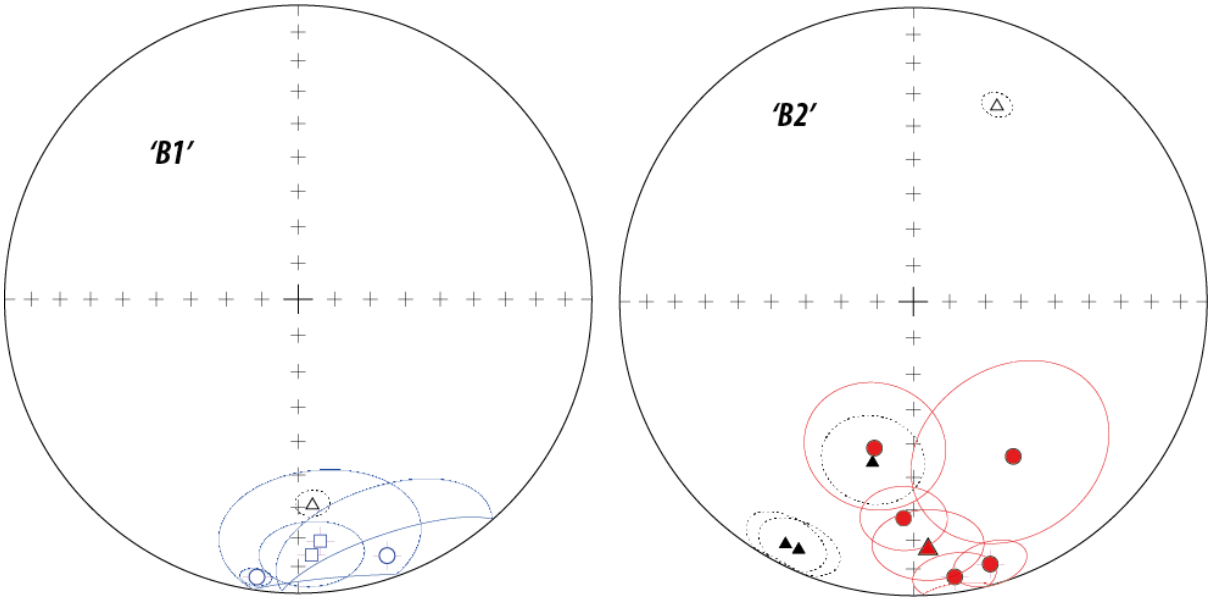

Figure 135: Possibly two sets of components seen in the volcanics.

Storetvedt and Otterå (1987) observed the possible counterclockwise rotation of their A and B components in comparison to the expected magnetic field (Fig. 11) when looking at the dikes. Looking at the components seen in this study in comparison to the latest data on the polar wander path for northwestern Europe we observe a similar eastward shift from where the expected pole should be at the time of emplacement for both our volcanic rocks and the dikes (Fig. 136).

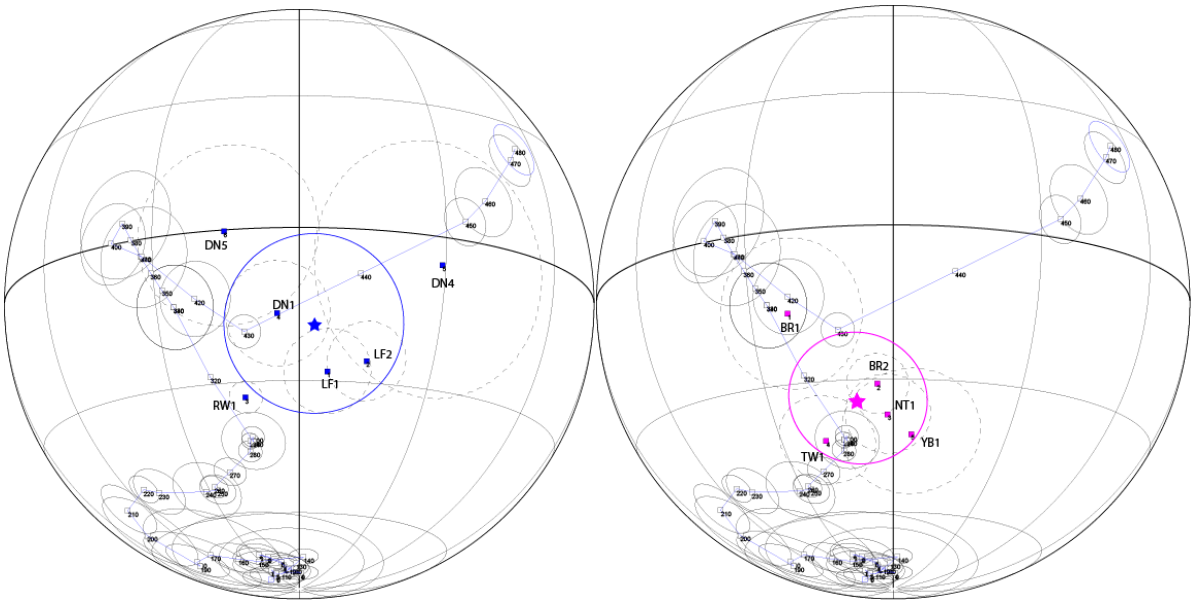

Figure 136: The two sets of samples and the APW reference. Devonian volcanics in Blue and Carboniferous Dikes in Purple.

Storetvedt and Otterå (1987) explained the shift in direction of the dikes by proposing the emplacement of the dikes happened at the tail end of a 600km sinistral movement along the Great Glen Fault (Fig. 137). This was then followed later by a dextral reactivation of the fault to achieve the counterclockwise rotation needed to explain the eastward shift of the directions in the dikes (Fig. 11).

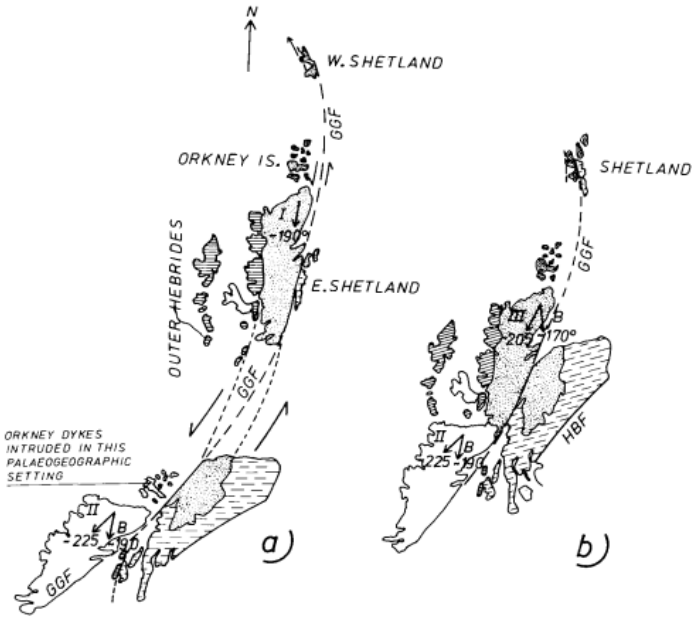

Figure 137: The proposed tectonic movements by Storetvedt and Otterå (1987) along the Great Glen Fault.

The Devonian components in this study seem to have experienced a greater displacement eastward than the Carboniferous dikes, which would indicate that any dextral movement along the fault started much earlier, before the emplacement of the dikes. The counterclockwise movement of the components looks to be mostly rotational, there is little latitudinal movement of the components seen, ending up just a little further south than the expected reference. This would indicate that the movement along the transcurrent faults in the area did not displace the Orkney Islands in any meaningful fashion, instead causing the rotation we see in the paleomagnetic data today along a rotational axis very close to the Orkneys.
Looking at the transcurrent faults around the Orcadian Basin (Fig. 2) the movements proposed along these should not induce a counterclockwise rotation of the Orcadian Basin, so there should have been an opposite movement in some of these faults in the Devonian and Carboniferous.

The lack of latitudinal movement in the paleomagnetic data from the Devonian rocks makes Storetvedt and Otterås (1987) proposal of a 600km sinistral movement during this time period incorrect, if there has been any sinistral displacement, it would have happened earlier, if at all. There

are no signs of the previously proposed large latitudinal displacements along the Great Glen Fault seen in the paleomagnetic data, nor in the structures of Orkney.

There is no structural evidence seen on the Orkney Islands of this rotation, so the rotating block would have to encompass the island group as well as some of the surrounding basin. There are some fault zones along the western edge of the Orcadian Basin (Fig. 1), and it would be interesting to see if there are any evidences of horizontal displacement in this area or further afield from seismic imagery of the seabed to see if there's any indication of how large the rotating block was.
The only large-scale structures around the Orcadian Basin is the transcurrent faults running from the northeast towards the southwest on either side of the basin and there's been no reported signs of any rotation reported on mainland Scotland, so the seabed between the Orkney Islands and mainland Scotland might be a place to look for any signs of this possible rotation, and to the north of the island group.

Further paleomagnetic surveys of the Orkney Islands would help narrow the A_{95} areas around the proposed site components and enable us to better pinpoint the actual displacement seen in the paleo pole. More data should also make this interpretation more robust if the same trend is seen. Sampling the younger dikes and sediments would help us further constrain the time of rotation, if the younger rocks falls around the expected references, we would know a little more of the end of rotation. Older rocks, below the sampled volcanics could also give further data on when the counterclockwise rotation started, or how quick the movement was. The fact that we can see the displacement in both the Devonian volcanics, the Carboniferous dikes, and the probable Carboniferous overprint seen in the volcanics gives us a "real time" view of the rotation. More datapoints both older and younger would help give us a better picture of the events.

Sampling further afield from Mainland (Orkney) and Hoy, on the northern islands as well as from Shetland and northern mainland Scotland could also be an angle of attack to find the extent of the rotating block. If there is no evidence of any rotation seen in these samples, we would know more about the extent of the rotating block.

Looking at seismic imagery of the seabed in the Orcadian basin would be a good place to start searching for the required structural evidences of the proposed rotation of the Orkneys suggested by the paleomagnetic data, as well as conducting newer paleomagnetic survey of the surrounding area. If there has been a large-scale rotation of the Orkneys, the evidence should still be visible in the subsurface somewhere.

7. Conclusion

Samples from the Hoy Volcanic member were drilled from three different localities, totaling four sets of samples. These were accompanied by four set of samples taken from the volcanic tuffs at Rackwick. Of these, only the volcanic basalts from Rackwick and the two sets of volcanic rocks from Lounders Fea yielded good results, though some evidence of stable end points can be seen in the Rackwick tuffs and from Melsetter.

The directions found in the Rackwick volcanics are close to the older results from previous studies, pointing to a shallow south-southwestern direction. The Lounders Fea sets have a ChRM at a shallow south-southeastern direction, slightly rotated in comparison to the older studies and the direction found at Rackwick, but still close by. The ever so slightly younger Deerness volcanics resembles the older studies by Robinson (1985), giving a south-southwestern ChRM which is steeper than the Hoy Volcanics.

The dikes gave few comparisons due to the choices of which dike to sample, but the overlap shows similarities between the old and new results. The dikes have a ChRM pointing towards a very shallow south-southeastern direction, a little rotated counterclockwise and upwards in comparison to the volcanics.

The paleo poles calculated for the Devonian volcanics and the Carboniferous dikes shows a rotation counterclockwise that has endured over the entire period, shifting the remanence seen in the Devonian rocks over 30° eastwards, while the Carboniferous dikes have been shifted less than 15° at the most when looking at the Nethertown and Yesnaby dikes. This would mean the proposed dextral movement along the Great Glen Fault started much earlier, long before the emplacement of the dikes at 304 Ma and that the previously modeled sinistral movement along the Great Glen Fault is incorrect.

8. References

Astin, T. R., (1985). “The palaeogeography of the Middle Devonian Lower Eday Sandstone, Orkney”. Scottish journal of geology, 1985-02, Vol.21 (3), p.353-375. doi: 10.1144/sjg21030353

Astin, T. R., (1990). “The Devonian lacustrine sediments of Orkney, Scotland; implications for climate cyclicity, basin structure and maturation history”. Journal of the Geological Society, 147(1), pp.141-151. doi: 10.1144/gsjgs.147.1.0141

Baxter, A. N. and Mitchell, J. G. (1984). “Camptonite-Monchiquite dyke swarms of Northern Scotland; Age relationships and their implications,” Scottish Journal of Geology. Geological Society of London, 20(3), pp. 297-308. doi: 10.1144/sjg20030297

Bird, P. C. (2014). “Tectono-stratigraphic evolution of the West Orkney Basin: implications for hydrocarbon exploration”. (Doctoral dissertation, Cardiff University).

Bjerga, A. D. (2017). “The Caledonian tectonomagmatic evolution of the Orkney Islands, Scotland”. (Master Thesis, Department of Geosciences, University of Oslo)

Brown, J. F. (1975). “Potassium-argon evidence of a Permian age for the camptonite dykes: Orkney,” Scottish Journal of Geology, 11(3), pp. 259-262. doi: 10.1144/sjg11030259.

Butler, R. F. (1992). “Paleomagnetism : magnetic domains to geologic terranes”. Boston: Blackwell Scientific Publications.

Chew, D. M. and Strachan, R. A. (2014). “The Laurentian Caledonides of Scotland and Ireland”. Geological Society, London, Special Publications, Vol. 390, pp. 45-91. doi: 10.1144/SP390.16

Cohen, K. M., Finney, S. C., Gibbard, P. L. & Fan, J. -X. (2013; updated 2020/03). “The ICS International Chronostratigraphic Chart”. Episodes, 2013, Vol.36 (3), p.199-204. doi: 10.18814/epiiugs/2013/v36i3/002

Coward, M. P., Enfield, M. A., & Fischer, M. W. (1989). “Devonian basins of Northern Scotland: extension and inversion related to Late Caledonian—Variscan tectonics”. Geological Society, London, Special Publications, 1989-01-01, Vol.44 (1), p.275-308. doi: 10.1144/GSL.SP.1989.044.01.16

Coward, M. P., Dewey, J. F., Hempton, M. and Holroyd, J. (2003). “Tectonic evolution. The Millennium Atlas: Petroleum Geology of the Central and Northern North Sea”. Geological Society, London, 17, 591 p.33

Delcamp, A., Petronis, M. S., Troll, V. R. (2014). “Discerning magmatic flow patterns in shallow-level basaltic dykes from the NE rift zone of Tenerife, Spain, using the Anisotropy of Magnetic Susceptibility (AMS) technique”. Geological Society special publication, 2015, Vol.396 (1), p.87-106. doi: 10.1144/SP396.2

Dewey, J. F. and Strachan, R. A. (2003) “Changing Silurian-Devonian relative plate motion in the Caledonides: sinistral transpression to sinistral transtension,” Journal of the Geological Society, 160(2), pp. 219-229. doi: 10.1144/0016-764902-085.

Domeier, M., & Torsvik, T. H. (2014). ”Plate tectonics in the late Paleozoic”. Geoscience Frontiers, 5(3), p. 303-350. doi: 10.1016/j.gsf.2014.01.002

Enfield, M. A. and Coward M. P. (1987). “The Structure of the West Orkney Basin, northern Scotland”. Journal of the Geological Society, London, Vol. 144, pp. 871-884. doi: 10.1144/gsjgs.144.6.0871

Fisher, R. (1953). “Dispersion on a sphere”. Proceedings of the Royal Society. A, Mathematical, physical, and engineering sciences, 1953-05-07, Vol.217 (1130), p.295-305. doi: 10.1098/rspa.1953.0064

Fossen, H. (2010). “Extensional tectonics in the North Atlantic Caledonides: a regional view”. Geological Society special publication, 2010, Vol.335 (1), p.767-793. doi: 10.1144/SP335.31

Geikie, A. (1897). “The ancient volcanoes of Great Britain (Vol. 1)”. Macmillan.

Gillen, C. (2003). “Geology and landscapes of Scotland”. Harpenden, Hertfordshire: Terra Publishing (UK).

Halliday, A. N., McAlpine, A. and Mitchell, J. G. (1977). “The Age of the Hoy Lavas, Orkney”. Scottish Journal of Geology, Vol. 13, pp. 43-52. doi: 10.1144/sjg13010043

Halliday, A. N., McAlpine, A. and Mitchell, J. G. (1982). “40Ar/39Ar age of the Hoy lavas, Orkney”. In Numerical Dating in Stratigraphy, Wiley, pp. 928-31.

Kendall, R. S. (2017). “The Old Red Sandstone of Britain and Ireland — a review,” Proceedings of the Geologists’ Association. 128(3), pp. 409-421. doi: 10.1016/j.pgeola.2017.05.002

Li, Z. X., Bogdanova, S. V., Collins, A. S., Davidson, A., De Waele, B., Ernst, R. E., Fitzsimons, I. C. W., Fuck, R. A., Gladkochub, D. P., Jacobs, J., Karlstrom, K. E., Lu, S., Natapov, L. M., Pease, V., Pisarevsky, S. A., Thrane, K., Vernikovsky, V. (2008). “Assembly, configuration, and break-up history of Rodinia: A

synthesis." Precambrian research, 2008-01, Vol.160 (1-2), p.179-210.
doi: 10.1016/j.precamres.2007.04.021

Lundmark, A. M., Gabrielsen, R. and Brown, J. F. (2011). "Zircon U–Pb age for the Orkney lamprophyre dyke swarm, Scotland, and relations to Permo- Carboniferous magmatism in northwestern Europe," Journal of the Geological Society, 168, pp. 1233–1236.
doi: 10.1144/0016-76492011-017

Lundmark, A. M., Augland, L. E., & Bjerga, A. D. (2019). Timing of strain partitioning and magmatism in the Scottish Scandian collision, evidence from the high Ba–Sr Orkney granite complex. *Scottish Journal of Geology*, *55*(1), 21-34.

Lundmark, A. M., Augland, L. E., Svebo, J. R., (2020) "Devonian magmatism in the Orcadian basin: evidence of large-scale coupling between transcurrent faulting and pull-apart extension?". Submitted to Journal of the Geological Society.

Macdonald, R. and Fettes, D. J. (2007). "The tectonomagmatic evolution of Scotland", Transactions of the Royal Society of Edinburg: Earth Sciences. 97 (3). pp. 213-295. doi: 10.1017/S0263593300001450

Marshall, J. E., Rogers, D. A., & Whiteley, M. J. (1996). "Devonian marine incursions into the Orcadian basin, Scotland". Journal of the Geological Society, 1996-05, Vol.153 (3), p.451-466.
doi: 10.1144/gsjgs.153.3.0451

Marshall, J., and Hewett, T. (2003), "Devonian, in The Millennium Atlas: Petroleum Geology of the Central and Northern North Sea", edited by D. Evans et al., Geol. Soc. of London, U. K.

Marshall, J. E., Brown, J. F., & Astin, T. R. (2011). "Recognising the Taghanic Crisis in the Devonian terrestrial environment and its implications for understanding land–sea interactions". Palaeogeography, palaeoclimatology, palaeoecology, 2011, Vol.304 (1), p.165-183.
doi: 10.1016/j.palaeo.2010.10.016

McAlpine, A. (1978). "The Upper Old Red Sandstone of Orkney, Caithness and Neighbouring Areas". (Doctoral dissertation, University of Newcastle upon Tyne).

McKerrow, W. S., Mac Niocaill, C., and Dewey, J. F. (2000). "The Caledonian Orogeny redefined" Journal of the Geological Society, 2000-11, Vol.157 (6), p.1149-1154. doi: 10.1144/jgs.157.6.1149

Monaghan, A. A. & Parrish, R. R. (2006). "Geochronology of Carboniferous–Permian magmatism in the Midland Valley of Scotland: implications for regional tectonomagmatic evolution and the

numerical time scale". Journal of the Geological Society, London, 163(1), p. 15-28. doi: 10.1144/0016-764904-142

Morris, W. A., Briden, J. C., Piper, J. D. A-. Sallomy, J. T. (1973). "Paleomagnetic Studies in the British Caledonides – V Miscellaneous New Data" Geophysical Journal of the Royal Astronomical Society, 1973-10, Vol.34 (1), p.69-105. doi: 10.1111/j.1365-246X.1973.tb02386.x

Mykura, W., Flinn, D. & May, F. (1976). "British regional geology: Orkney and Shetland". Stationery Office Books (TSO).

Odling, N. W. A. (1999a). "Too of the Head". Geological Conservation Review, Vol. 17: Caledonian Igneous Rocks of Great Britain, Chapter 9: Late Silurian and Devonian volcanic rocks of Scotland, 4 pages

Odling, N. W. A. (1999b). "Point of Ayre". Geological Conservation Review, Vol. 17: Caledonian Igneous Rocks of Great Britain, Chapter 9: Late Silurian and Devonian volcanic rocks of Scotland, 3 pages

Ort, M. H., Porreca, M., Geissman, J. W. (2015). "The use of palaeomagnetism and rock magnetism to understand volcanic processes: introduction". Geol Soc Lond, Spec Publ 396:1-11. doi: 10.1144/SP396.17

Parnell, J., Rogers, D., Astin, T., and Marshall, J. (1994). "Devonian Orcadian Basin, northern Scotland, UK". Global Geological Record of Lake Basins, 1, pp.73-79

Prave, A. R., Fallick, A. E., Thomas, C. W., Graham, C. M. (2009). "A composite C-isotope profile for the Neoproterozoic Dalradian Supergroup of Scotland and Ireland". Journal of the Geological Society, 2009-09, Vol.166 (5), p.845-857. doi: 10.1144/0016-76492008-131

Pueyo Anchuela, Ó., Gil, A., Lago, M., França, Z. & Galé, C. (2006). "Magma flow directions in Azores basaltic dykes from AMS data: preliminary results from Corvo island". Geogaceta, 40, 83– 86

Raposo, M. I. B., Ernesto, M. (1995). "Anisotropy of magnetic susceptibility in the Ponta Grossa dike swarm (Brasil) and its relationship with magma flow direction". Physics of the earth and planetary interiors, 1995-01, Vol.87 (3-4), p.183-196. doi: 10.1016/0031-9201(94)02970-m

Rian, M. T. (2018). "A re-evaluation of the age and significance of lamprophyre dikes of Orkney, Scotland". (Master Thesis, Department of Geosciences, University of Oslo).

Rock, N. M. S. (1983). “The Permo-Carboniferous camptonite-monchiquite dyke-suite of the Scottish Highlands and Islands: distribution, field and petrological aspects,” British Geological Survey, 14(82), p. 42

Robinson, M. A. (1985). “Palaeomagnetism of volcanics and sediments of the Eday Group, Southern Orkney”. Scottish journal of geology, 1985-02, Vol.21 (3), p.285-300. doi: 10.1144/sjg21030285

Smythe, D. K., Russel, M. J. and Skuce, A. G. (1995). “Intra-continental rifting inferred from the major late Carboniferous quartz-dolerite dyke swarm of NW Europe” Scottish Journal of Geology. Geological Society of London, 31(1), pp. 151-162. doi: 10.1144/sjg31020151

Speed, J. (1666). “England, Wales, Scotland and Ireland described”. London

Storetvedt, K. M. and Meland, A. H. (1985). “Geological interpretation of palaeomagnetic results from Devonian rocks of Hoy, Orkney”. Scottish journal of geology, 1985-02, Vol.21 (3), p.337-352. doi: 10.1144/sjg21030337

Storetvedt, K. M. and Otterå, L. E. (1987). “Palaeozoic reconfigurations of north Scotland based on palaeomagnetic results from Orkney dykes”. Physics of the earth and planetary interiors, 1988-11, Vol.52 (3-4), p.243-255. doi: 10.1016/0031-9201(88)90118-5

Storetvedt, K. M. and Pettersen, N. (1972). “Palaeomagnetic properties of the Middle-Upper Devonian Volcanics of the Orkney Islands”. Earth and planetary science letters, 1972-03, Vol.14 (2), p.269-278. doi: 10.1016/0012-821x(72)90019-2

Strachan, R. A. (2003). “The metamorphic basement geology of Mainland Orkney and Graemsay”. Scottish journal of geology, 2003-11, Vol.39 (2), p.145-149. doi: 10.1144/sjg39020145

Tarling, D. H. (1985). “Palaeomagnetic studies of the Orcadian Basin”. Scottish journal of geology, 1985, Vol.21 (3), p.261-273. doi: 10.1144/sjg21030261

Tauxe, L., Gee, J. S. & Staudigel, H., (1998). “Flow directions in dikes from anisotropy of magnetic susceptibility data: the bootstrap way”, Journal of Geophysical Research: Solid Earth, 1998-08-10, Vol.103 (B8), p.17775-17790. doi: 10.1029/98JB01077

Thirlwall, M. F. (1979). “The petrochemistry of the British Old Red Sandstone volcanic province”. (Doctoral dissertation, University of Edinburgh).

Wilson, G. V and Knox, J. (1936). “The geology of the Orkney and Shetland Islands”. Proceedings of the Geologists’ Association, 47(3), p. IN15-IN17. doi: 10.1016/S0016- 7878(36)80015-7

9. Appendix

9.1 Tables from previous studies

Storetvedt and Petersen, 1971

Samples collected from Rackwick and the Old Man of Hoy.

N	R	*k*	A_{95}	Dec	Inc	Pole	Remarks
7	6.9	44.8	9.1	205	8.4	23.7N 149.5E	Unit Weight on specimens. Statistical parameters are according to Fisher.

Orkney Volcanics	Devonian (Middle – Upper)	149.5° E 23.7° N	R	Pole position considered somewhat inaccurate owing to the problems of estimating single remanence components.

Storetvedt and Meland, 1985

Samples collected from Rackwick and the Old Man of Hoy.

Site no.	Specimen	Dec	Inc	Group	Range	Locality
1	OR 1-A	032	-26°	B1	440-635°C	Old Man of Hoy Lavas
2	8-A	023	-27°	B1	450-580°C	Old Man of Hoy Lavas
	11-A	018	-33°	B1	400-635°C	Old Man of Hoy Lavas
	12-A	031	-25°	B1	440-635°C	Old Man of Hoy Lavas
3	13-A	017°	-39°	B1	NRM-660°C	Old Man of Hoy Lavas

	14-A	031°	-30°	B1	3-70 mT + 100-400°C	Old Man of Hoy Lavas
	16-B	199°	19°	B2	400-635°C	Old Man of Hoy Lavas
	18-A	206°	12°	B2	585°, 635°C	Old Man of Hoy Lavas
	19-A	025°	-35°	B1	440-550°C	Old Man of Hoy Lavas
5	31-B	354°	-30°	B1	530-620°C	Old Man of Hoy Lower Eday Sst. Baked contact
	32-Ba	189°	-30°	A	v.s. 200-360°C	Old Man of Hoy Lower Eday Sst. Baked contact
	32-Bb	032°	-26°	B1	360-605°C	Old Man of Hoy Lower Eday Sst. Baked contact
	33-A	027°	-24°	B1	405-605°C	Old Man of Hoy Lower Eday Sst. Baked contact
	34-B	041°	-22°	B1	500-670°C	Old Man of Hoy Lower Eday Sst. Baked contact
	35-B	027°	-22°	B1	560°, 590°C	Old Man of Hoy Lower Eday Sst. Baked contact
6	36-A	027°	-34°	B1	360-605°C	Old Man of Hoy Lower Eday Sst. Baked contact
	37-Ba	173°	-30°	A	v.s. 200-300°C	Old Man of Hoy Lower Eday Sst. Baked contact
	37-Bb	030°	-28°	B1	500-620°C	Old Man of Hoy Lower Eday Sst. Baked contact
	38-A	016°	-21°	B1	510-575°C	Old Man of Hoy Lower Eday Sst. Baked contact
	38-B	014°	-26°	B1	400-625°	Old Man of Hoy Lower Eday Sst. Baked contact
	39-A	020°	-21°	B1	450-530°	Old Man of Hoy Lower Eday Sst. Baked contact

7	45-Aa	174°	-30°	A	v.s. 250-400°C	Old Man of Hoy Lower Eday Sst. 20cm from the baked contact
	45-Ab	029°	-25°	B1	400-600°C	Old Man of Hoy Lower Eday Sst. 20cm from the baked contact
	45-Ba	175°	-32°	A	v.s. 200-350°C	Old Man of Hoy Lower Eday Sst. 20cm from the baked contact
	45-Bb	021°	-22°	B1	500-590°C	Old Man of Hoy Lower Eday Sst. 20cm from the baked contact
	46-Aa	170°	-35°	A	v.s. 200-320°C	Old Man of Hoy Lower Eday Sst. 20cm from the baked contact
	46-Ab	017°	-27°	B1	410-545°C	Old Man of Hoy Lower Eday Sst. 20cm from the baked contact
	46-B	018°	-25°	B1	400-540°C	Old Man of Hoy Lower Eday Sst. 20cm from the baked contact
8	49-A	176°	-28°	A	v.s. 250-450°C	Old Man of Hoy Lower Eday Sst. 30cm from the baked contact
10	57-A	021°	-40°	B1	300-530°C	Old Man of Hoy Lower Eday Sst. 100cm from the baked contact
	57-B	175°	-32°	A	v.s. 250-400°C	Old Man of Hoy Lower Eday Sst. 100cm from the baked contact
11	60-A	206°	14°	B2	300-450° C	Rackwick
	61-A	211°	13°	B2	9-40 mT	Rackwick
	64-A	209°	12°	B2	350-450° C	Rackwick
12	66-A1	214°	14°	B2	9-20 mT	Rackwick

	66-B2	218°	6°	B2	9-14 mT	Rackwick
	66-C2	207°	4°	B2	12-20 mT	Rackwick
13	67-C2	230°	19°	B2	3-12 mT	Rackwick
14	68-A1	211°	8°	B2	200-460° C	Rackwick
	68-B2	216°	17°	B2	6-30 mT	Rackwick
15	70-B1	195°	22°	B2	15-40 mT	Rackwick
16	71-A1	202°	-12°	B2	460-520° C	Rackwick
	71-A2	201°	-8°	B2	100-460° C	Rackwick
	71-B1	204°	5°	B2	22,24 mT	Rackwick
	71-B2	200°	1°	B2	3-30 mT	Rackwick
	71-C1	203°	7°	B2	9-39 mT	Rackwick

Formation	Group	Dec	Inc	A_{95}	K	Pole
Hoy Lavas	A	176°	-31°	4.2	206	47.7° N 182.2° E
	B1	023°	-28°	3.8	66	
	B2	208°	9°	5.5	43	22.7° N 146.3° E

Storetvedt and Otterå, 1987

Samples collected from the Orkney dikes.

Table of dikes

Site	Samples	Location	Strike	Dyke width (m)	Rock type
1	OD 1 – 5	Birsay Bay	070	~1	Camptonite
2	6 – 10	Birsay Bay	070	1.0	Camptonite
3	11 – 15	Ch. of Orphir	090	0.5	Camptonite
4	16 – 20	Ch. of Orphir	040	0.5	Camptonite
5	21 – 25	Midland Ness	170	~1	Monchiquite
6	26 – 29	Midland Ness	170	0.5	Monchiquite
7	30 – 34	Billia Croo	090	0.5	Camptonite
8	35 – 39	Garson, Strom.	054	~1	Camptonite
9	40 – 45	Rennibister	066	~2	Camptonite
10	46 – 48	Widewall Bay	060	0.8	Camptonite
11	49 – 52	Widewall Bay	060	1.0	Camptonite
12	53 – 57	Grim Ness	040	1.0	Monchiquite

13	58 – 61	Petertown	138	2.5	Monchiquite

Table of results

Formation	Pal. group	Dec	Inc	A_{95}	*K*	Pole
Orkney dykes	B	169°	4	3.1	67	189.5° E 28.4° N
Orkney dykes (Kiaman age overprint)	A	172°	-24°	3.3	51	188.9° E 43.2° N

Robinson, 1985

Table of results

Location/group	Dec	Inc	N	k	A_{95}	Pole
Orkney (Eday)	193.8°	40.8°	6	20	15.2°	164.3° E 7.3° N

Site mean results

Site no	Formation	Location	GDec	GInc	Tectonic correction	TDec	TInc	N	k	A_{95}
19	Contact Zone	Deerness	173.7°	51.8°	090/10 (Strike/Dip)	174.8°	41.8°	11	21.3	10.1°
20	Eday Lavas	Deerness	192.5°	44.0°	090/10 (Strike/Dip)	190.8°	34.2°	8	6.0	24.8°
34	Eday Lavas	Deerness	224.8°	53.5°	334/26 (Strike/Dip)	201.5°	69.7°	8	3.8	33.1°

38	Eday Lavas	Deerness	189.5°	45.3°	090/10 (Strike/Dip)	188.1°	35.4°	7	20.5	13.7°
17	M. Eday Sst.	Deerness	205.3°	-4.5°	355/18 (Strike/Dip)	205.2°	4.6°	5	16.0	19.7°

9.2 Field Magnetic measurements

Dates in mm/dd/yyyy

Sample	Azimuth	Plunge	Sun Reading	Time (local)	Time (GMT)	Corr. Azimuth	Sun Azimuth	Residual	Residual Avg	Notes	State	Exist?	AMS
Melsetter - MS1		**58.778N**	**3.273W**	**08/27/2019**					**-1**				Decently clustered
MS1-1	063	7	078	12:24	11:24	61	62	-1					
MS1-2	057	27				55							
MS1-3	332	6				330							
MS1-4	015	10				13							
MS1-5	330	8				328							
MS1-6	169	16				167							
MS1-7	093	47				91							
MS1-8	012	41				10							
Lounders Fea - LF1		**58.917N**	**3.366W**	**08/28/2019**					2				Well clustered
LF1-1	219	11	225	12:48	11:48	217	216	1					
LF1-2	179	82				177							
LF1-3	319	17	324	12:52	11:52	317	317	0					
LF1-4	295	75	296	12:54	11:54	293	289	4					
LF1-5	200	56				198							
LF1-6	276	32				274							
LF1-7	245	45				243							
LF1-8	233	37				231							
LF1-9	238	73				236							
Lounders Fea - LF2		**58.919N**	**3.369W**	**08/28/2019**									Well Clustered
LF2-1	220	51				218							
LF2-2	046	22				44							
LF2-3	266	67				264							
LF2-4	329	16				327							
LF2-5	242	67				240							

LF2-6	212	75				210							
LF2-7	175	54				173							
LF2-8	031	14				29							
Rackwick - RW1		**58.869N**	**3.399W**	**08/29/2019**	**09/01/2019**				1				Decently clustered
RW1-1	264	70	243	14:13	13:13	262	262	0					
RW1-2	336	84				334							
RW1-3	233	70	248	12:17	11:17	231	230	1		**New date: 1/9**			
RW1-4	255	79	270	12:19	11:19	253	253	0					
RW1-5	344	50				342							
RW1-6	017	73				15							
RW1-7	283	79	294	12:29	11:29	281	280	1					
RW1-8	274	67	283	12:36	11:36	272	271	1					
Rackwick - RW2		**58.869N**	**3.400W**	**08/31/2019**									Looks scattered, might follow a great-circle
RW2-1	214	17				212				Bottom sandy layer			
RW2-2	029	30				27							
RW2-3	355	17				353							
RW2-4	311	48				309							
RW2-5	350	16				348							
RW2-6	202	25				200				Possibly unconformed/faults			
Rackwick - RW3		**58.869N**	**3.400W**	**08/31/2019**									Looks a bit scattered
RW3-1	009	31				7							
RW3-2	033	23				31							
RW3-3	313	21				311							
RW3-4	053	21				51							
RW3-5	043	17				41							
RW3-6	343	12				341							
Rackwick - RW4		**58.869N**	**3.400W**	**08/31/2019**									Some clustering, some scattered
RW4-1	354	22				352							
RW4-2	313	23				311							
RW4-3	333	20				331							

RW4-4	293	54				291							
RW4-5	340	44				338							
RW4-6	315	12				313							
Rackwick - RW5		**58.869N**	**3.400W**	**08/31/2019**									Sort of clustered, but a bit widely distributed
RW5-1	317	68				315							
RW5-2	351	62				349							
RW5-3	355	66				353							
RW5-4	000	60				358							
RW5-5	319	88				317							
RW5-6	010	80				8							
RW5-7	003	65				1							
Rackwick - RW6		**58.869N**	**3.407W**	**09/01/2019**									
RW6-1	011	51								STRIKE/DIP - HANDSAMPLE			
RW6-2	139	33								STRIKE/DIP - HANDSAMPLE			
RW6-3	189	81								STRIKE/DIP - HANDSAMPLE			
RW6-4	198	67								STRIKE/DIP - HANDSAMPLE			
RW6-5	073	78								STRIKE/DIP - HANDSAMPLE			
Deerness - DN1		**58.920N**	**2.713W**	**08/30/2019**					0				Clustered, one outlier
DN1-1	241	67	194	15:31	14:31	239	237	2					
DN1-2	340	22	294	15:38	14:38	338	339	-1					
DN1-3	338	48				336							
DN1-4	040	58				38							
DN1-5	326	17				324							
DN1-6	154	22	100	16:10	15:10	152	153	-1					
DN1-7	219	19	162	16:20	15:20	217	218	-1					
DN1-8	315	62	255	16:24	15:24	313	312	1					
DN1-9	295	51	233	16:38	15:38	293	293	0		More reddish color			
Deerness - DN2		**58.920N**	**2.713W**	**08/30/2019**					1				Decently Clustered
DN2-1	269	72	194	17:25	16:25	267	265	2		Baked contact			

DN2-2	226	32	152	17:29	16:29	224	224	0					
DN2-3	206	49				204							
DN2-4	240	76				238							
DN2-5	321	87	244	17:39	16:39	319	319	0					
DN2-6	337	91	259	17:43	16:43	335	334	1					
Deerness - DN3		**58.920N**	**2.713W**	**08/30/2019**					-1				A little widely clustered
DN3-1	310	27	232	17:48	16:48	308	309	-1		Bleached Zone			
DN3-2	274	26	194	17:57	16:57	272	273	-1		Grey/red sandstone			
DN3-3	342	36	261	18:04	17:04	340	341	-1		Red sandstone			
DN3-4	046	18				44							
DN3-5	295	35				293							
DN3-6	336	74				334							
DN3-7	296	20				294							
Deerness - DN4		**58.920N**	**2.713W**	**08/30/2019**									Scattered, maybe a pattern
DN4-1	301	21				299							
DN4-2	093	19				91							
DN4-3	275	19				273							
DN4-4	320	16				318							
DN4-5	013	55				11							
DN4-6	305	56				303							
Deerness - DN5		**58.920N**	**2.712W**	**09/02/2019**									One axis clustered, rest maybe following a great circle
DN5-1	258	76				256				1.5m "pillow"			
DN5-2	307	65				305				same "pillow"			
DN5-3	283	72				281				0.8-1m "pillow"			
DN5-4	307	66				305				60cm "pillow"			
DN5-5	173	27				171				50cm "pillow"			
DN5-6	026	59				24				1m "pillow"			
DN5-7	343	37				341				1m "pillow", edge			
DN5-8	126	15				124				2-3m "pillow"			
Bay of Skaill - BS1		**59.057N**	**3.338W**	**09/03/2019**					0				Some clustering, maybe along a great circle

BS1-1	234	31	273	10:56	09:56	232	232	0		55cm from edge			
BS1-2	161	36	201	11:00	10:00	159	161	-2		71cm from edge			
BS1-3	311	38	347	11:04	10:04	309	308	1		35cm from edge			
BS1-4	061	55				59				19cm from edge			
BS1-5	154	26				152				32cm from edge			
BS1-6	186	18				184				28cm from edge			
BS1-7	117	23				115				28cm from edge			
BS1-8	038	18				36				23cm from edge			
Yesnaby - YB1		**59.025N**	**3.359W**	**09/03/2019**					-3				Good clustering, two outliers
YB1-1	343	72	322	14:08	13:08	341	339	2		South side			
YB1-2	130	31	108	14:23	13:23	128	130	-2		Top			
YB1-3	156	37	134	14:25	13:25	154	157	-3		Top			
YB1-4	079	59	059	14:28	13:28	77	82	-5		Top			
YB1-5	075	83	055	14:33	13:33	73	80	-7		Top			
YB1-6	131	90				129				North side			
YB1-7	161	44				159				North side			
YB1-8	144	35				142				North side			
Nethertown - NT1		**58.952N**	**3.319W**	**09/03/2019**					-4				Decent clustering
NT1-1	070	56				68							
NT1-2	275	25				273							
NT1-3	286	41				284							
NT1-4	047	32				45							
NT1-5	060	30				58							
NT1-6	239	67				237							
NT1-7	103	56	038	17:10	16:10	101	105	-4					
NT1-8	245	53				243							
Tingwall - TW1		**59.087N**	**3.039W**	**09/04/2019**					1				Decent clustering
TW1-1	217	21	253	11:00	10:00	215	213	2					
TW1-2	222	25	256	11:02	10:02	220	217	3					
TW1-3	204	22	243	11:03	10:03	202	204	-2					
TW1-4	132	16	170	11:05	10:05	130	132	-2					

TW1-5	252	22	288	11:06	10:06	250	250	0					
TW1-6	232	34				230							
TW1-7	206	14	235	11:20	10:20	204	201	3					
TW1-8	223	27	250	11:28	10:28	221	218	3					
Birsay - BR1		**59.138N**	**3.307W**	**09/04/2019**									Good clustering, one a little off
BR1-1	127	26				125							
BR1-2	157	26				155							
BR1-3	263	73				261							
BR1-4	167	77				165							
BR1-5	008	21				6							
BR1-6	102	24				100							
BR1-7	111	22				109							
BR1-8	254	78				252							
Birsay - BR2		**59.138N**	**3.307W**	**09/04/2019**									One axis clustered, the other two seems to fall into two groups
BR2-1	113	13				111							
BR2-2	132	20				130							
BR2-3	144	20				142							
BR2-4	122	22				120				Further east			
BR2-5	140	17				138				Slightly messy line			
BR2-6	152	10				150				Bottom half unmarked			
BR2-7	101	18				99							
BR2-8	204	32				202				4 bits, top marked			
BR2-9	132	23				130							
BR2-10	134	20				132							
BR2-11	256	60				254							
BR2-12	341	62				339							
Birsay - BR3		**59.138N**	**3.307W**	**09/04/2019**									One axis clustered, the others follow a great-circle
BR3-1	159	21				157							
BR3-2	212	16				210							
BR3-3	171	22				169							

BR3-4	344	68				342							
BR3-5	346	66				344							